Breaking with tradition: Fischer—Tropsch gas loops and modelling vapor—liquid—liquid equilibrium

by

Braden Kelly

A thesis submitted in partial fulfillment of the requirements for the degree of

Master of Science

in

Chemical Engineering

Department of Chemical and Materials Engineering
University of Alberta

Abstract

Fischer—Tropsch gas loops have been in use for nearly a century, producing synthetic fuels and petrochemicals. Yet there still remain many opportunities to expand its uses, update the gas loop with new technology, as well as better understand at a fundamental level the way the products behave. The following chapters address each of these three points, trying to bring new insight into the uses and behavior of one of the most promising technologies currently available for producing synthetic fuels and petrochemicals.

Rather than focusing on the synthetic fuel production of Fischer—Tropsch synthesis, the gas loops significant by-product of steam was applied to the steam assisted gravity drainage recovery of bitumen. It was found that Fischer—Tropsch technology can be used in tandem with traditional once through steam generation methods to produce the necessary steam, while also lowering the CO_2 emissions and producing liquid hydrocarbon products, diluent for bitumen transport, and solvent for steam co-injection.

In the second part of the thesis water electrolysis is integrated into cobalt and iron based Fischer—Tropsch gas loops and compared with traditional Fischer—Tropsch gas loops which use air separation units instead. The carbon efficiency of the Fischer—Tropsch gas loop was found to be significantly increased for both cases and renewable energy was found to work well with the iron-based Fischer—Tropsch gas loop design.

The syncrude recovery section of the Fischer—Tropsch gas loop has received little attention in literature regarding oxygenate partitioning between the aqueous and organic liquid phases and gas phase. Several thermodynamics models were tested for accuracy in oxygenate liquid—liquid and vapor—liquid—liquid equilibrium partitioning. The UNIQUAC model was found to be the best model for liquid—liquid calculations and when using the Hayden O'Connell was found to be the most reliable model for predicting vapor—liquid—liquid equilibrium compositions.

Keywords: Fischer—Tropsch, SAGD, water electrolysis, gas loops, thermodynamics, phase equilibria.

Preface

Chapter-10 in this thesis and parts of Chapter-9 are under review as “Kelly, B.; De Klerk, A. Modelling vapor—liquid—liquid phase equilibria in Fischer—Tropsch syncrude. Industrial & Engineering Chemistry Research, 2015. I was responsible for data collection, model selections, model optimizations, model evaluations and manuscript composition. Dr. Arno de Klerk was the co-author involved in concept formulation and manuscript composition.

In loving memory of my brother, Bryce Arthur Kelly. Even after all this time I still think of you.

Acknowledgements

The following work was done without the aid of supernatural powers.

I first and foremost owe my supervisor Dr. Arno de Klerk for allowing me to work under him and learn. I learned so much. His patience is nearly as great as his sense of humor. His editing skills are also unparalleled. For two years he offered me a platform from which I could see further than I ever could have on my own. Occasionally I would stand up, but it usually made me dizzy.

I owe special thanks to Professors John Shaw and Janet Elliott, both for their assistance and guidance over the last two years, but also for being on my thesis committee. It was humbling to have an NSERC and a CRC professor in thermodynamics on my defense committee.

I am a huge fan of music, and must express my gratitude to Paul Kalkbrenner, Burial, Robert Babicz and many more. They kept me company while I worked.

I would not be the man I am without shaping from several significant literary writers. I would like to thank the late David Foster Wallace, Kurt Vonnegut, Hermann Hesse, and John Steinbeck. I would also like to thank the still with us: Thomas Pynchon and Richard Adams. I eye the campus rabbit (hares) with suspicion of great intelligence thanks to Watership Down.

Speaking of writing, I did a pretty sloppy job of this thesis, and I owe a lot to my fiancé Kaitlyn Leroux, and her sister Kailey Leroux, for looking it over and being liberal with the red ink.

Several other people have had significant influences on my life. I would like to thank all of my friends for being my friends, because if they weren't I would have no friends. Making a list would be futile; I have been made better by all of you. I would also like to thank my family for being my family, even though I don't have a choice. For some reason my mom, Carolyn, and dad

(old guy) Glenn, and sister, Bryanna, never ribbed me too much about dropping out of undergrad three times and I appreciate that. My failings led to some of my most treasured memories and I met a lot of great people during my downtimes. I would be nothing without my failures.

I would like to also thank my soon to be parent-in-laws Pam and Kerry Leroux for their incredible generosity and kindness. It will be an honor to be part of your wonderful family.

I also need to thank the people who provided me a roof over my head at the beginning, as well as the end, of this thesis when I was in the awkward stages of moving from one location to another. Kim Engelbertink, your cooking is only matched by my mothers, and your own generosity; and Ray, while oddly last named, you are also a kind, warm hearted person who leaves a positive and lasting impression on people.

I would also like to acknowledge the funding provided by the Canadian Government through the Helmholtz-Alberta Initiative (HAI).

There are two people I need to thank again, because they are the reason this has all been possible. First: my supervisor Dr. Arno de Klerk. You are the reason I found a love for chemical engineering after dropping out of third year twice. Your knowledge and humor in design CH E 464 has indefinitely changed my life. It is the reason I pursued grad school and managed to attain a Master's degree (first try I might add).

Second: I really *really* need to again thank my beautiful fiancé Kaitlyn for her amazing and incandescent love, support, understanding, kindness, generosity and thoughtfulness. You are my infinite improbability drive. You have made me a better human than I could ever be on my own, which is more important than anything University could ever give me (but I am still doing a PhD *wink*).

Table of Contents

List of Tables

Figures **List of Figures** **Page**

Nomenclature

AAPD – Average absolute percentage difference
ASU – Air separation unit
ATR – Auto-thermal reformer
Bbl. – Barrel, unit of volume
COSIA – Canada's Oil Sands Innovation Alliance
CTL – Coal-to-liquids
EOS – Equation of state
FT – Fischer—Tropsch
G^E – Excess Gibbs energy
HC – Hayden O'Connell equation of state
HHV – Higher heating value
HTFT – High temperature Fischer—Tropsch
LHV – Lower heating value
LLE – Liquid—liquid equilibria
LTFT – Low temperature Fischer—Tropsch
M – Modulus number
MS – Mutual Solubility
NC – Number of components
NP – Number of phases
NRTL – Non-random two liquids
OTSG – Once through steam generation
PR – Peng—Robinson equation of state
PRSV – Peng—Robinson —Stryjek—Vera equation of state
PSA – Pressure swing adsorption
RK – Redlich-Kwong equation of state
SAGD – Steam assisted gravity drainage
SMR – Steam methane reforming
SN – Stoichiometric number
SRK – Soave—Redlich—Kwong equation of state
Syncrude – Synthetic crude oil
Syngas – Synthesis gas
UNIFAC – Universal Functional Activity Coefficient model
UNIQUAC – Unified Quasi Chemical
vdW – Van der Waals equation of state
VLE – Vapor—liquid equilibria
VLLE – Vapor—liquid—liquid equilibria
VMGSim – Virtual Materials Group Simulator
WEU – Water electrolysis unit
WGS – Water—gas—shift

Symbols

a – Activity or dimensionless parameter in equation of state
A – Intensive Helmholtz energy, or dimensionless constant for equation of state, or parameter defined for the Hayden O'Connell equation of state
b – Dimensionless parameter in equation of state
b_o– Equivalent hard sphere volume of molecules
B – Second Virial coefficient, or dimensionless constant for equation of state
C_{ij} – Energy interaction parameter used by Huron— Vidal for the NRTL
f – Pure fluid fugacity
$\hat{f}i$ – Fugacity of component in mixture
g_{ij} – Interaction energy parameter
G – Intensive Gibbs energy
H – Intensive enthalpy
ΔH – Effective enthalpy of formation of physically bound pairs
ig – Ideal gas property
is – Ideal solution property
k - Boltzmann constant
k_{ij} – Binary interaction coefficient
l_{ij} – Binary interaction coefficient
n – Number of moles
N_o – Avagadro's number, 6.0225x10-23 molecules/mol
P – Pressure
q_i – Molecular shape
r – Property reduced by critical constant or
r_i – Molecular size
R – Universal gas constant (8.3143 $\frac{cm^3-MPa}{mole-K}$)
s_i – Parameter in NRTL
S_i – Parameter in UNIQUAC
sat – Saturated fluid
T – Temperature
$T^{*,}$ – Reduced Temperature
U – Intensive internal energy
u – internal energy
V – Volume
x – Composition of the liquid phase
y – Composition of the vapor phase
z – Composition of the bulk phase
Z – Compressibility factor or coordination number

SUBSCRIPTS
c – Critical property
i – Component i
j – Component j
R – Reference state

SUPERSCRIPTS

E – Excess property for a mixture
L – Liquid phase
o – Standard state property
sat – Saturated property
V – Vapor phase

GREEK

$\hat{\varphi}_i$ – Component fugacity in a mixture
μ_i – Chemical potential for a component in a mixture
τ_{ij} – Boltzmann factor
Δ – Denotes change
m – Parameter for cubic equations of state
Φ – Volume fraction
α – Non-randomness parameter in the NRTL model
γ – Activity coefficient
μ – Pure component chemical potential, or molecular dipole moment
φ – Pure component fugacity coefficient
ϑ – Surface area fraction
η – Association parameter for pure components, solvation parameter for unlike interactions
ω' – Non-polar acentric factor
ε – Energy parameter
σ – Molecular size parameter
μ' – Reduced dipole moment
ω – Acentric factor

Chapter 1 – Introduction

Background

The research that follows this introductory chapter hinges on Fischer—Tropsch (FT) technology, therefore it is best to begin by describing what Fischer—Tropsch technology is. Afterwards, the three main roles in which Fischer—Tropsch technology is encountered in the subsequent chapters is discussed. Namely, for use in steam generation, gas loop design with water electrolysis, and a specific look into the thermodynamic modelling of oxygenates such as alcohols and carboxylic acids in the Fischer—Tropsch synthesis products. Necessary terminology such as "gas loops" will also be discussed in this chapter. Kinetics, reaction mechanisms, hydrodynamics, and thermodynamics that occur *inside* a Fischer—Tropsch reactor are not investigated; while these are active research areas, they have garnered a lot of attention in literature and industry. The effort put into this work aims at either integrating Fischer—Tropsch technology into new fields, integrating new technology into Fischer—Tropsch gas loops, or modelling aspects of Fischer—Tropsch synthesis products that have received little to no attention in literature this far. To summarize, everything is done with the goal of achieving something new, despite Fischer—Tropsch technology being very mature.

The beginning and short history of the Fischer—Tropsch process

The etymology of the name Fischer—Tropsch is derived from its two inventors Franz Fischer and Hans Tropsch. Both were German scientists working at the Kaiser Wilhelm Institute for Coal Research in the Ruhr, Germany.[1] During the year of 1923, their efforts to take coal and convert it into synthetic hydrocarbons came to fruition. An immensely useful technology was born. Anything of carbonaceous content can be turned into hydrocarbons using Fischer—

Tropsch synthesis, and the products can then be upgraded into fuels (or petrochemicals) of the refiner's choice. The two most common feed sources are coal and natural gas. In Germany at the time of its discovery the source of carbon was coal, and later when South Africa began using Fischer—Tropsch technology it too was based on coal. [2] South Africa has been the largest user of Fischer—Tropsch technology since the mid 1950's when the first South African Fischer—Tropsch refinery opened in Sasolburg. Germany had up to nine refineries running by the Second World War, but they were all closed down after the war. [3] Because of the vast reservoirs of crude oil discovered in the Middle East in the 1970's, the price of crude was too low for Fischer—Tropsch synthesis to compete and no new plants were built until the 1980's when two, both in South Africa and both based on coal, were constructed. The first major refineries using natural gas as a feed were the Mossgas plant in South Africa and the Bintulu plant in Malaysia, both constructed in the early 1990's.[4] The United States invested in a gas—to—liquids (GTL) facility in Brownsville Texas in the 1940's, but it was short lived. Several other GTL Fischer—Tropsch facilities have been built in Qatar and Nigeria. China has invested in coal—to—liquids (CTL).

The Fischer—Tropsch reactor is the center of the conversion process, but is actually just one of many parts. Figure 1.1 below shows a simple process flow diagram for the Fischer—Tropsch process. The most expensive block in the process is the production of syngas which takes up ~60% of the cost and provides the necessary syngas to the Fischer—Tropsch reactor. [5] Syngas is the term used to describe the partial combustion products of the reformer or gasifier depending on if the material being used as feed is a gas/light liquid or solid/dense liquid respectively. Syngas is meant mainly to be a combination of carbon monoxide (CO) and hydrogen (H_2), but also contains carbon dioxide (CO_2), water (H_2O), and trace by-products. Syngas often needs to

be adjusted with water—gas—shift (WGS) reactions – Equation 1.1, or addition/subtraction of CO_2 or H_2. While there are many by-products created in the Fischer—Tropsch reactor the primary reaction is the production of alkanes according to equation 1.2:

WGS $$CO + H_2O \leftrightarrow CO_2 + H_2 \quad 1.1$$

Alkanes $$(2n+1)H_2 + nCO \rightarrow C_nH_{(2n+2)} + nH_2O \quad 1.2$$

Iron and cobalt are the only industrially used catalysts in Fischer—Tropsch reactors. In reactors using cobalt as a catalyst there is no WGS reaction and the usage ratio or stoichiometric number (SN), corresponds to Equation 1.3. In reactors using iron catalysts the WGS reaction is active inside the Fischer—Tropsch reactor and the usage ratio is Equation 1.4.

$$\frac{H_2}{CO} \sim 2.0 \quad 1.3$$

$$(H_2 - CO_2)/(CO + CO_2) \sim 2.0 \quad 1.4$$

Figure 1.1 Fischer—Tropsch open gas loop.

Shown above in Figure 1.1 is a simple process flow diagram for Fischer—Tropsch, which also forms the basis for the simplest type of gas loop: the open gas loop. A gas loop is all of the steps required to go from the feed to the final Fischer—Tropsch products. In an open gas loop there is no recycling, everything makes one pass through each unit. This requires the process to be very efficient, and conversion to be very high. If there is a low conversion rate, most of the syngas, which was very expensive to make, passes through, is not converted and is wasted. For this reason Fischer—Tropsch technology is almost always closed loop as shown in Figure 1.2.

Closed loop designs are a lot more complicated and can have many recycle streams. There is not a default closed loop design, since everything depends on what variables are considered the most important, (i.e., carbon efficiency, energy efficiency, cost, type of feed material, etc.).

Figure 1.2 Fischer—Tropsch closed gas loop design.

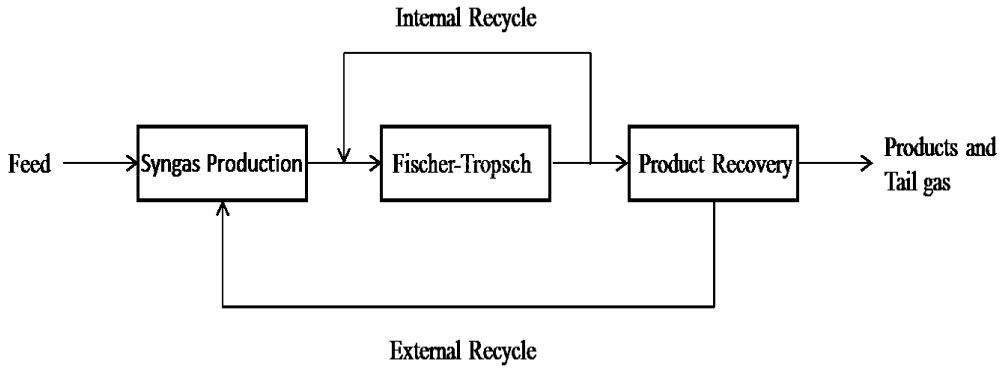

Objectives and scope of work

There are three main goals to the following chapters. Each of these goals is thoroughly investigated in chapters 3, 4 and 10. Chapters 2, 5, 6, 7, 8, and 9 provide the auxiliary fundamentals for understanding the scientific principles which are used to investigate and arrive at conclusions for each goal.

1. In Chapter 3 the objective was to assess the use of Fischer—Tropsch technology for steam production in steam assisted gravity drainage (SAGD) recovery of bitumen. By exploiting the high temperature of syngas production as well as the exothermic heat released from Fischer—Tropsch synthesis, steam can be produced for SAGD. The unconverted syngas (i.e., tail gas - see Figures 1.1 and 1.2) can be used as fuel gas and be combusted in the once through steam generators (OTSG) which traditionally (currently) use natural gas. In addition to steam, Fischer—Tropsch technology provides diluent for

bitumen transport, solvent for steam co-injection, and clean hydrocarbon products to be added to the recovery of bitumen.

2. In Chapter 4 the objective was to determine the influence a water electrolysis unit would have on a Fischer—Tropsch gas loop. The hydrogen benefit to splitting water molecules into hydrogen and oxygen is an often discussed topic; however, in syngas generation auto-thermal reformers (ATR) depend on a source of oxygen, which can also be had through the use of water electrolysis. Oxygen from a water electrolysis unit is also free of inerts such as nitrogen and argon that inevitably make their way into Fischer—Tropsch gas loops and build up when an air separation unit is used for supplying oxygen. Inerts lower the partial pressures of other key elements such as hydrogen and carbon monoxide and also increase the size of purges, resulting in more waste. The addition of hydrogen from the water electrolysis unit can be used to condition syngas for the Fischer—Tropsch reactor as well for use in downstream hydro-processing units.
3. In Chapter 10 the objective was to determine suitable thermodynamic models for predicting oxygenate phase partitioning in Fischer—Tropsch products after exiting the reactor. There is very little research available in the literature for understanding and determining the partitioning of oxygenates once Fischer—Tropsch products are cooled and form vapor—liquid—liquid equilibrium (VLLE). Oxygenates are non-ideal and models used strictly for hydrocarbons are inadequate for predicting the composition of oxygenates in the aqueous and hydrocarbon phases. This has a negative impact on plant longevity if corrosive carboxylic acids are not kept strictly to the aqueous phase, and instead make their way to the downstream hydrocarbon processing units.[6]

References

(1) Jager, B. Developments in Fischer—Tropsch technology. *Studies in Surface Science and Catalysis* **1998**, *Vol. 119*, pp. 25-34.
(2) Schulz, H. A short history of Fischer—Tropsch and present trends of Fischer—Tropsch synthesis, *Applied Catalysis A: General*, **1999,** 3-12**.**
(3) Storch, H.H.; Golumbic, N.; Anderson, R.B. The Fischer—Tropsch and related syntheses, Wiley, New York, 1951
(4) Dry, M.E.; The Fischer—Tropsch Process: 1950-2000. *Catalysis Today*, **2002**, 71, 227
(5) Rostrup-Nielsen, J.; Christiansen, L. J. *Concepts in syngas manufacture;* Imperial College Press: London, 2011.
(6) De Klerk, A. Hydroprocessing peculiarities of Fischer—Tropsch syncrude. *Catalysis Today*, **2008,** *130*, 439-445

Chapter 2 – Literature review on Fischer—Tropsch applications

Introduction

Literature review on OTSG and Fischer—Tropsch steam generation

Fischer—Tropsch technology is expanding globally, however there has been no industrial implementation of it anywhere in Canada. Due to the fact that western Canada contains 95 % of North America's bitumen reserves[1], and as stated, Fischer—Tropsch technology is not industrially employed in Canada, a literature review into SAGD production of bitumen paired with Fischer—Tropsch technology was expected to yield little. This was indeed the case – no references were found that dealt with the integration of Fischer—Tropsch technology to SAGD. A limited review was done for the SAGD process [2-5] and the use of solvent co-injection [1][6][7] to make sure Fischer—Tropsch could provide the correct solvents.

From their conception Fischer—Tropsch reactors have required cooling for the reactors to keep them near isothermal, and producing steam is an obvious method. The steam generated by Fischer—Tropsch gas loops is utilized by industry for either doing work or producing electricity.[9] No published data was found indicating that Fischer—Tropsch has been considered as a supplier of hydrocarbons and steam for SAGD. Some literature was found in which Fischer—Tropsch was utilized in the upgrading of heavy bitumen residues into liquid products,[10] but the purpose was not to use steam to enhance SAGD, but rather to use heavy residue as a feed for Fischer—Tropsch hydrocarbon production.

Literature review on Fischer—Tropsch gas loops and the incorporation of water electrolysis

An overview was completed to see how past and current gas loops have been used in Fischer—Tropsch processes, and also to see what other alternatives have been tried with the Fischer—

Tropsch gas loop as far as oxygen and hydrogen supply go. The literature revealed that the idea of incorporating water electrolysis into industrial designs has been around since the 1970's, and Fischer—Tropsch synthesis is a name often associated with the use of closed carbon loop schemes. Graves et al. gives a thorough examination beginning in the 1970's until present of the ideas associated with electrolysis and industrial designs.[11]

Several keywords tend to be associated with the use of electrolysis: renewable energy and techno-economic evaluation. Much has been published on generating syngas using electrolysis[12-14], and while many have mentioned Fischer—Tropsch synthesis in passing, it has remained a black box on the process flow diagram where hydrogen and carbon monoxide flow in, and hydrocarbons flow out. Quite recently there has been interest in developing an interface between electrolysis processes and Fischer—Tropsch, taking into account the Fischer—Tropsch process[15][16]. Again, the keywords tend to be techno-economic evaluation and the Fischer—Tropsch gas loop has been used as an open loop where high conversions (>80%) have been assumed; or, even when kinetics are modelled, the process remains modelled as an open loop, which is a simple take on a complex process. While these evaluations show the usefulness of Fischer—Tropsch technology, they have no impact on improving its design. A large number of publications dealing with electrolysis to create syngas also assume a feed of CO_2 is present for the use of solid oxide electrolyser cells (SOEC). CO_2 is not available in purified form at an industrial scale in many locations aside from power plants utilizing carbon capture.

On the other hand, natural gas is readily available in many locations and can make use of the oxygen and hydrogen from water electrolysis in natural gas reforming coupled with Fischer—Tropsch synthesis.[17] Both natural gas reforming and Fischer—Tropsch synthesis are mature, readily available technologies. Whereas in the renewable research sector, the emphasis is on

details regarding electrolysis and the Fischer—Tropsch process is kept as a black box into which H_2 and CO go and out of which comes oil. Now it is the Fischer—Tropsch process that is under the microscope.

It is therefore necessary to understand gas loops in a general sense, as well as the specific units that comprise the Fischer—Tropsch gas loop. Gas loops have been discussed extensively by De Klerk[18] for every Fischer—Tropsch refinery completed between 1950-2009, also with discussion on the designs of German refineries pre-1950. Steynberg and Dry[19] also thoroughly discussed the nature and necessity of several current gas loops being used by industry. The term gas loop is not restricted to the Fischer—Tropsch process, and can be found in several other areas, a few being ammonia production,[20] hydrogen production,[21] and methanol synthesis.[22]

Literature review on the thermodynamics of Fischer—Tropsch product separation

In the literature a lot of attention has been paid to what happens inside the Fischer—Tropsch reactor[19], as well as the processes occurring before it to generate the required syngas for the reaction.[17] The product refining that follows the Fischer—Tropsch reactor is also well documented and available in literature.[18] An important step lying between the Fischer—Tropsch reactor and product refining is the cooling and separation of Fischer—Tropsch products. This step involves VLLE as condensation creates aqueous and organic liquid phases. Due to a small fraction of oxygenate by-products (Table 2.1), the mixture is non-ideal and is much harder to accurately describe with many of the models currently available in industrial process simulators. There is a shortage of guidance for which models to use in designing conceptual product separation. What thermodynamics have been done in Fischer—Tropsch have focused mainly on the VLE inside the reactor.[23-26]

Table 2.1 Fischer—Tropsch syncrude product compositions.

Product Fraction	Carbon range	Compound Class	Syncrude composition[a] (mass %)		
			Fe-HTFT[b]	Fe-LTFT[c]	Co-LTFT
Tail gas	C_1	Alkane	12.7	4.3	5.6
	C_2	Alkene	5.6	1.0	0.1
		Alkane	4.5	1.0	1.0
LPG	C_3-C_4	Alkene	21.2	6.0	3.4
		Alkane	3.0	1.8	1.8
Naphtha	C_5-C_{10}	Alkene	25.8	7.7	7.8
		Alkane	4.3	3.3	12.0
		Aromatic	1.7	0	0
		Oxygenate	1.6	1.3	0.2
Distillate	C_{11}-C_{22}	Alkene	4.8	5.7	1.1
		Alkane	0.9	13.5	20.8
		Aromatic	0.8	0	0
		Oxygenate	0.5	0.3	0
Residue/wax	C_{22} +	Alkene	1.6	0.7	0
		Alkane	0.4	59.2	44.6
		Aromatic	0.7	0	0
		Oxygenate	0.2	0	0
Aqueous Product	C_1-C_5	Alcohol	4.5	3.9	1.4
		Carbonyl	3.9	0	0
		Carboxylic Acid	1.3	0.3	0.2

[a]The syncrude composition is expressed as the total mass of product from Fischer—Tropsch synthesis, excluding inert gases (N_2 and Ar) and water gas shift products (H_2O, CO, CO_2, and H_2). Zero indicates low concentration and not necessarily a total absence of such compounds. [b] HTFT stands for high—temperature—Fischer—Tropsch. [c] LTFT stands for low—temperature—Fischer—Tropsch. Reproduced with permission.[18]

Literature regarding the Fischer—Tropsch thermodynamics occurring inside the reactor is mainly regarding the solubility of gases in the liquid phase formed inside the reactor. It is only the hydrocarbons and non-condensable gases that were of concern, since only the heavy

hydrocarbons condense inside the reactor; water, light to medium weight hydrocarbons, and oxygenates remain in the vapor phase.

Initial investigation of vapor—liquid equilibrium (VLE) began by assuming the vapor phase was ideal enough for Raoult's law to be applicable,[23] and also that no oxygenates were present, so the thermodynamics were kept fairly minimal. Work also began in the late 1980's to investigate the solubility of light gases in Fischer—Tropsch products,[27-29] mainly the heavy n-paraffin waxes and a range of equations of state were used often incorporating Flory—Huggins mixing rules: the Soave—Redlich—Kwong[27, 30] and Lacombe-Sanchez.[28] In the mid 1990's work that was focused on the VLE of Fischer—Tropsch products was done by Marano[25] using the Peng—Robinson but also with modified mixing rules to account for the long polymer chains. Since then the Lee—Kesler has been used to calculate VLE compositions and viscosity in long chain Fischer—Tropsch hydrocarbon products.[30] Work focused on hydrocarbons and light gases has been done with regular and modified versions of the Peng—Robinson and Soave—Redlich—Kwong equations as well as with Henry constants.[31, 32] Recently work has been done which returned to using Raoult's law in order to keep calculations as simple as possible due to the presence of other hydrodynamic and kinetic calculations in modelling the inside of the reactor.[26]

The thermodynamics of Fischer—Tropsch wax formation has been investigated by one group[33] and several models were used including the Lee—Kesler, Hildebrandt—Scott, and Non—Random—Two—Liquids (NRTL). A simplified Fischer—Tropsch system using a ternary system of water-n-butanol-n-hexane was modelled using the Peng—Robinson —Stryjek—Vera (PRSV) equation of state with the modelling platform HYSYS. Satisfactory results were found for the VLE ternary for both liquid and vapor phase, however vapor—liquid—liquid equilibria

(VLLE) was not attempted; this paper highlighted the need for further work in determining a suitable model for oxygenate partitioning.[34]

The majority of work done on Fischer—Tropsch thermodynamics has either focused on the hydrocarbon VLE inside the reactor, the solubility of light gases in heavy paraffin's, the thermodynamics of wax formation or in one case that pertained to Fischer—Tropsch reactor effluent, the VLE composition of long-chained paraffin hydrocarbons as well as viscosity. The paper by Rodriguez—Vallejo et al. was the only paper found that directly attempted to model oxygenates in the context of Fischer—Tropsch products outside the reactor.

Summary

There is nothing in the literature on using Fischer—Tropsch technology to improve SAGD recovery of bitumen. The first objective which is detailed in Chapter 3 is a first step towards expanding the use of Fischer—Tropsch technology from the production of hydrocarbons, to the production of steam, and in doing so indirectly producing hydrocarbons from SAGD recovery of bitumen.

For several decades research has been directed at water electrolysis, and it can now be considered a mature technology, although not a mature industrial technology. This work investigated water electrolysis on an industrial scale by including water electrolysis into hydrogen production and the Fischer—Tropsch gas loops. The goal was also to utilize all of the atoms produced by the water electrolysis unit. In literature attention is frequently paid to only the hydrogen that is produced, however the oxygen is a valuable feed for syngas production.

The last part of this work deals with modelling the syncrude recovery section of a Fischer—Tropsch gas loop. This has not been properly dealt with in literature. Oxygenates are nearly always excluded, and in no case has VLLE syncrude recovery been investigated with the intent

of accurately modelling oxygenate partitioning. This was the focus of Chapters 9 and 10: to accurately model oxygenate partitioning in the VLLE encountered in syncrude recovery, and provide guidelines for future research into this area.

References

(1) Keshavarz, M. Mechanistic simulation study of steam-solvent co-injection for bitumen and heavy oil recovery; Masters. Thesis, University of Alberta, **2013**.
(2) Doscher, T.M. Factors influencing success in steam soak operations. *Proc. Pet. Ind.* Conference on thermal oil recovery. Los Angeles, **1966**, 70-80.
(3) Butler, R.M. *Thermal recovery of oil and bitumen*, Prentice-Hall, **1991.**
(4) Butler, R.M. *Horizontal wells for the recovery of oil, gas, and bitumen*, Petroleum Society, **1994.**
(5) Farouq Ali, S.M. Canada's super strategy for oil sands. *Journal of Canadian Petroleum Technology*, **1994**, 16-19.
(6) Nasr, T.N.; Isaacs, E.E., Process for Enhancing Hydrocarbon Mobility Using a Steam Additive; US Patent # 6,230,814, May 15, 2001.
(7) Babadagli, T.; Al-Bahlani, A.M.: Hydrocarbon Recovery Process for Fractured Reservoirs, Canadian Patent Application, Serial No: 2,639,997 filed in Oct. 6, 2008.
(8) Schulz, H. A short history of Fischer—Tropsch and present trends of Fischer—Tropsch synthesis, *Applied Catalysis A: General*, **1999,** 3-12**.**
(9) Vosloo, A. C. Fischer–Tropsch: a futuristic view. *Fuel processing technology*, **2001**, *71*(1), 149-155.
(10) Kresnyak, S. Process for co-producing commercially valuable products from byproducts of heavy oil and bitumen upgrading process, US Patent # US20150038599, Feb 5, **2015**.
(11) Graves, C.; Ebbesen, S.D.; Mogensen, M.; Lackner, K.S. Sustainable hydrocarbon fuels by recycling CO_2 and H_2O with renewable or nuclear energy. *Renewable and Sustainable energy Reviews* **2011**, *Vol. 15*, 1-23.
(12) Graves, C.R. *Recycling CO_2 into sustainable hydrocarbon fuels: electrolysis of CO_2 and H_2O*. PhD Thesis, Columbia University, **2010.**
(13) Nguyen, V.N.; Blum, L. Syngas and synfuels from H_2O and CO_2: current status. *Chemie Ingenieur Technik* **2015**, *Vol. 87*, 354-375
(14) Jensen, S.H.; Larsen, P.H.; Mogensen, M. Hydrogen and synthetic fuel productions from renewable energy sources. *International Journal of Hydrogen Energy* **2007**, *Vol. 32*, 3253-3257.
(15) Becker, W.L.; Braun, R.J.; Penev, M.; Melaina, M. Production of Fischer—Tropsch liquid fuels from high temperature solid oxide co-electrolysis units. *Energy* **2012**, *Vol.47*, 99-115.
(16) Stempian, J.P.; Ni, M.; Sun, Q., Chan, S.H. Thermodynamic analysis of combined Solid Oxide Electrolyzer and Fischer—Tropsch processes. *Energy* **2015**, Vol. 81, 682-690.
(17) J. Rostrup-Nielsen and L. J. Christiansen, *Concepts in syngas manufacture*, Imperial College Press: London, **2011**.
(18) De Klerk, Arno. *Fischer—Tropsch Refining*; Wiley-VCH: Germany, 2010.
(19) Dry, M. E.;Steynberg, A. P. Commercial FT process applications. *Studies in Surface Science and Catalysis*, **2004,** *152*, 406-481.

(20) Holladay, J. D.; Hu, J.; King, D. L.; Wang, Y. An overview of hydrogen production technologies. *Catalysis Today* ***2009***, *139*(4), 244-260.
(21) Aika, K. I.; Christiansen, L. J.; Dybkjaer, I.; Hansen, J. B.; Nielsen, P. H.; Nielsen, A.; Tamaru, K. *Ammonia: catalysis and manufacture*. A. Nielsen (Ed.). Springer Science & Business Media, **2012**.
(22) Bertau, M.; Plass, H.O.L.; Wernicke, F.S.H-J. (Eds), *Methanol: The basic chemical and energy feedstock of the future: Asinger's vision today,* Springer-Verlag: Berlin, **2014**.
(23) Caldwell, L.; Vuuren, D.S. On the formation and composition of the liquid phase in FT reactors. *Chemical Engineering Science* **1986**, *Vol. 41*, 89-96.
(24) Wang, Y.N.; Li, Y.W.; Bai,L.; Zhao, Y.L, Zhang, B.J. Correlation of gas-liquid equilibrium prediction in Fischer—Tropsch synthesis. *Fuel* **1999**, *Vol. 78*, 911-917.
(25) Marano, J.J.; Holder, G. D.; Characterization of Fischer—Tropsch liquids for vapor—liquid equilibria calculations. *Fluid Phase Equilibria* **1997,** *Vol 138*, 1-21.
(26) Masuku, C.M.; Ma, W.; Hildebrandt, D.; Glasser, D.; Davis, B.H. A vapor—liquid equilibrium thermodynamic model for a Fischer—Tropsch reactor. *Fluid Phase Equilibria* **2012**, *Vol. 314*, 38-45.
(27) Tsai, F.N.; Huang, S.H.; Lin, H.M.; Chao, K.C. Solubility of methane, ethane, and carbon dioxide in a Mobile Fischer—Tropsch wax and in n-paraffins. *The Chemical Engineering Journal* **1988**, *Vol. 38*, 41-46.
(28) Chou, J.S.; Chao, K.C. Correlation of synthesis gas solubility in n-paraffin solvents and Fischer—Tropsch waxes. *Fluid Phase Equilibria* **1989**, *Vol. 46,* 179-195.
(29) Huang, S. H.; Lin, H. M.; Tsai, F. N.; Chao, K. C. Solubility of synthesis gases in heavy n-paraffins and Fischer—Tropsch wax. *Ind. Eng. Chem. Res.* **1988**, *27*, 162-169.
(30) Derevich, I.V.; Ermdaev, V.S.; Mordkovich, V.Z. Modelling the thermal and physical properties of liquid and gas mixtures of Fischer—Tropsch products. *Theoretical Foundations of Chemical Engineering* **2011**, *Vol. 45*, 221-226.
(31) Karimi, Z.; Rahmani, M.; Mogadam, M. A study on the vapor—liquid equilibria in Fischer—Tropsch synthesis. *Procedia Engineering* **2012**, *Vol. 42*, 25-33.
(32) Derevich, I.V.; Ermdaev, V.S.; Mordkovich, V.Z. Liquid-vapor thermodynamic equilibrium in Fischer—Tropsch synthesis products. *Theoretical Foundations of Chemical Engineering* **2008**, *Vol. 42*, 216-219.
(33) Derevich, I.V.; Ermdaev, V.S.; Zol'nikova, N.V.; Mordkovich, V.Z. Thermodynamics of wax formation in the Fischer—Tropsch Synthesis products. *Theoretical Foundations of Chemical Engineering* **2013**, *Vol. 47*, 191-200.
(34) Rodriguez—Vallejo, D.F.R.; De Klerk, A. Improving the interface between Fischer—Tropsch synthesis and refining. *Energy and Fuels* **2013**, *Vol. 27*, 3137-3147.

Chapter 3 – Once-Through Steam Generation

Background

Classical methods of gathering bitumen use open pit mining to manually excavate the bitumen, and then process it into a higher quality product. While this technique is still used, it has been found that the majority of bitumen lies underground in formations too deep to be mined using open pit mining methods. A popular method known as steam assisted gravity drainage (SAGD) was developed to allow the recovery of highly viscous bitumen, without the need to physically excavate the oil sands ore.[1]

SAGD derives its name from the use of twin boreholes drilled through a bitumen formation, one above the other, usually separated by 5 meters. The upper borehole is pressurized with steam which heats the surrounding formation, decreasing the viscosity of the bitumen, and allowing it to flow with the assistance of gravity into the lower borehole, along with the condensed (produced) water. The bitumen and produced water is pumped to the surface where the bitumen is separated, and transported to an upgrading facility. Typically diluent must be mixed with bitumen to keep the viscosity of the bitumen low enough for it to be transportable. The produced water is recycled at a rate higher than 90 %.[2] The source of water for the steam often contains undesired contaminants from the brackish sources used for fresh water intake as well as from the recycled produced water. Fresh water intake is kept to a minimum. It is common for steam to be generated at the surface at 75-80% quality, where quality refers to the amount of vapor formed relative to the total amount of water. By keeping some of the water as a liquid, non-volatile components such as salts are kept in the liquid phase, helping to eliminate fouling. The vapor phase is then separated afterwards so that steam at 100% quality is transported to the injection wells.

Once through steam generation (OTSG) units are used on the surface to generate the initial steam at 75-80% quality. Combustion of natural gas provides the heat for generating steam and a consequence of this is the production of CO_2, which, while not the worst greenhouse gas, due to its quantity, purportedly has the largest effect on the environment. Two large fields have been created to cope with CO_2 generation: Carbon capture and Carbon storage. Any designs that can limit the production of CO_2 are favourable not only environmentally, but also have the added benefit of a supply of carbon in a more useful form than CO_2. In today's world and in the context of being on the top of a bitumen formation, the most useful form of carbon is that of hydrocarbons.

Fischer—Tropsch is a very flexible process which produces hydrocarbons from any type of carbonaceous material. Fischer—Tropsch and the bitumen industry both have in common the end goal of hydrocarbon production. It is actually quite natural for the two to be paired together. Since the development of SAGD, a lot of research has gone into using solvents with steam to heat and extract the bitumen.[3][4] The natural gas traditionally used as fuel for heat generation by OTSG can be used instead by Fischer—Tropsch to produce steam, offgas as fuel for a smaller OTSG unit, and hydrocarbon liquids. The final hydrocarbon products of Fischer—Tropsch liquids are final products themselves, however a portion can be used directly in the SAGD production of bitumen as solvents, and also as diluent for the transportation of the bitumen once it has been brought to the surface and separated from the produced water.

The generation of the syngas used by the Fischer—Tropsch reactor typically leaves the reformer at approximately 1050 °C, and is required to be cooled prior to entering the Fischer—Tropsch reactor. The heat that is necessary to be removed to lower the temperature of the syngas to the Fischer—Tropsch reactor inlet temperature is recoverable as steam. The exothermic

Fischer—Tropsch synthesis is kept at a relatively constant temperature by transferring the reaction heat to boiler water and generating steam. Both the syngas cooling, and Fischer—Tropsch synthesis, generate steam that can be used by SAGD.

The light gaseous hydrocarbon Fischer—Tropsch products as well as unconverted syngas can be sent to an OTSG as fuel gas feed for final combustion and steam generation. In order for Fischer—Tropsch synthesis to produce the high pressure steam (>10 MPa) necessary for a cold reservoir it must be run at high temperature, which has an effect on the product distribution. When run at high temperatures the final products inevitably contain a larger amount of methane and lighter gaseous products.

In the following, the Fischer—Tropsch reactor model selected uses cobalt catalyst. There are consequences, both good and bad to this selection. Cobalt catalysts are used industrially for converting natural gas to liquids. However, synthesis with cobalt catalysts is done below temperatures of 230 °C. Cooling for this temperature can produce steam at a maximum pressure of 2.3 MPa. By running at a slightly elevated temperature of ~240 °C, steam can be generated at 3 MPa, which is sufficient for heating a reservoir when it is already hot, and not far outside typical reactor operating temperatures. In the case of producing high pressure steam as is needed for the initial start-up of a SAGD borehole, steam pressure must be greater than 10 MPa, which requires the cobalt catalyst to be operated at temperatures higher than 320 °C. At these temperatures cobalt catalysts produce high amounts of methane and are not viable for producing liquid hydrocarbons. The consequence of running cobalt catalysts at a very high temperature is that much of the syngas energy in converting natural gas to syngas is undone and wasted. In a realistic setting where hydrocarbons were the desired product, the use of cobalt catalysts above 230 °C would never occur. At elevated temperatures the levels of methanation makes the process

unrealistic. That said, the goal is not to make liquid hydrocarbons, but to make steam, and have the benefit of liquid hydrocarbons, without as high a regard for the product selectivity as would be the case in a refinery.

Another issue in using cobalt catalysts at elevated temperature is that since it is not realistic and not done in industry, the literature cited by VMGSim for kinetics, contains kinetics for cobalt catalysts that only apply to the low pressure case (i.e., the kinetics were taken from experiments at low temperature; Bartholomew and Farrauto (2006), and Steynberg and Dry (2004)). Therefore, any outlet compositions for the high pressure case in which cobalt is run at over 320 °C, cannot be trusted and would require experimental verification. This is not as large of a weakness as it may seem. While the actual results may not be quantitatively true for the high temperature case, insight can still be gained into the possibilities of using Fischer—Tropsch synthesis for SAGD steam production. For instance, should the outlet composition have a very high percentage of methane for the high temperature case, while the number will be dubious to say the least, that number can still be used to evaluate the process; i.e., if a Fischer—Tropsch synthesis reactor produced as exorbitantly high of an amount of methane as the simulation predicted, what effect will this have on the scenario, will it still be viable? For this reason the simulation is still very useful. A quantitative discussion can take place based on results that are likely to be only qualitatively correct.

Design Basis

The metric used to evaluate the proposed pairing of Fischer—Tropsch technology with steam generation for SAGD consists of a mass and energy balance which considers a base case OTSG developed by Canada's Oil Sands Innovation Alliance (COSIA) against that of steam being generated in tandem with Fischer—Tropsch technology. Reservoirs initially are cold and require

high pressure steam in the range of 10-15 MPa to heat up the formation and to get the bitumen flowing. Once heated, lower pressure steam in the range of 1.5 – 5 MPa is used to continue production. Two scenarios were investigated for each design basis: a low pressure steam (3 MPa) case as well as a high pressure steam (13 MPa) case since the operation must be capable of producing for both cold and hot reservoirs. The pre-cleaned natural gas composition is given in Table 3.1. The base case provided by COSIA for OTSG is given as follows:

- OTSG produces 1600 GJ/h lower heating value (LHV) of combined heat input with radiation losses of 32 GJ/h and stack losses of 100 GJ/h.
- By producing 1600 GJ/h (LHV) of combined heat input, the SAGD process produces 33,000 barrels of bitumen per day.
- Has steam quality of 75% or higher.
- Has a reservoir pressure range of (1.5 to 5 MPa (gauge)) when the reservoir is hot, and (10-15 MPa (gauge)) when the reservoir is cold.
- CO_2 production is 2195 Mt/day (67.3 kg CO_2/ bbl. bitumen) from direct combustion and 328 Mt/day (10.2 kg CO_2/bbl. bitumen) from indirect sources such as powering pumps from sources that produce CO_2.

Table 3.1 Natural gas composition

Property	Value
Lower heating value ($MJ \cdot kg^{-1}$)	47.7
Higher heating value ($MJ \cdot kg^{-1}$)	52.9
Composition (mol %) [a]	
methane	95.0
ethane	0.5
carbon dioxide	1.5
nitrogen	3.0

[a] Average molar mass of 0.01746 $kg \cdot mol^{-1}$ and normal gas density of 0.754 $kg \cdot m^{-3}$.

Both cases were then scaled to 17,000 GJ/day of energy production as this was viewed as a more feasible scale for possible implementation by COSIA. The objective of this study was to see if SAGD production could benefit from the inclusion of Fischer—Tropsch technology (Figure 3.1). The main goal was to see if the CO_2 footprint could be reduced; however there are also the benefits of producing solvents for steam, diluent for bitumen transportation, and hydrocarbon products.

Figure 3.1 Block diagram of VMGSim simulations steps and products.

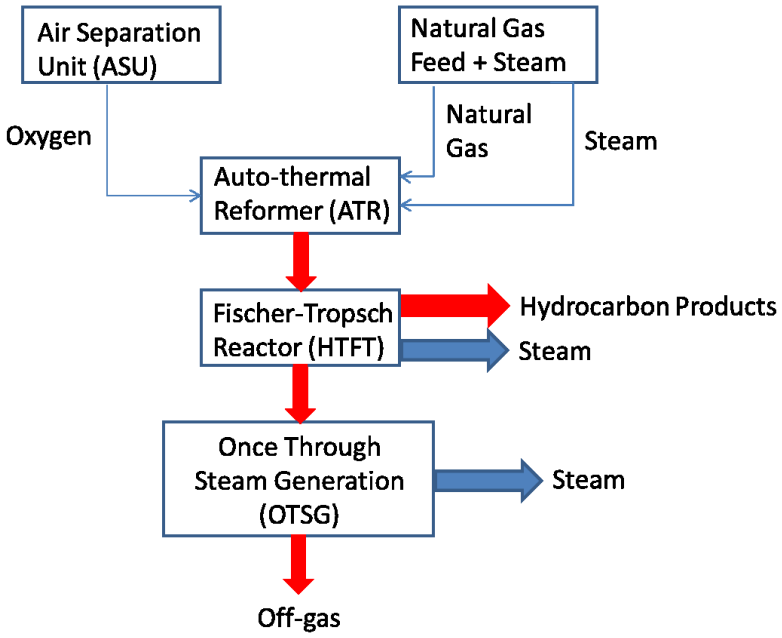

Modelling the Fischer—Tropsch gas loop.

There are two industrially relevant choices for the type of Fischer—Tropsch reactor to use: iron or cobalt based catalyst. For this assessment cobalt catalysts were used in the Fischer—Tropsch reactor although in practice cobalt catalyst cannot be used at such high temperatures unless methanation is the intended reaction route. The industrial thermodynamic process simulator VMGSim was used to model the air separation, syngas generation, and Fischer—Tropsch reactor blocks (Figure 3.1). The OTSG was calculated manually outside of the simulation using the details of the base case scenario. Given that the components are all typical of the oil and gas industry, the Advanced Peng—Robinson Natural Gas equation of state was used as the thermodynamic model. The "advanced" portion comes from VMGSim modifying the original Peng—Robinson according to the Mathias—Copeman adjustment, providing volume translation correction for phase densities and special handling of water and hydrogen. The natural gas portion comes from VMGSim in house improvements to the Advanced Peng—Robinson to make it more suitable for relatively weak polar components often found in natural gas mixtures such as acid gases (i.e., H_2S and CO_2).

Simulation assumptions are as following:

- No piping heat losses.
- 100 kPa pressure drop across reactors.[5]
- 50 kPa pressure drop across heat exchangers and boilers for steam generation.[5]
- 80 % adiabatic efficiency in the centrifugal Fischer—Tropsch compressor.
- 80 % adiabatic efficiency in the multi-stage centrifugal oxygen compressor.

- Combustion chamber of the syngas auto-thermal reformer (ATR) was modelled as a conversion reactor; the reformer bed was modelled as a Gibbs free energy calculation.
- Steam/carbon inlet ratio of 0.60 to the ATR.[6]
- Oxygen/carbon inlet ration of 0.55 to the ATR.[6]
- Fischer—Tropsch compressor outlet temperatures cannot exceed 200 °C.[5]
- Oxygen compressor outlet temperature could not exceed 170°C.[7] Four stages were used at a compression ratio of 2.5 per stage.

Figure 3.1 (above) shows the straight forward methodology used to calculate the steam and CO_2 contribution of Fischer—Tropsch technology paired with OTSG. The simulation was run to calculate the material balances of the ASU, ATR and Fischer—Tropsch reactor blocks, and then the resulting offgas from the Fischer—Tropsch reactor was used as fuel gas in an OTSG according to the specifications above to further generate steam. VMGSim was used for the energy balance on the ATR and Fischer—Tropsch reactor, pumps, heat exchangers and Fischer—Tropsch recycle compressor however literature was consulted for the ASU energy requirements since it is a highly integrated and specialised field, as well as the necessary oxygen compression. Data from COSIA was used for energy requirements of the OTSG. Once complete, the results were scaled to meet the 17,000 GJ/day specifications.

Air-Separation Unit

For the purpose of mass balance requirements VMGSim was used to simulate the ASU. In reality ASU's are highly integrated and efficient units that are a specialty in themselves so for the purpose of energy balance requirements (i.e., power consumption), literature was consulted and a value of 0.35 kWh/m^3 O_2[8] at a pressure of 1 atm and 99.5% oxygen purity was used. A compressor to pressurize the oxygen to ATR inlet conditions was calculated separately.

According to Gunardson, centrifugal compressors are used for compressing the low pressure oxygen to reformer pressures, although to get to high pressures requires alternating with reciprocal compressors.[9]

Auto-thermal Reformer

The ATR simulation was done in two parts. First the hydrocarbons were combusted in a reaction chamber with oxygen, in this case the highly exothermic methane and ethane combustion reactions according to:

$$CH_4 + 1.5\ O_2 \rightarrow CO + 2\ H_2O\ (g) \qquad \Delta\hat{H}_c^\circ = -519\ kJ/mol \qquad 3.1$$

$$C_2H_6 + 3.5\ O_2 \rightarrow 2\ CO_2 + 3\ H_2O\ (g) \qquad \Delta\hat{H}_c^\circ = -1428\ kJ/mol \qquad 3.2$$

An equilibrium bed using Gibbs free energy minimization then calculated equilibrium compositions in the second part of the reactor, the steam-methane-reforming (SMR) bed. If the ATR had been modelled as a conversion reactor the following equations describe the SMR bed of an ATR: exothermic water-gas-shift (equation 1.1 and 3.3) and endothermic SMR (equation 3.4) reactions:

$$CO + H_2O\ (g) \leftrightarrow CO_2 + H_2 \qquad \Delta\hat{H}_R^\circ = -41\ kJ/mol \qquad 3.3$$

$$CH_4 + H_2O\ (g) \leftrightarrow CO_2 + 3H_2 \qquad \Delta\hat{H}_R^\circ = 206\ kJ/mol \qquad 3.4$$

Fischer—Tropsch reactor

Steam production is required to be between 10-15 MPa (gauge) when the reservoir is cold, but only needs to be between 1.5-5 MPa (gauge) once the reservoir is heated. In both cases cobalt catalysts were used in the Fischer—Tropsch synthesis. Cobalt is used often with natural gas feeds because they produce syngas with high hydrogen yields, so the reactor does not need to be WGS active, as in the case for coal and other hydrogen deficient feeds. In those cases iron catalysts are used to promote WGS activity.

Since natural gas is the feed and will have a sufficient H_2/CO ratio leaving the reformer, cobalt catalysts are a natural fit for the low pressure scenario. Unfortunately, for the case which requires being run at high pressures, and as a result high temperatures, cobalt catalysts are not practical for Fischer—Tropsch synthesis as already mentioned above. Large amounts of methane are produced at elevated temperatures. There are therefore pro's and con's to cobalt. At start-up of a cold reservoir it would be at its poorest performance, producing large amounts of methane that would need to be sent to the OTSG. Performance would steadily get better as the steam pressures required were lowered and the reactor temperature could also be lowered.

VMGSim offers a reactor specifically for Fischer—Tropsch synthesis, basing its kinetics on published data from Bartholomew and Farrauto (2006), and Steynberg and Dry (2004). This was chosen because it allowed the simulation of the entire gas loop, and the quick calculations of thermodynamic properties by an equation of state gave useful insight into the duty requirements and practicality of using Fischer—Tropsch technology to produce steam for SAGD.

Results and Discussion

A brief explanation will detail the methodology employed when using Fischer—Tropsch technology with OTSG, and then mass and energy balances will be given and discussed. In OTSG natural gas is combusted and the heat is used to produce steam at the required pressure and this generally has a thermal efficiency of 91.5% as calculated from the COSIA energy balance. The losses are due to stack and line losses. In using Fischer—Tropsch technology, the natural gas is instead reformed to make syngas ($CO + H_2$ rather than $CO_2 + H_2O$ as in combustion), which is then cooled to the Fischer—Tropsch reactors inlet temperature through steam generation. The Fischer—Tropsch synthesis is kept near isothermal by generating steam with the exothermic heat of reaction. The temperature of the reactor determines the maximum

pressure that the steam can be, or in this case, the pressure of required steam determines the temperature that the reactor must be run.

After the reactor, the products are cooled to condense out the hydrocarbon products and water, and more steam is generated. The light hydrocarbons and non-condensables remain in the vapor phase, and after being partly recycled to increase the hydrocarbon yield in the reactor, the tail gas is sent as fuel gas to the OTSG. The tail gas employed as fuel gas has a significantly lower LHV than natural gas (Table 3.1 and Table 3.2). The OTSG combusts the fuel gas producing the final amount of steam for SAGD bitumen recovery.

In the high pressure steam scenario where the Fischer—Tropsch reactor is run at high temperature there was a significant amount of methane produced (~40 mol %). High amounts of methane are to be expected, however the number cannot be quantitatively trusted since the temperature is outside of the simulator's kinetic models temperature range. As a result of the high methane production, the amount of steam generated by the OTSG is twice what is generated by the Fischer—Tropsch gas loop. In the case of the low pressure steam production significantly more liquid hydrocarbons are formed and much less methane (~7 mol %). The low pressure (and subsequently lower temperature) Fischer—Tropsch gas loop produced the same amount of steam as the OTSG, and also produced twice as much liquid hydrocarbon product as the high pressure case.

Both scenarios investigated have simple mass balances shown below in (Figures 3.2 and 3.3) as well as energy balances provided in Table 3.2 and 3.3. Figure 3.1 above shows the block diagram step approach to calculating steam generation for the Fischer—Tropsch process. From Table 3.4 the pros and cons of the two methods in comparison with the standard base case OTSG case can be evaluated.

Figure 3.2 Mass balance for high pressure steam production.

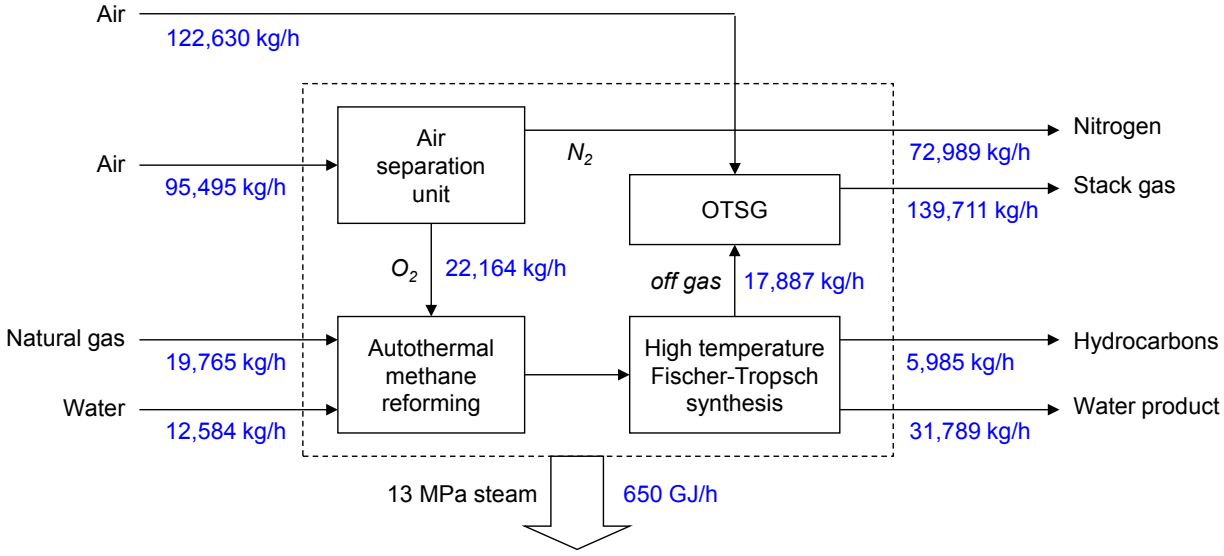

Table 3.2 Energy balance for high pressure steam production

Feed Stream Summary Stream name	Flowrate (kg/h)	LHV (MJ/kg)	LHV (MW)	MJ/bbl. FT Oil[a]
Natural Gas	19,765	48	262	17831
Oxygen	22,164	0	0	0
Water	14,644	0	0	0
Gas Stream				
Off gas	17,887	21	105	7147
Liquid Stream				
Hydrocarbons	5,985	41	69	4691
Thermal Efficiency	LHV (MW)	%		
Natural gas	261.9	100		
Hydrocarbons	68.9	26.3		
OTSG Steam Export	96.0	36.7		
FT Steam Export	45.1	17.2		
FT Utilities	-21.8	-8.3		
OTSG Utilities	-6.1	-2.3		
Total	**188.2**	**69.5**		

[a]A density of 715 kg/m^3 was calculated by VMGSim for Fischer—Tropsch oil.

Figure 3.3 Mass balance for low pressure steam production.

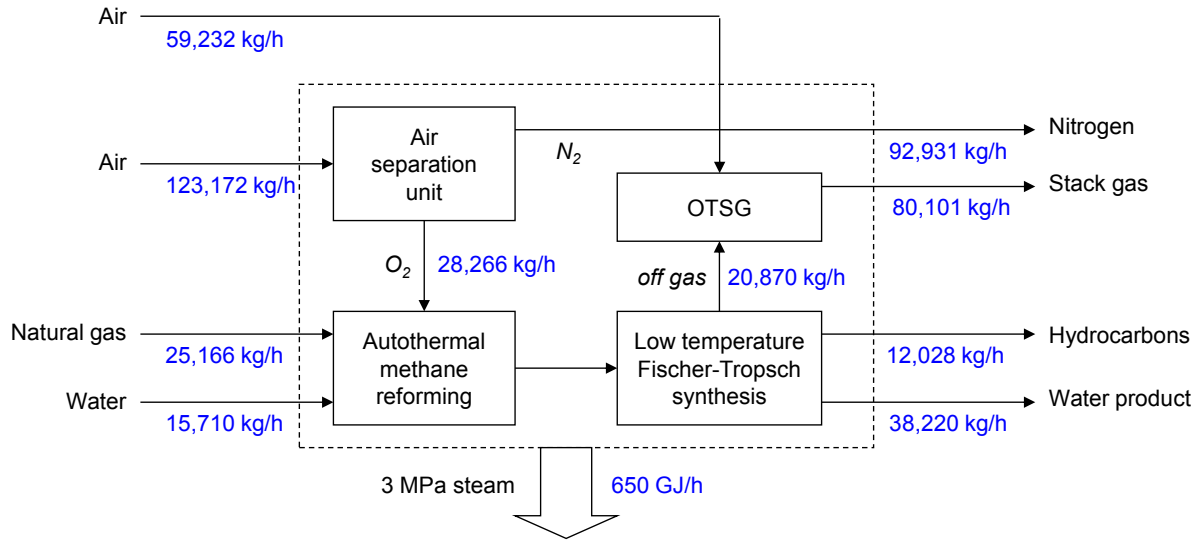

Table 3.3: Energy balance for low pressure steam production

Feed Stream Summary Stream name	Flowrate (kg/h)	LHV (MJ/kg)	LHV (MW)	MJ/ bbl. FT oil[a]
Natural Gas	25,166	48	333	11397
Oxygen	28,266	0	0	0
Water	15,710	0	0	0
Gas Stream				
Off gas	20,870	15	89	3036
Liquid Stream				
Hydrocarbons	12,028	43	144	4915
Thermal Efficiency	LHV MW	%		
Natural gas	333.4	100		
Hydrocarbons	143.8	43.1		
OTSG Steam Export	81.3	24.4		
FT Steam Export	80.5	24.1		
FT Utilities	-27.5	-8.2		
OTSG Utilities	-4.6	-1.4		
Total	**273.5**	**82.0**		

[a]A density of 715 kg/m^3 was calculated by VMGSim for Fischer—Tropsch oil.

The thermal efficiencies for both cases are given in Tables 3.2 and 3.3. Thermal efficiencies were 69.5 % and 82.0 % for high and low pressure steam production respectively. They are much higher than is typically found in natural gas conversion processes. Steynberg and Nel give a range of 60-66 % as being normal for a natural gas conversion process.[12] Thermal efficiency

was calculated as being the amount of energy in the natural gas feed compared to the amount of energy in the hydrocarbon products as well as all sources of steam, since they are final products. The energy in the natural gas feed and hydrocarbon products are their respective lower heating values, and the energy in the steam is the amount of energy added to the boiler water to promote the phase change into steam.

The off gas stream is sent to the OTSG and converted to steam. The high thermal efficiency is due to two things unique to this process: steam is a final product, so it is not being used to produce power and losing efficiency due to conversion of steam energy to electricity or work, and the off gas which is being used to produce steam as a final product in the OTSG is producing steam with a thermal efficiency of 91.5 %. Because steam is a desired final product and not an intermediate stream that eventually gets converted to a different form of energy or work at a loss, a larger portion of the thermal energy from combustion of natural gas is retained.

Using Fischer—Tropsch technology with OTSG immediately decreased the amount of CO_2 exiting the process per barrel of combined Fischer—Tropsch synthesis oil and bitumen via direct combustion by a half or more. Generating low pressure steam has a much better carbon efficiency; however a process must be capable of starting with a cold reservoir and gradually achieving equilibrium at low pressure. The amount of CO_2 produced by the Fischer—Tropsch process per barrel of combined bitumen and oil produced is increased by approximately 30 % when steam is required at high pressure (Table 3.3).

Steam is required to be at high pressures at the start of SAGD when the reservoir is cold. In this case using Fischer—Tropsch technology with OTSG generated the same amount of CO_2 per barrel of combined bitumen and oil (the base case is only bitumen) as the base case OTSG, but the Fischer—Tropsch synthesis liquid hydrocarbon yield when combined with the bitumen

recovery increased total SAGD hydrocarbon yield by 8.5%. There is also the convenient benefit of having diluent for bitumen transport as well as light hydrocarbons for solvent co-injection if the SAGD site is using that method.[11]

As the reservoir is heated the pressure requirements drops continuously to reach 1-5 MPa (gauge) and the reactor can correspondingly be run at lowering temperatures. In the low pressure steam case there still remains the added benefit of having diluent and solvent available, but now the major benefits are a reduction in CO_2 per barrel of combined oil and bitumen by 29.0 % and an increase in SAGD combined bitumen and Fischer—Tropsch synthesis liquid products yield of 17.2 %. These results are significant as they represent an increase in production as well as an increase in carbon efficiency.

Table 3.4 Analysis of the CO_2 footprint of 17,000 GJ/day OTSG steam production for SAGD[a].

Description	Base case OTSG	Proposal (Low Pressure)	Proposal (High Pressure)
Natural gas feed (kg/h)	14893	25166	19765
CO_2 emissions (kg/h)	47153	39225	51236
Direct from OTSG	40957	11247	24129
Indirect from OTSG[b]	6196	1701	3650
Direct from synthesis process	0	5322	6813
Indirect from synthesis[b] process	0	20954	16644
Oil production (bbl./h)	609	714	661
from SAGD	609	609	609
from synthesis process	0	105	53
kg CO_2/bbl. oil production (Direct)[c]	**67.3**	**23.2**	**46.8**
kg CO_2/bbl. oil production (Indirect)[d]	**10.2**	**31.7**	**30.7**
kg CO_2/bbl. oil production (Total)	**77.5**	**54.9**	**77.5**

[a] Based on the data provided, the thermal efficiency for OSTG energy transfer to steam is 91.8 % and 17,000 GJ/day OTSG steam production will yield around 14,600 bbl./day bitumen. [b] Based on 763 kg CO_2/MW-hr.[c] Direct means CO_2 is produced from combustion.[d] Indirect means CO_2 is produced via power use for units i.e., compressors etc.

The energy requirements for the Fischer—Tropsch gas loop are provided below in Table 3.4. Overall, the power consumption for utilities is highest for the low pressure case, but more

hydrocarbons are produced and less CO_2 per barrel of product, which more than balances the extra utility cost in favor of the low pressure case. Once the reservoir is heated the necessary steam pressure would steadily decline, becoming continuously more profitable for production with the greater liquid hydrocarbon yield. The CO_2 emissions would also be highest at the start-up of a cold reservoir and then steadily decline.

Table 3.5 Fischer—Tropsch utility balance for low and high pressures.

	Low Pressure		High Pressure	
Duty	(MW)	(MJ/bbl. Oil)[a]	(MW)	(MJ/bbl. Oil)
Compressors				
Oxygen Compressor	3.25	16	2.55	14
FT Compressor	0.03	0	0.02	0
Heat Exchangers				
ATR Nat Gas Preheat	10.98	55	8.88	48
ATR Oxygen Preheat	3.19	16	2.50	14
Steam Preheat	2.99	15	2.35	13
Pumps				
Boiler Water	0.00	0	0.01	0
ASU				
Entire Unit	7.05	36	5.53	30
TOTAL	**27.51**	**139**	**21.85**	**119**

[a]A density of 715 kg/m^3 was assumed for Fischer-Tropsch oil.

It may at first seem puzzling that the high pressure case required less utility energy per barrel of combined oil and bitumen (Table 3.4). The high pressure case required less natural gas to meet the steam production requirements (Table 3.3). Accordingly, less oxygen needed to be compressed and preheated, less steam was preheated, and less natural gas was preheated. In the OTSG base case, even less natural gas than the high pressure case was required to meet the steam quota and less energy was required for utilities than either the low or high pressure case. The main reason for the energy differences lies in how the three scenarios utilized natural gas to get the necessary energy for steam generation. In the base case all of the steam came from the OTSG which got the heat for steam generation from Equation 3.5:

$$CH_4 + 2O_2 \rightarrow CO_2 + 2H_2O \qquad \Delta\widehat{H}_c^{\circ} = -802\ kJ/mol \qquad 3.5$$

Equation 3.5 provides more heat from combustion than the combination of Equations 1.2 and 3.1 to 3.5. Therefore the OTSG required less natural gas, and less utilities to produce steam. However, all of the CH_4 is converted to CO_2, which is not a useful form of carbon, so steam is generated but nothing else of use. In the Fischer—Tropsch gas loop cases as more energy is invested in utilities, substantially more carbon is made useful alongside the steam that is generated. Rather than getting steam from creating CO_2, the Fischer—Tropsch cases get the energy for steam, albeit less energy, from creating CO and in turn CH_2 (CH_2 is the basic monomer of Fischer—Tropsch synthesis polymers). CH_2 is a more useful form of carbon than CO_2.

Conclusion

In assessing the possible advantages of using Fischer—Tropsch technology to generate steam for SAGD bitumen recovery, two cases were compared with the traditional OTSG. The low pressure steam case represented how Fischer—Tropsch technology could contribute to an already heated reservoir, and the high pressure case represented what Fischer—Tropsch technology could contribute to a cold reservoir. Several things can be concluded from the results of this assessment:

a) The traditional OTSG case requires much less power consumption and is much simpler than either of the Fischer—Tropsch gas loop cases. However carbon leaves the process as CO_2 which is an undesirable and inconvenient form.

b) Pairing Fischer—Tropsch technology with OTSG increased the utility requirements of the process, generated the same amount of steam as the OTSG case, but reduced CO_2 emissions by also generating syncrude.

c) When the reservoir is hot and the steam requirements dictate that the Fischer—Tropsch reactor can be run at low temperature, a 29 % reduction in CO_2 produced per barrel of combined syncrude/bitumen is had as benefit to the pairing.

d) When the reservoir is cold and the steam requirements dictate that the Fischer—Tropsch reactor run at high temperature, the pairing breaks even, CO_2 emission wise, with the base case at a level of 40 mol % production of methane from the Fischer—Tropsch reactor outlet. Should more methanation occur, then at start-up of a cold reservoir the pairing would lose its CO_2 benefit until the steam requirements dropped to a temperature producing less than 40 mol % methane from the Fischer—Tropsch synthesis.

e) In both Fischer—Tropsch cases the increased yield of combined syncrude/ bitumen was significant, 8.5 % and 17.2 % increase for the high and low pressure cases respectively.

f) Fischer—Tropsch would remove the need for diluent and solvents to be transported to SAGD sites.

g) Despite Fischer—Tropsch technology integration with OTSG appearing to be an economical benefit through increased production of combined syncrude/ bitumen, the capital costs associated with Fischer—Tropsch have not been investigated, and they would be significant.

h) In order for Fischer—Tropsch technology to be used in a realistic manner with OTSG, it would need to be used on a small and portable scale. Fischer—Tropsch benefits from economy of scale, so the scale requirement, as well as being portable, poses large obstacles.

i) The production of much higher quality products by the Fischer—Tropsch gas loop than the bitumen which is recovered by SAGD operation would also create positive economic

incentive since the SAGD would be sending higher quality products to the downstream upgrading facilities.

References

(1) Butler, R.M. Thermal recovery of oil and bitumen; Prentice-Hall **1991**.
(2) Canadian Oil Sands Innovation Alliance, COSIA challenge: down hole steam generation, **2014**
(3) Gupta, S.C.; Gittins, S.D.; Field implementation of solvent aided process "waxy" mixtures. Paper 2002-299 presented at the Canadian International Conference, Calgary, Alberta, Canada, June 11-13, **2002**.
(4) Nasr, T.N.; Beaulieu, G.; Golbeck, H.; Heck, G. Novel expanding solvent-SAGD process "ES-SAGD". *Journal of Canadian Petroleum Technology* **2003**, *Vol. 42*, 13-16.
(5) Ulrich, G.D.; Vasudevan, P.T. *Chemical engineering: process design and economics a practical guide*, Process Publishing: Durham, New Hampshire, **2004**.
(6) Rostrup-Nielsen, J.; Christiansen, L. J., *Concepts in syngas manufacture*, Imperial College Press: London, **2011**.
(7) Asia Industrial Gases Association. Reciprocating compressors for oxygen service, code of Practice AIGA 048/08; AIGA: Singapore, **2008**.
(8) Häring, H-W(Ed). *Industrial Gases Processing;* Wiley-VCH: Germany, **2008**.
(9) Gunardson, H. H. (Ed.). *Industrial gases in petrochemical processing: chemical industries*. CRC Press, **1997**.
(10) Steynberg, A.P.; Nel, Herman G., Clean coal conversion options using Fischer—Tropsch technology. *Fuel* **2003**, *Vol. 83*, 765-770.
(11) Gray, M.R. *Upgrading oilsands bitumen and heavy oil;* University of Alberta Press: Edmonton, AB, **2015**, 241-245.

Chapter 4 – The potential role of water electrolysis in carbon producing gas loops

Introduction

Synthesis gas, which is a mixture of H_2 and CO, is the starting point for the synthesis of Fischer—Tropsch syncrude as well as the production of hydrogen. Syngas is industrially produced by natural gas reforming,[1] or gasification.[2] Syngas can also be produced by other means, such as by solar-driven thermochemical gasification,[3][4] or by electrochemical reactions by employing the reverse water gas shift (Equation 3.3) to generate syngas from H_2 and CO_2.

Water electrolysis accounts for about 5 % of global H_2 production.[5] Electrolysis of water is generally considered only when cheap electric power is available. Despite the apparent low carbon-footprint of H_2 production by water electrolysis using solar, wind or hydroelectric power, the process potentially violates three of the Green Chemistry principles: to prevent waste, increase of energy efficiency and maximize atom economy. Central to the potential violation of the aforementioned Green Chemistry principles is the wasteful co-production of O_2.

In this chapter it will be shown how water electrolysis can be incorporated into gas loop designs so that H_2 and O_2 both have value. Previous studies on the use of water electrolysis in gas loop designs explored mainly the combined use of biomass as a renewable energy source with water electrolysis to produce chemicals (methanol and hydrogen peroxide).[6-11] In this study the focus is on gas loop design and the more general benefit that can be derived form combining water electrolysis with synthesis gas generation.

Three industrially relevant cases are considered to illustrate the potential benefits.

First, the gas loop design for the production of only H_2, as is typical for petroleum refining applications. Second, the gas loop design for cobalt-based Fischer—Tropsch synthesis, where the consumption ratio of H_2:CO ≈ 2 and CO_2 should ideally be excluded from the synthesis gas feed. Third, the gas loop design for the production of synthesis gas for iron-based Fischer—Tropsch synthesis. Iron-based Fischer—Tropsch catalysts catalyse the water gas shift reaction and are capable of performing Fischer—Tropsch synthesis using a wide range of synthesis gas compositions.

Process concept

The incorporation of water electrolysis into a gas loop for the generation of synthesis gas is shown (Figure 4.1).

The first major benefit of water electrolysis in the gas loop design (Figure 4.1) is the production of O_2, which is employed as an oxidant for synthesis gas generation. Producing O_2 is particularly useful when the gas reformer or gasifier requires O_2 as process feed, e.g. autothermal reforming as opposed to steam reforming of natural gas. In such cases the O_2 from water electrolysis replaces purified O_2 obtained from a cryogenic air separation unit (ASU).

A related benefit is that the O_2 from water electrolysis does not contain Ar as an impurity. Purified O_2 from an ASU usually contains Ar, typically 0.5 % Ar or more, because it is difficult to separate Ar from O_2 by distillation.[5] The normal boiling point of Ar (–185.9 °C) is close to that of O_2 (–183.0 °C). Whenever synthesis gas is employed in a gas loop with a recycle, such as the gas loop for Fischer—Tropsch synthesis, the purity of O_2 affects the purge loss. The extent of purge loss is determined by the build-up of difficult to separate

material in the recycle, such as Ar;[12] hence the benefit of having an Ar-free O_2 feed from water electrolysis.

Fig. 4.1 Integration of water electrolysis with a gas loop design for synthesis gas production from a carbon-based feed.

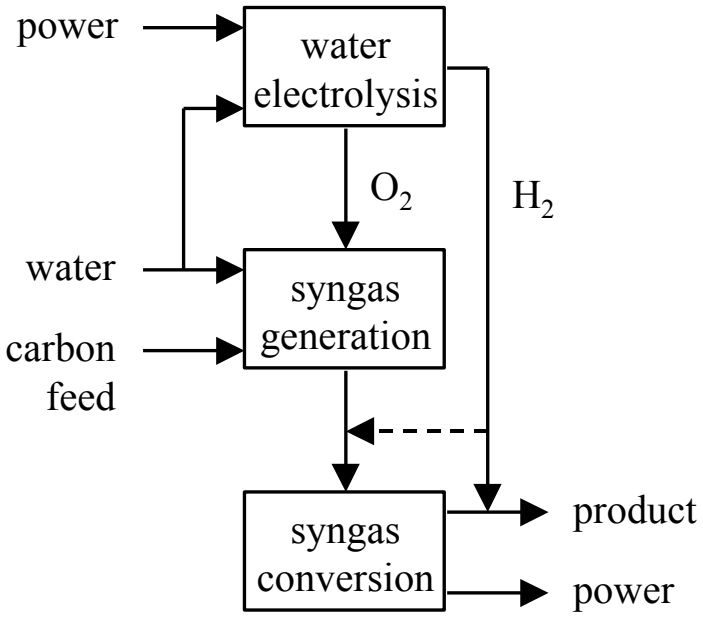

Another advantage is that water electrolysis can be performed at high pressure, so that the O_2 is produced at process pressure. This avoids oxidant compression, which is necessary when O_2 is produced by cryogenic air separation. Not only does it avoid the use of mechanical equipment with moving parts, but it also reduces the utility footprint (energy and cooling water use) associated with an ASU and O_2 compression. To put this into perspective, when evaporative cooling is employed the water consumption associated with the ASU and O_2 compression in Fischer—Tropsch facilities amounts to 2 kg water consumed per 1 kg oil produced.[13]

Collectively, the reduced utility footprint that results from incorporating water electrolysis in an autothermal reformer based gas loop, might enable realistic small-scale designs for gas-to-liquids facilities.[14]

The second major benefit of water electrolysis in the gas loop design (Figure 4.1) is the production of H_2. When the objective of the process is to produce hydrogen specifically, then the H_2 from water electrolysis contributes directly to the production of the final product.

A related advantage is that the H_2 obtained from water electrolysis is already a high purity H_2 stream. When H_2 is produced from synthesis gas, the H_2 is purified by pressure swing adsorption (PSA). Although very high purity H_2 can be produced by PSA, recovery is in the range 70-90 % depending on design and operation.[5] Obtaining high purity H_2 directly from water electrolysis is therefore more valuable than that H_2 in synthesis gas that must still be purified for applications requiring pure H_2. Even in applications that involve syngas-to-liquids conversion, having a pure H_2 stream available is valuable when downstream hydroprocessing is performed, or when the H_2:CO ratio in the gas loop must be regulated.

Design basis

The objective of this work is to demonstrate how gas loop designs can benefit from incorporating water electrolysis. Designs were not individually optimised. Throughout the discussion the main design assumptions will be indicated.

Syngas generation

Pre-cleaned natural gas (Table 3.1) was selected as carbon feed and syngas generation is accomplished by natural gas reforming.

In all instances the base-case gas loop designs employed an autothermal reformer (ATR) in combination with an ASU to supply purified O_2. A discussion on the relative merits of selecting different reformer and oxidant types can be found in the literature.[1] To keep the analysis uncomplicated, it was further decided to employ excess steam to produce electric power and to use electric power as energy input for the ASU. Another option for the use of excess steam could be to use the steam in conjunction with OTSG as was done in Chapter 3.

The ASU is capable of producing O_2 at a purity of 99.5 %. The air must be preconditioned to remove water vapor and CO_2 before the ASU. For material balance purposes it was assumed that the air was preconditioned. The energy required to produce purified, but unpressurised O_2, is 0.89 $MJ \cdot kg^{-1}$ O_2.[5]

The ATR operation was fixed at an O_2:C ratio of 0.59 for hydrogen production and 0.55 for Fischer—Tropsch synthesis; the typical range is 0.35 to 0.6.[1] One of the advantages of ATR is the high methane conversion. The methane content in the dry syngas gas is usually 1 mol % or less.[1] To keep the basis constant, the methane conversion was fixed such that at the ATR outlet it was between 0.5 % to 1.0 % of the dry syngas composition. The ATR was modelled using a Gibbs minimization reactor. While exit temperatures for ATRs are widely available in literature, the presence of recycle streams inevitably affects the reactions inside the ATR and consequently the temperature and composition of the ATR outlet stream, which influences the syngas composition due to a change in WGS equilibrium. Therefore it was not realistic to assume a set outlet temperature for all designs, and instead modelling was done using the relatively simple but reliable Gibbs minimization technique[15][16] with published correlations for the heats of formation of the components[1]. Outlet temperatures ranged from 970 °C to 1150 °C depending on the amount and composition of recycle. The gas phase in

ATRs is typically very ideally behaved at high temperatures, however the Peng—Robinson equation of state was used to provide additional reliability.[15]

Water gas shift conversion

The final syngas composition obtained by water gas shift conversion was calculated based on equilibrium conversion. In all cases the temperature of water gas shift conversion was selected to ensures operation above the dewpoint of water at the gas loop pressures.[17]

CO_2 removal

There is a variety of methods currently practiced by industry for the removal of CO_2. These include chemical absorption such as by amines or alkali salts, physical absorption such as by Selexol or Rectisol, and membrane or cryogenic separation.[18-20] The Benfield chemical absorption process using hot potassium carbonate (alkali salts) is well suited for removing syngas since a large bulk is required to be removed, but not down to very low part-per-million levels. There are also over 600 Benfield units currently in operation around the world for syngas cleaning of CO_2.[20] Energy requirements are available from literature for the Benfield process.[20] For the basic Benfield process without any heat conservation features, the net heat duty is typically around 0.49 to 0.54 MJ/kg CO_2 (45,000-50,000 Btu/lbmol CO_2). Benfield has a process known as the LoHeat option which can reduce energy requirements to 0.33 to 0.38 MJ/kg CO_2 (30,000 to 35,000 Btu/ lbmol CO_2), a hybrid LoHeat option with duty requirements of 0.27 to 0.30 MJ/kg CO_2 (25,000 to 28,000 Btu/ lbmol CO_2), and an enhanced hybrid LoHeat option with duties of 0.20 to 0.27 MJ/kg CO_2 (18,000 to 25,000 Btu/ lbmol CO_2).[20] For comparison purposes between the WEU and ASU gas loops, the lowest value of the basic Benfield process without heat conservation was chosen (0.49 MJ/kg CO_2).

Gas loop purging

The inert content of the recycle loops were not optimized on a case-by-case basis. The purging rate was adjusted to ensure that the inert content remained equal to 15 mol % at the Fischer—Tropsch reactor inlet for all Fischer—Tropsch gas loop designs. This represented a trade-off between gas conservation, energy consumption and equipment sizing.

Water electrolysis unit

The power consumption for the water electrolysis unit was taken from literature.[10] A value of 21.1 MJ/kg O_2 was used. This corresponds to a water electrolysis unit working at ~70 % efficiency. This falls in the efficiency range currently employed by alkaline electrolysers.

Fischer—Tropsch synthesis

The Fischer—Tropsch hydrocarbon products were lumped into three categories as given in Table 4.1 for simplification. Published literature for thermodynamic correlations such as heats of formation and heat capacities are limited for hydrocarbons larger than heptane. By simplifying, published temperature dependant correlations were able to be used and group contribution methods were avoided.

Table 4.1 Fischer—Tropsch product distribution

Product	Distribution (%)
CH_4	7.5
C_2 to C_5	15
C_7 and heavier	77.5

The same distribution was used for each case to have consistency.

Design considerations

In order to compare typical gas loops using air separation units with gas loops using water electrolysis units, a design basis was set. Since the objective was to highlight strengths and weaknesses, the values used facilitate comparison and are representative of reality, rather than being specific to an industrial case study.

(a) Carbon feed: Natural gas from a lean natural gas source and that has a high heating value (Table 3.1).

(b) Capacity: The design is sized based on a production capacity of 100 $mol \cdot s^{-1}$ (0.2 $kg \cdot s^{-1}$) H_2, delivered as 99.9 % or higher purity H_2 at near ambient temperature and process pressure.

(c) Utilities: Cooling water is available at 20 °C and the maximum cooling water return temperature is 40 °C. Steam is available and can be produced from demineralized water, which is available.

(d) Centrifugal compressors were used with efficiencies of 80 %. Oxygen compressors had maximum outlet temperatures of 170 °C, otherwise temperatures were limited to a maximum of 200 °C.

(e) Centrifugal pumps were used with efficiencies of 60 %.

(f) Fischer—Tropsch inlet contained 15 mol % inerts.

(g) Fischer—Tropsch reactor conversion was set at 60 mol % CO.

(h) Gas loop designs were manipulated such that the stoichiometric ratios (Equations 1.3 and 1.4) were met at the Fischer—Tropsch reactor inlet.

Gas loop for hydrogen production

Base case (Case A)

The base case gas loop design for hydrogen production is shown in Fig. 4.2.

Natural gas (stream 1), steam (stream 2), purified O_2 (stream 3) are co-fed to the ATR. Since the objective was to produce H_2, the steam-to-carbon ratio was set at 2.5, which favoured production of a more H_2-rich syngas.

Fig. 4.2 Base case gas loop design for hydrogen production.

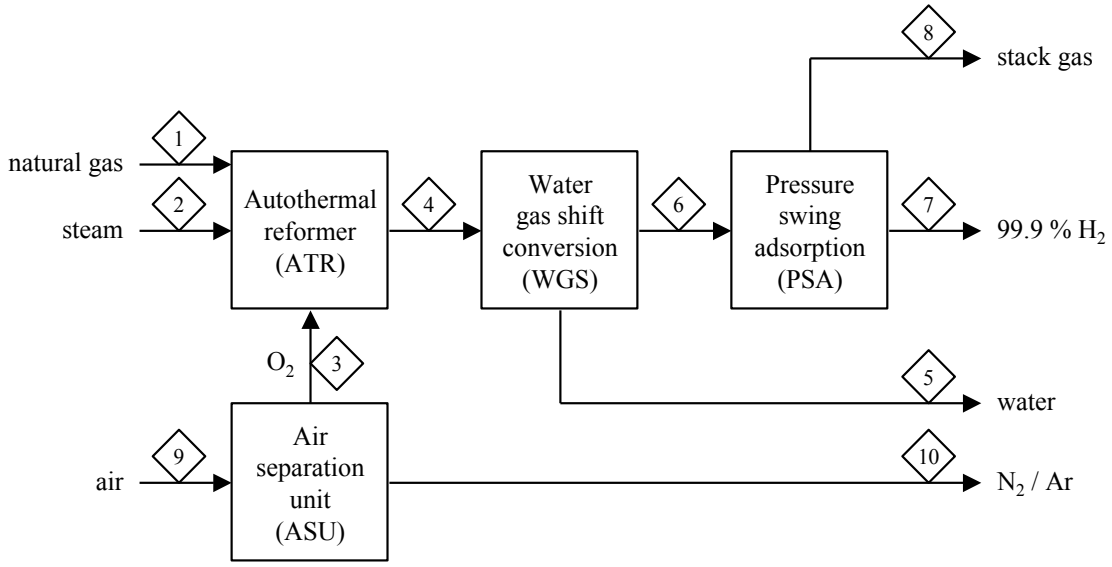

The raw syngas (stream 4) is converted over a water gas shift catalyst at ~220 °C to convert most of the CO with water to H_2 and CO_2. Unconverted water (stream 5) in the syngas is separated by condensation. The hydrogen-rich syngas (stream 6) is then purified through pressure swing adsorption to produce a pure H_2 product (stream 7) with 90 % recovery of hydrogen.[6] The low pressure tail gas from the PSA unit (stream 8) is CO_2-rich and is sent to the stack.

Due to the high methane conversion in the ATR and the CO_2-rich nature of the PSA tail gas, there is little incentive to change from an open gas loop design as shown, to a closed gas

loop with recycling of the PSA tail gas. The material balance for the base case is given below in Table 4.2. Only the main feed and product streams are listed.

Table 4.2 Material balance for base case H_2 production from syngas [a]

Description	ATR feed (1) to (3)	Water (5)	Pure H_2 (7)	Stack gas (8)
Total flow rate ($kg \cdot s^{-1}$)	15.39	4.92	1.00	9.47
Compound flow ($kg \cdot s^{-1}$)				
methane, CH_4	3.05	0	0	0.10
ethane, C_2H_6	0.30	0	0	0
carbon dioxide, CO_2	0.13	0	0	8.99
nitrogen, N_2	0.17	0	0	0.17
oxygen, O_2	4.03	0	0	0
argon, Ar	0.03	0	0	0.03
water, H_2O	7.69	4.92	0	0
carbon monoxide, CO	-	0	0	0.08
hydrogen, H_2	-	0	1.00	0.11

[a] Process flow diagram shown in Fig. 2.

Water electrolysis integration (Case B)

The integration of water electrolysis into the gas loop design (Figure 4.3) replaces the ASU as source of purified O_2, while at the same time being a source of pure H_2. With the exception of this change, the rest of the design is similar to that of the base case (Figure 4.2).

The water electrolysis unit takes water as feed (stream 1) and produces pure H_2 (stream 2) and pure O_2 (stream 3) as products.

The pure O_2 (stream 3) is used as co-feed with natural gas (stream 4) and steam (stream 5) to produce syngas in the ATR. The raw syngas (stream 6) from the ATR is converted over a water gas shift catalyst. Water (stream 7) is condensed and the H_2-rich gas (stream 8) is the feed for the PSA unit. In the PSA pure H_2 (stream 9) is produced, which is mixed with the pure H_2 from water electrolysis (stream 2) to produce the final pure H_2 product (stream 10).

The PSA tail gas (stream 11) is sent to the stack. For the same reasons as in the base case this is an open gas loop design.

Fig. 4.3 Water electrolysis integrated gas loop design for hydrogen production.

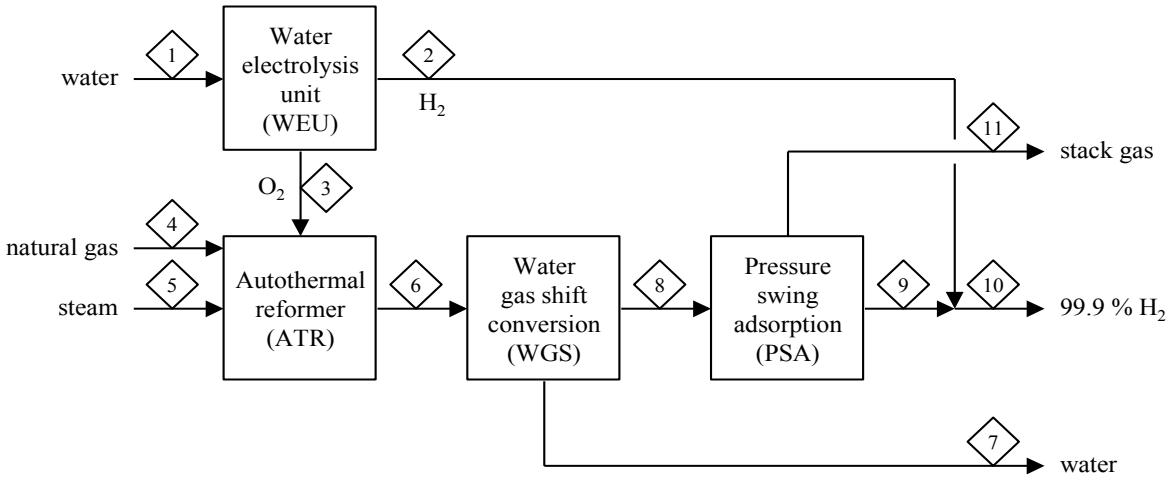

The material balance for the gas loop with integrated water electrolysis is given in Table 4.4. The flow rates were scaled to have the same H_2 production rate as the base case.

The relative contributions of water electrolysis and natural gas reforming to the production of H_2 is affected by the O_2:C ratio of the ATR. On the lower end, with an O_2:C = 0.35, the relative contribution of water electrolysis to H_2 production decreases to 20 %. On the higher end, with an O_2:C = 0.6, the relative contribution of water electrolysis to H_2 production is 34 %.

Table 4.3 Material balance for H_2 production from gas loop with water electrolysis integration [a]

Description	WEU feed (1)	ATR feed (3) to (5)	ex WGS (7) & (11)	Pure H_2 (10)
Total flow rate ($kg \cdot s^{-1}$)	3.01	10.19	9.53	1.00
Compound flow ($kg \cdot s^{-1}$)				
methane, CH_4	-	2.03	0.07	0
ethane, C_2H_6	-	0.20	0	0
carbon dioxide, CO_2	-	0.09	5.96	0
nitrogen, N_2	-	0.11	0.11	0
oxygen, O_2	-	2.67	0	0
water, H_2O	3.01	5.10	3.27	0
carbon monoxide, CO	-	-	0.05	0
hydrogen, H_2 (WEU)	-	-	0	0.34
hydrogen, H_2 (PSA)	-	-	0.07	0.66

Energy balances

The utilities required to power the hydrogen production gas loop as well as generate steam are shown below in Table 4.4. In the gas loop containing the WEU, ~34 mol % of the total hydrogen was generated by the WEU, resulting in less methane needing to be processed via the hydrogen gas loop. This is obvious from the large difference in high pressure (HP) steam produced by the base case. This led to the base case also creating more tail gas to be used as fuel gas for power generation, as well as more steam being generated from cooling the ATR outlet and WGS reactor. So while the WEU gas loop used less natural gas, it required more power for the WEU and didn't contribute as much steam for onsite power generation. This is further looked into in the discussion section where CO_2 emission is looked at closely.

Table 4.4 Utility requirements for hydrogen production.

	Case A Base Case	Case B Water electrolysis integration
	(MW)	(MW)
HP (70 bar) Saturated Steam Source		
Reformer outlet waste heat boiler	29	19
HP Superheated Steam Users		
HP steam turbine	34	23
MP (19 bar) Saturated steam source		
WGS Reactor cooling	23	15
MP saturated steam user		
MP steam turbine	26	17
Fuel gas source		
Tail gas LHV	239	159
Power Generation		
HP Steam Turbine	11	7
MP Steam Turbine	8	5
Fuel Gas Turbine	80	52
Electrical power users		
HP Boiler feed pump	0.1	0.1
WEU/ASU	4	56
Oxygen compressor	2	-
Fuel gas user		
HP saturated steam	6	4
MP saturated steam	0.1	2
ATR preheat	34	23
Without WEU		
Power Export	93	65
With WEU		
Power Import	-	8
Natural Gas for Power (kg/s)	-	0.5
Resulting CO_2 production (kg/s)	-	1.2

Cobalt based Fischer—Tropsch gas loop

Base case (Case C)

The base case gas loop design for Fischer—Tropsch syncrude production is shown in Figure 4.4.

Natural gas (stream 1), steam (stream 2), purified O_2 (stream 3) are co-fed to the ATR. Since the objective was to produce syncrude, the steam-to-carbon ratio was set at 2.5, which is a typical number for mature industrial ATRs used with Fischer—Tropsch . Newer ATRs can use ratios below 1. This leads to less hydrogen and a greater chance of carbon deposition so pre-reforming is typically applied before the ATR. In the case of using a steam-carbon ratio of 2.5 this was not necessary, and the additional hydrogen was favorable for both the base case and water electrolysis case. The use of a high steam-carbon ratio for the ATR feed does not have a negative impact on the environment assuming the process water is properly treated.

The raw syngas (stream 5) is sent to a water-gas-shift reactor. Because of the high H_2/CO ratio leaving the ATR either H_2 needed to be removed, which could be done with a PSA, or CO_2 needed to be added prior to the WGS. Conveniently cobalt-based Fischer—Tropsch reactors are not WGS active so it is necessary to remove CO_2 from the WGS outlet (stream 7) prior to the reactor (stream 8); CO_2 acts as an inert in the Fischer—Tropsch reactor, increasing its size and decreasing the partial pressure of H_2 and CO. The CO_2 removed was recycled back to the inlet of the WGS reactor (stream 6), thus providing the necessary CO_2 to get the syngas to a H_2/CO ratio of 2. At the inlet to the reactor CO_2 concentration was constrained to 0.5 mol % for both the base case and WEU case. While the H_2/CO ratio was high leaving the ATR, it was not so high as to make use of all of the CO_2 removed, resulting

in a CO_2 purge stream being required (stream 9). The WGS is run at 700 °C to facilitate reverse WGS reaction.

Conversion was set at 60 mol % of CO in the Fischer—Tropsch reactor at a temperature of 220 °C. Fischer—Tropsch products (stream 11) were cooled to 40 °C and syncrude (stream 12) and water (stream 13) were seperated. A portion of the syngas was recycled to the Fischer—Tropsch reactor (stream 10) and the rest was recycled to the ATR (stream 15) with a small portion purged (stream 16) to keep the inert concentration in the Fischer—Tropsch inlet at 15 mol %.

Figure 4.4 Cobalt Fischer—Tropsch synthesis with oxygen from ASU.

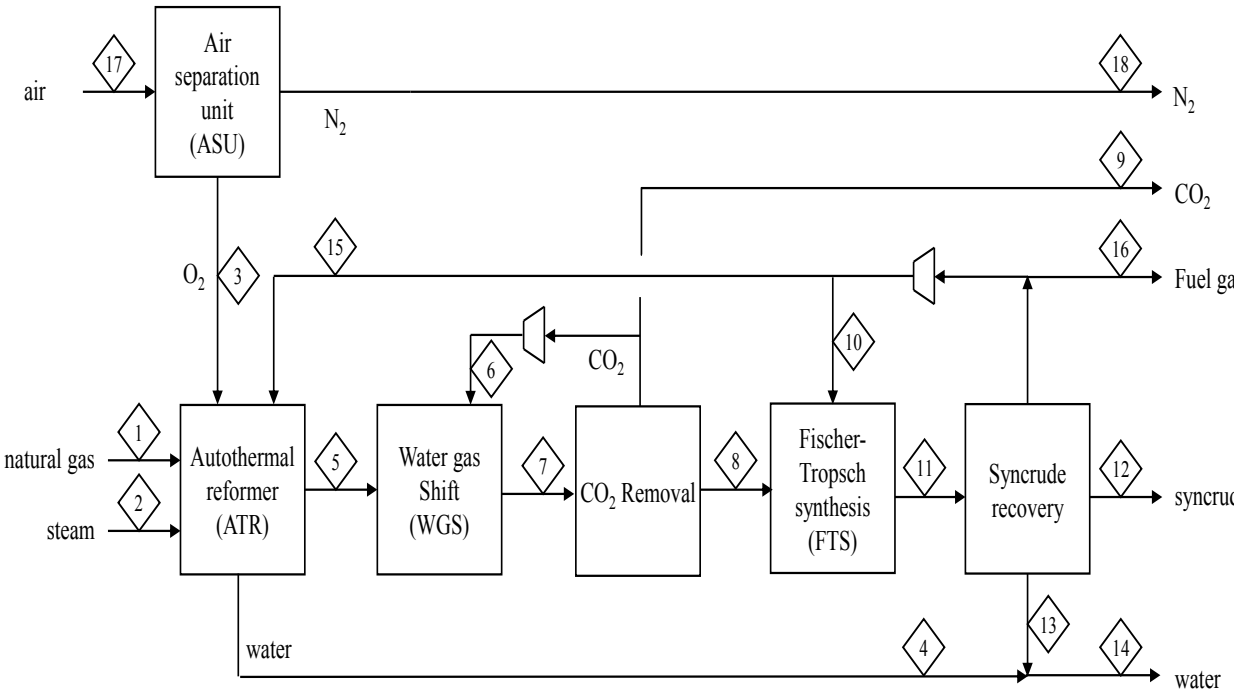

Table 4.5 Material balance for base case cobalt Fischer—Tropsch production from syngas.

Compound	ATR feed (1 to 3)	Water (14)	Syncrude (12)	Fuel gas & CO_2 purge (16) & (9)
Total flow rate (kg/s)	11.44	8.74	1.00	1.64
Composition (kg/s)				
methane (CH_4)	1.65	0	0	0.07
ethane (C_2H_6)	0.16	0	0	0.08
carbon dioxide (CO_2)	0.07	0	0	1.04
nitrogen (N_2)	0.09	0	0	0.09
oxygen (O_2)	2.65	0	0	0
argon (Ar)	0.017	0	0	0.017
water (H_2O)	6.79	8.74	0	0
carbon monoxide (CO)	-	0	0	0.31
hydrogen (H_2)	-	0	0	0.04
Syncrude (C_7+)	-	0	1.00	0

Water electrolysis integration (Case D)

The integration of water electrolysis into the gas loop design (Figure 4.5) replaces the ASU as source of purified O_2, while at the same time being a source of pure H_2. With the exception of this change, the rest of the design is similar to that of the base case (Figure 4.4).

The water electrolysis unit takes water as feed (stream 17) and produces pure H_2 (stream 6) and pure O_2 (stream 3) as products.

The pure O_2 (stream 3) is used as co-feed with natural gas (stream 1) and steam (stream 2) to produce syngas in the ATR. The raw syngas (stream 5) goes directly to the reverse WGS reactor where hydrogen (stream 6) is co-fed. As a result of the hydrogen stream the syngas is conditioned to the necessary H_2/CO ratio of 2 without the need of ejecting recycled CO_2 as in the base case. The WGS is run at 700 °C to facilitate the necessary reverse WGS reaction as in the base case. The WGS outlet (stream 8) has CO_2 removed such that the inlet of the

Fischer—Tropsch reactor contains 0.5 mol % CO_2, and is recycled (stream 7) to the inlet of the WGS unit.

Conversion is set at 60 mol % of CO in the Fischer—Tropsch reactor at 220 °C. Products from the reactor (stream 11) are cooled and the condensed syncrude (stream 12) and water (stream 13) are seperated. The unconverted syngas is recycled, partly to the Fischer—Tropsch reactor (stream 10) and the rest to the ATR (stream 15) with a small purge (stream 16) being removed to keep the inert concentration in the Fischer—Tropsch reactor inlet at 15 mol %.

Figure 4.5: Cobalt-based Fischer—Tropsch synthesis using water electrolysis.

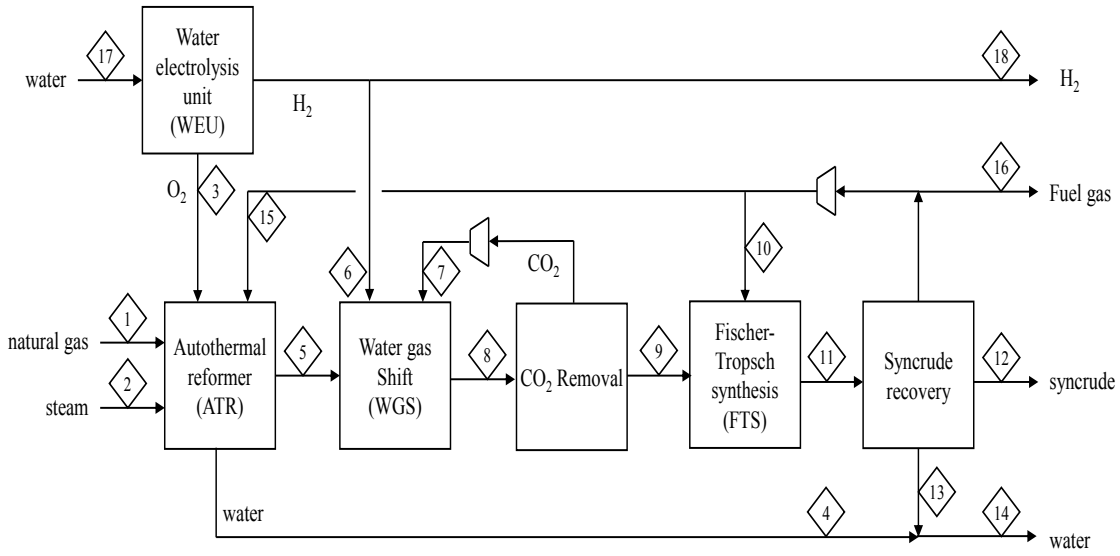

Table 4.6 Material balance for cobalt-based Fischer—Tropsch production from gas loop with water electrolysis integration.

Compound	ATR feed (1 to 3)	Hydrogen (6)	Water (14)	Syncrude (12)	Fuel gas (16)
Total flow rate (kg/s)	10.13	0.18	8.95	1.00	0.35
Composition (kg/s)					
methane (CH_4)	1.16	-	-	0	0.02
ethane (C_2H_6)	0.11	-	-	0	0.03
carbon dioxide (CO_2)	0.05	-	-	0	0.01
nitrogen (N_2)	0.06	-	-	0	0.06
oxygen (O_2)	2.46	-	-	0	0
water (H_2O)	6.29	-	8.95	0	0
carbon monoxide (CO)	-	-	-	0	0.19
hydrogen (H_2)	-	0.18	-	0	0.02
Syncrude (C_7+)	-	-	-	1.00	0

Energy Balance

Table 4.7 Utility balance on cobalt-based Fischer—Tropsch

	Case C Base case	Case D Water electrolysis integration
	(MW)	(MW)
HP (70 bar) Saturated Steam Source		
Reformer outlet waste heat boiler	42.3	32.0
MP (19 bar) Saturated Steam Source		
FT reactor cooling	21.1	21.8
HP Superheated Steam Users		
HP steam turbine	50.5	38.2
MP Superheated Steam User		
MP steam turbine	23.5	24.3
Fuel Gas source		
Tail Gas (LHV)	39.4	22.5
Excess H2 from WEU (LHV)	-	140.7
Power Generation		
HP Steam Turbine	15.8	11.9
MP Steam Turbine	7.4	7.6
Fuel Gas Turbine	-	56.3
Electrical power users		
CO2 Removal	0.5	0.8
CO2 recycle compressor	0.0001	0.003
External recycle compressor	0.04	0.1
Oxygen compressor	1.3	-
HP Boiler feed pump	0.2	0.1
MP Boiler feed pump	0.03	0.03
WEU/ASU	2.4	51.9
Fuel Gas user		
ATR preheat	27.9	13.9
MP saturated steam	2.4	2.5
HP saturated steam	8.2	6.2
Without WEU Power Export	27.6	74.8
With WEU Power Export	27.6	22.8

The importance of the utility requirements is looked at in detail in the discussion section further down. One interesting point worth noting is that the gas loop with the WEU was able to generate enough onsite power to supply the WEU provided some of the excess hydrogen from the WEU was used in a gas turbine to generate electricity.

Iron-based Fischer—Tropsch gas loop

Base Case (Case E)

The base case gas loop design for Fischer—Tropsch syncrude production is shown in Figure 4.6.

Natural gas (stream 1), steam (stream 2), purified O_2 (stream 3) are co-fed to the ATR. Since the objective was to produce syncrude, the steam-to-carbon ratio was set at 2.5 as explained above for the cobalt-based Fischer—Tropsch gas loop.

The raw syngas (stream 5) is sent directly to the Fischer—Tropsch reactor. While having a high stoichiometric ratio (Equation 1.4, $[H_2\text{-}CO_2]/[CO+CO_2]$), which is above 2, the iron catalysts used in the Fischer—Tropsch reactor are WGS active (Equation 1.2). With the aid of recycling CO_2 (stream 6) shifted the stoichiometric ratio to ~2, which is the usage ratio inside the Fischer—Tropsch reactor. A separate WGS unit was not necessary as in the case of the cobalt catalysts, which were not WGS active. The Fischer—Tropsch reactor inlet condition restricted inerts to 15 mol %, however in this case CO_2 is not treated as an inert, rather it is accounted for in the stiochiometric ratio (Equation 1.4). Conversion in the Fischer—Tropsch reactor was set at 60 mol % CO at a temperature of 280 °C. Fischer—Tropsch products (stream 11) had CO_2 removed (~ 90 mol %) and recycled to the Fischer—Tropsch reactor (stream 6). A portion of the CO_2 was purged (stream 16) to keep the stoichiometric ratio from dropping below 2. In the base case (Case E) ~ 25 mol % of the

removed CO_2 had to be purged before being recycled. The rest of the products (stream 8) were cooled to 40 °C and syncrude (stream 9) and water (stream 10) were seperated. The unconverted syngas was recycled to the ATR (stream 12) and a portion was purged as fuel gas (stream 13).

Figure 4.6 Iron Fischer—Tropsch synthesis with oxygen from ASU.

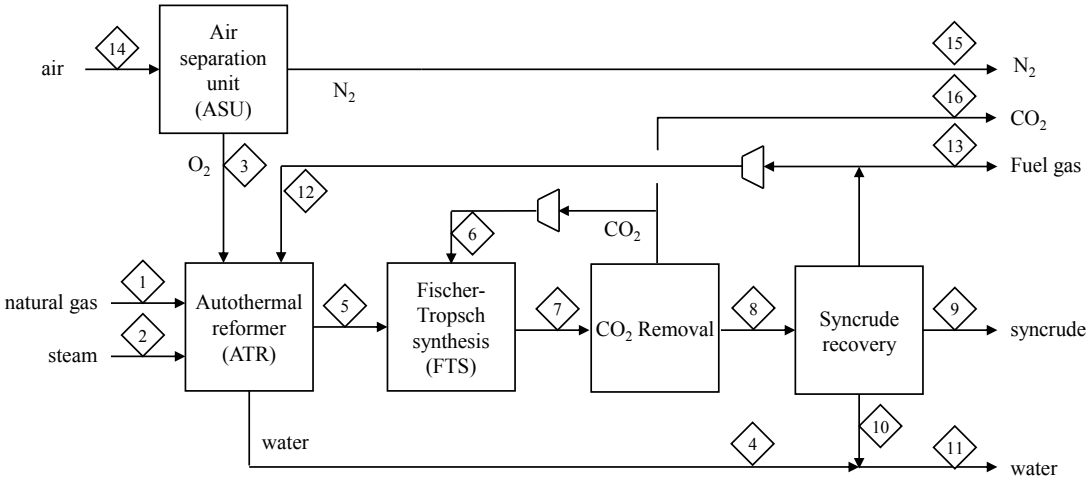

Table 4.8 Material balance for base case iron Fischer—Tropsch production from syngas.

Compound	ATR feed (1 to 3)	Water (11)	Syncrude (9)	Stack gas (13)
Total flow rate (kg/s)	16.41	12.87	1.00	2.56
Composition (kg/s)				
methane (CH_4)	1.79	0	0	0.01
ethane (C_2H_6)	0.18	0	0	0
carbon dioxide (CO_2)	0.08	0	0	2.37
nitrogen (N_2)	0.10	0	0	0.10
oxygen (O_2)	4.00	0	0	0
argon (Ar)	0.025	0	0	0.025
water (H_2O)	10.24	12.87	0	0
carbon monoxide (CO)	-	0	0	0.02
hydrogen (H_2)	-	0	0	0.03
Syncrude	-	0	1.00	0

Material balance closes to within 0.02 kg/s.

Water electrolysis integration (Case F)

The integration of water electrolysis into the gas loop design (Figure 4.7) replaces the ASU as source of purified O_2, while at the same time being a source of pure H_2. With the exception of this change, the rest of the design is similar to that of the base case (Figure 4.6).

The water electrolysis unit takes water as feed (stream 15) and produces pure H_2 (stream 6) and pure O_2 (stream 3) as products.

The pure O_2 (stream 3) is used as co-feed with natural gas (stream 1) and steam (stream 2) to produce syngas in the ATR. The raw syngas (stream 5) goes directly to the Fischer—Tropsch reactor as in the base case, except in this case hydrogen is also fed to the inlet of the reactor. At the outlet of the ATR due to the high ratio of H_2O the syngas is above the usage ratio of ~2. However, by following the same path as the base case and recycling CO_2 (stream 7) after the Fischer—Tropsch reactor the stoichiometric ratio is adjusted to 2. In this case however with the additional hydrogen, only ~ 1 mol % of the removed CO_2 is required to be purged (stream 17), compared with ~ 25 mol % of the base case. Due to different recycle and purge rates and subsequently different stream compositions, the flow rates of stream 8 in (Figure 4.6) and stream 9 in (Figure 4.7) are not the same.

Conversion in the Fischer—Tropsch reactor is the same as the base case, 60 mol % CO conversion at 280 °C with the inlet constrained to 15 mol % inerts. Fischer—Tropsch products (stream 9) had CO_2 removed (~ 75 mol %) and recycled to the Fischer—Tropsch reactor (stream 6). A portion of the CO_2 was purged (stream 17) to keep the usage ratio from dropping below 2. The rest of the products (stream 9) were cooled to 40 °C and syncrude (stream 10) and water (stream 11) were seperated. The unconverted syngas was recycled to the ATR (stream 13) and a portion was purged as fuel gas (stream 14).

Figure 4.7 Iron-based Fischer—Tropsch synthesis using water electrolysis

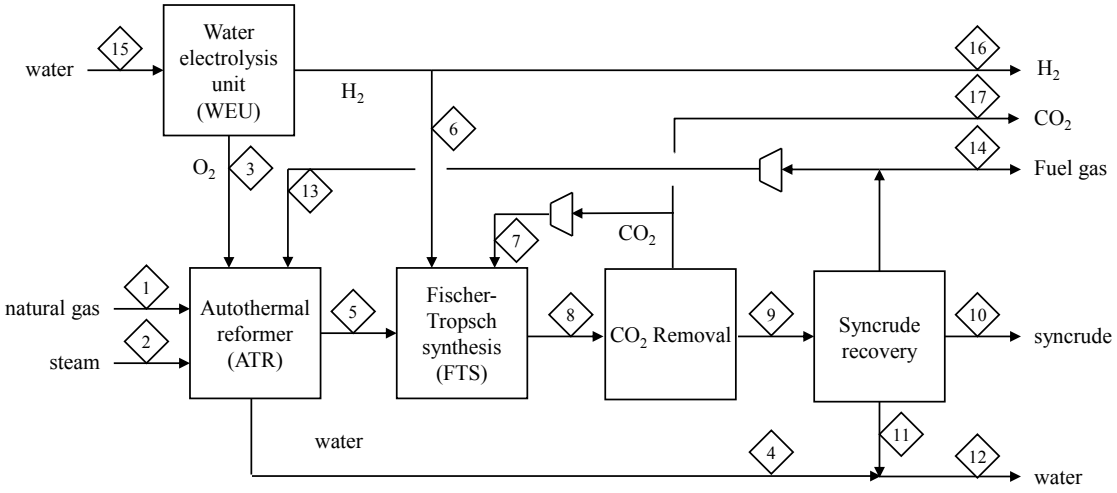

Table 4.9 Material balance for iron-based Fischer—Tropsch production from gas loop with water electrolysis integration.

Compound	ATR feed (1 to 3)	Hydrogen (6)	Water (12)	Syncrude (10)	Stack gas (14) & (17)
Total flow rate (kg/s)	14.97	0.38	14.19	1.00	0.16
Composition (kg/s)					
methane (CH_4)	1.03	0	0	0	0.00
ethane (C_2H_6)	0.10	0	0	0	0
carbon dioxide (CO_2)	0.04	0	0	0	0.08
nitrogen (N_2)	0.06	0	0	0	0.06
oxygen (O_2)	3.86	0	0	0	0
argon (Ar)	0.00	0	0	0	-
water (H_2O)	9.88	0	14.19	0	0
carbon monoxide (CO)	-	0	0	0	0.01
hydrogen (H_2)	-	0.38	0	0	0.01
Syncrude (C_7+)	-	-	0	1.00	0

Energy Balance

The utility balance for the iron-based Fischer—Tropsch case is shown below in Table 4.11 and is analysed in the next section. Unlike the cobalt-based Fischer—Tropsch case, there was not enough excess hydrogen to provide onsite power for the WEU, and natural gas had to be used.

Table 4.10 Utility balance on iron Fischer—Tropsch

	Case E Base case	Case F Water electrolysis integration
	(MW)	(MW)
HP (70 bar) Saturated Steam Source		
Reformer outlet waste heat boiler	42.4	47.0
MP (40 bar) Saturated Steam Source		
FT reactor cooling	19.3	19.7
HP Superheated Steam Users		
HP steam turbine	50.6	56.2
MP Superheated Steam User		
MP steam turbine	21.8	26.4
Fuel Gas source		
Tail Gas (LHV)	17.8	9.3
Excess H2 from WEU (LHV)	-	114.7
Power Generation		
HP Steam Turbine	15.8	17.6
MP Steam Turbine	6.8	8.2
Fuel Gas Turbine	-	48.7
Electrical power users		
CO2 Removal	1.8	4.3
CO2 recycle compressor	0.03	0.04
External recycle compressor	0.4	0.5
Oxygen Compressor	2.0	0.0
HP Boiler feed pump	0.2	0.2
MP Boiler feed pump	0.01	0.1
WEU/ASU	3.6	81.6
Fuel Gas user		
MP saturated steam	2.5	2.6
HP saturated steam	8.2	6.7
ATR preheat	7.0	0.0
Without WEU		
Power Export	14.6	69.4
With WEU		
Power Import	-	12.2
Natural Gas for Power (kg/s)	-	0.64
Resulting CO2 Production (kg/s)	-	1.60

Discussion

Hydrogen production

The process flow diagrams for the ASU and WEU gas loops involving hydrogen production are shown above in Figures 4.2 and 4.3. The material balances for both cases are shown above in Tables 4.2 and 4.3. The utility balances are given above in Table 4.4. The CO_2 emissions for both cases are given below in Table 4.11.

As was brought up briefly in the energy balance section of the hydrogen production results, the nature of the WEU providing pure hydrogen reduces the requirements of the reforming gas loop. This has two important consequences, one for the mass balance and the other for the energy balance. First, for the mass balance, as can be seen in Tables 4.2 and 4.3, much less natural gas is required when a WEU is employed for oxygen production. This reduces the amount of CO_2 generated. It is necessary to note that in terms of percentage, both scenarios have the same carbon efficiency in the gas loop, the ASU case simply has more natural gas to convert. Since the tail gas was used as fuel gas, all of the carbon in the natural gas leaves as CO_2 for both cases. The WEU case benefits from not using as much natural gas, and thus, having less CO_2 emissions.

Table 4.11 CO_2 emission for Hydrogen production.

				Indirect Energy	
				From renewables	From natural gas
	Direct(kg/s)	Indirect (kg/s)	Total (kg/s)	Total kg CO_2/kg H_2	Total kg CO_2/kg H_2
WEU	5.96	1.2	7.2	6.0	7.2
ASU	8.99	-	9.0	9.0	9.0

From an energy balance perspective (Table 4.4), because of the smaller reforming gas loop for hydrogen production the WEU gas loop generates less power. The WEU has large power requirements that benefit from on-site power generation. For the process to run, natural gas is

needed to be combusted in a gas turbine to generate power. In this case only combustion in a gas turbine was used, however, additional power could have been created through co-generation with a steam turbine to make use of the heat left in the gas turbine effluent. The CO_2 emissions for both hydrogen production cases are shown above in Table 4.11. The carbon efficiency of the process is impacted negatively by the additional combustion of natural gas to power the WEU. From the reforming gas loop alone the WEU case generated 34 % less CO_2 per kg H_2 than the ASU; however to power the WEU required an increase in CO_2 emission of 20 %.

If power for the WEU comes from a renewable source of energy then the CO_2 savings will remain at 34 %, but if natural gas must be used to generate power for the WEU, the benefits drop to 20 % less CO_2 per kg of hydrogen for the WEU.

Cobalt-based Fischer—Tropsch syncrude production

The process flow diagrams for the ASU and WEU cases involving cobalt Fischer—Tropsch were shown above in Figures 4.4 and 4.5. The material balances for the two cases are shown above in Tables 4.5 and 4.6. The utility balances were given above in Table 4.7. The CO_2 emissions for both cases are shown below in Table 4.12.

Having the additional feed of pure hydrogen helped the WEU case significantly in increasing carbon efficiency as well as providing the electricity required to power the WEU. Gains in carbon efficiency were made in two areas: first in the WGS where conversion was high enough to not require the purging of any CO_2 from the CO_2 recycle loop which co-fed the WGS, along with the syngas and H_2 feeds; second, the lower amounts of inerts (i.e., no argon) led to a slightly smaller purge loss of CO_2. The savings caused by the absence of argon were not as large as expected due do the presence of methane and ethane which were

treated as inerts and dominated the inert conentration at the Fischer—Tropsch reactor inlet. In the ASU case CO_2 made up 13.1 mol % of the external purge, and in the WEU case CO_2 made up 12.5 mol % of the external purge. This difference, while small, can be attributed mainly to the absence of argon.

The much higher power requirements of the WEU stands out in all comparisons, however, other notable differences in power usage are increased compression due to larger recycles in the WEU case, and the lack of O_2 compression being needed in the WEU case (Table 4.7). The utility cost of the CO_2 removal unit before the Fischer—Tropsch reactor is also substantially larger since there is no purge on the CO_2 that is recycled. Despite having larger recycles, and thus a larger ATR, the amount of HP steam produced by the WEU is lower. The outlet of the reformer is cross exchanged in all cases with the inlet to act as a preheat and increase thermal efficiency. Tail gas is used as fuel gas, and after superheating the saturated HP and MP steam streams, the remainder of the tailgas energy is used up preheating the ATR feed streams, thus allowing less of the ATR outlet stream to go to preheating, and more HP steam to be generated. This is relevant because the ASU case has more tail gas purged (i.e., has more fuel gas energy for preheating), and the ASU case also has a smaller external recycle, so that there is less energy consumed in preheating. This benefits the ASU case by increasing the electric power generation.

The WEU case has a slight edge in MP steam generated by the Fischer—Tropsch reactor since the WGS created a significant amount more CO, while simultaneously ensuring that the H_2/CO ratio remains at ~ 2 by using the necessary amount of hydrogen from the WEU (i.e, the Fischer—Tropsch synthesis is exothermic, and there is more CO to react). The reverse WGS reactor used 58 % of the pure hydrogen generated by the WEU. The rest of the

hydrogen from the WEU was converted into electrical power. Not all of the hydrogen was needed to provide power for the WEU, so there is opportunity to store a portion of the hydrogen and use it for other purpose such as hydroprocessing.

Table 4.12 CO_2 emission for cobalt-based Fischer—Tropsch syncrude production

				Indirect Energy	
				From renewables[a,b]	From natural gas
	Direct(kg/s)	Indirect (kg/s)	Total (kg/s)	kg CO_2/bbl oil	kg CO_2/bbl oil
WEU	0.5	-	0.5	53	53
ASU	2.0	-	2.0	227	227

[a]In this case all of the renewables energy is supplied by excess hydrogen from the WEU. No external renewable energy is required.
[b]A density of 715 kg/m^3 was calculated by VMGSim for cobalt-based Fischer-Trospch oil.

If the WEU is not run on renewable power, natural gas must be used in a gas turbine to provide power. The gas turbine effluent also contains usable heat that can be used to create steam from which more power can be generated. This is generally only viable for larger operations and was not considered for any of these cases.[(18)]

The contribution to CO_2 emission by the WEU gas loop was smaller than the ASU gas loop. Only 1.5 kg CO_2 per barrel of syncrude came directly from the gas loop. The majority of the WEU gas loop CO_2 emission came from using the tail gas as fuel gas for superheating steam and preheating the ATR. Of the 53 kg CO_2 per barrel of syncrude, 51.5 kg CO_2 came from using the tail gas as fuel gas. The WEU gas loops CO_2 emissions are 23 % of the ASU gas loops (Table 4.12).

Using the excess hydrogen from the WEU led to a carbon efficiency of 86.9 mol % in the WEU gas loop compared to only 60.8 mol % in the ASU gas loop. These results are quite positive towards the inclusion of a WEU into cobalt-based Fischer—Tropsch gas loops. Large increases in carbon efficiency make the process more profitable since more saleable

products are provided, and there is also a net export of power, so the gas loop is self sustaining (Table 4.8).

Iron-based Fischer—Tropsch syncrude production

The process flow diagrams for the ASU and WEU cases involving iron Fischer—Tropsch were shown above in Figures 4.6 and 4.7. The material balances for the two cases are shown above in Tables 4.8 and 4.9. The utility balances were given above in Table 4.10. The CO_2 emissions for both cases are shown below in Table 4.13.

Similar to the cobalt cases, there was significant carbon efficiency gains when a WEU was used to create syncrude, this time with iron catalyst Fischer—Tropsch . Iron catalysts are WGS active, which changes the design of the gas loop. CO_2 is no longer an inert, and the stoichiometric ratio is given by Equation 1.4. Rather than removing CO_2 before the inlet, iron-based Fischer-Trospch takes advantage of the WGS that is active inside the Fischer—Tropsch reactor and CO_2 removal occurs after the reactor (Figures 4.6 and 4.7). CO_2 removal is not as stringent as in the case of the cobalt case where CO_2 needed to be reduced to control inert concentration entering the Fischer—Tropsch synthesis.

CO_2 is recycled because its addition lowers the stoichiometric ratio of the ATR outlet gas, which leaves the ATR higher than the Fischer—Tropsch synthesis usage ratio of 2. This is mainly from the high steam to carbon ratio. Care has to be taken in how much CO_2 is recycled to the ATR, especially in the ASU case where there isn't external H_2 available to regulate the stoichiometric ratio if the ATR outlet stoichiometric ratio is too low.

This is actually a significant determiner of how much of the removed CO_2 gets purged, since there is a minimum amount of CO_2 that must be removed prior to recycle to the ATR or else the stoichiometric ratio will be immediately too low for Fischer—Tropsch synthesis

usage from the ATR outlet; and of the CO_2 removed, there is a maximum amount that can be recycled to the Fischer—Tropsch reactor – recycling too much will drop the stoichiometric ratio below the Fischer—Tropsch synthesis usage ratio of 2, thus the need to purge. In the ASU case 43.2 mol % of the natural gas feed carbon is purged as CO_2 in stream 16 of Figure 4.6. In the WEU case only 1.7 mol % of the natural gas feeds carbon is purged as CO_2 in stream 17 of Figure 4.7.

Two things stand out over the cobalt-based Fischer—Tropsch gas loop when WEU is used. First, the direct carbon efficiency of the WEU iron-based Fischer—Tropsch gas loop is 97 mol % which is significantly higher than the ASU iron Fischer—Tropsch gas loop (55.9 mol %), as well as the WEU cobalt-based Fischer—Tropsch gas loop (86.9 mol %). Second, the WEU iron-based Fischer—Tropsch gas loop is the only case out of the four Fischer—Tropsch gas loops that is not self-sustaining. It required natural gas combustion to power the WEU in addition to the excess hydrogen from the WEU being used. The main reason for both of these two results is that the WEU iron-based Fischer—Tropsch gas loop used 78 % of the hydrogen produced by the WEU in the gas loop. This led to a very high conversion of the natural gas feed into syncrude. Unfortunately, too little hydrogen was left over to provide power for the WEU without using natural gas.

When natural gas is used to provide power for the WEU, the carbon efficiency of the iron-based Fischer—Tropsch gas loops decreases to 54.5 %, which is slightly less than the base case ASU gas loop. A renewable energy source would be well put to use by the WEU iron-based Fischer—Tropsch gas loop. Available below in Table 4.13 is the CO_2 emissions for the two cases. If a renewable energy source was available to supplement the onsite power generation, the iron Fischer—Tropsch would be able to produce sycrude at only 11 kg CO_2

per barrel of syncrude. If natural gas is used in the place of a renewable energy source, the CO_2 emission climbs to 247 kg CO_2 per barrel of syncrude. This is still slightly lower than the 254 kg CO_2 per barrel of syncrude produced when an ASU is used in the gas loop.

Table 4.13 CO_2 emission for iron based Fischer—Tropsch syncrude production.

				Indirect Energy	
				From renewables[a,c]	From natural gas[b]
	Direct(kg/s)	Indirect (kg/s)	Total (kg/s)	Total kg CO_2/bbl oil	Total kg CO_2/bbl oil
WEU	0.11	2.3	2.37	11	247
ASU	2.44	-	2.44	254	254

[a]In this case renewable energy other than the excess hydrogen from the WEU is required.
[b]Hydrogen is first used to generate electricity, then natural gas generates the remainder. This would be the case if no renewable energy was available.
[c]A density of 655 kg/m^3 was calculated by VMGSim for iron based Fischer-Trospch oil.

It is worthwhile noting that a supply of renewable energy would not benefit the ASU case since the ASU case already exports more power than it needs. The mass balance is the source of the ASU's CO_2 emissions, not the energy balance; whereas the energy balance is the source of the WEU CO_2 emissions and not the mass balance.

Conclusions

The use of a water electrolysis unit in the hydrogen gas loops as well as cobalt and iron based Fischer—Tropsch gas loops has been compared against the traditional use of an air separation unit. Several things have been found that are of use for potential designs utilizing renewable energy:

1) Water electrolysis provides pure O_2 and H_2 which can help decrease purge waste.
2) Carbon efficiency is not affected by the presence of a water electrolysis unit in hydrogen production. Much less natural gas is needed to provide the same amount of hydrogen.

3) The use of water electrolysis led to significant gains in carbon efficiency in Fischer—Tropsch gas loops. In the case of cobalt-based Fischer—Tropsch the carbon efficiency was improved from 60.8 % to 86.9 %, and for the iron-based Fischer—Tropsch gas loops the carbon efficiency was improved from 55.9 % to 97 %.
4) When using a WEU within a cobalt-based Fischer—Tropsch gas loop, the excess hydrogen can be used to generate the necessary power for the WEU, which is the main draw of electricity. The WEU gas loop has a significantly lower CO_2 emission than the ASU gas loop.
5) When using a WEU in a iron-based Fischer—Tropsch gas loop there is not enough excess hydrogen to supplement the power generation from steam, and either a renewable energy resource is needed to power the WEU, or natural gas can be used to generate the required electricity.
6) In designing the gas loops, care must be taken in determining the internal, external, and purge amounts. If convergence is difficult, it is quite likely that the design is not a plausible one. Plausible designs, while still requiring iteration, generally converge in a somewhat linear fashion. Implausible or very rigid designs tend to be very finicky to small changes and prone to underdamped oscillatory behavior.
7) Keeping in mind how a change will effect not just the Fischer—Tropsch reactor, but also the ATR and WGS reactors is important. A change at the Fischer—Tropsch reactor will ripple through the recycles and effect everything not just after, but also before the Fischer—Tropsch reactor. This is particularily amplified as the external recycle grows in size.

References

(1) Rostrup-Nielsen, J.; Christiansen, L.J., *Concepts in syngas manufacture*, Imperial College Press: London, **2011**.
(2) Higman, C.; van der Burgt, M., *Gasification*, 2ed, Elsevier: Amsterdam, **2008**.
(3) Chueh, W.C.; Falter, C.; Abbott, M.; Scipio, D.; Furler, P.; Haile, S.M.; Steinfeld, A., *Science*, **2010**, *330*, 1797.
(4) Piatkowski, N.; Wieckert, C.; Weimer, A.W.; Steinfeld, A., *Energy Environ. Sci.*, **2011**, *4*, 73.
(5) Häring, H-W. ed. *Industrial gases processing*, Wiley-VCH: Weinheim, **2008**.
(6) Graves, C.; Ebbesen, S.D.; Mogensen, M.; Lackner, K.S. Sustainable hydrocarbon fuels by recycling CO_2 and H_2O with renewable or nuclear energy. *Renewable and Sustainable energy Reviews* **2011**, *Vol. 15*, 1-23.
(7) Pinaud, B.A.; Benck, J.D.; Seitz, L.C.; Forman, A.J.; Chen, Z.; Deutsch, T.G.; James, B.D.; Baum, K.N.; Baum, G.N.; Ardo, S.; Wang, H.; Millere, E.; Jaramillo, T.F., *Energy Environ. Sci.*, 2013, *6*, **1983**.
(8) Specht, M.; Bandi, A.; Baumgart, F.; Murray, C.N.; Gretz, J., In *Greenhouse gas control technologies*, B. Eliasson, P.W.F. Riemer and A. Wokaun Eds., Pergamon Press: Amsterdam, **1999**, 723
(9) Romero M.; Steinfeld, A., *Energy Environ. Sci.*, **2012**, *5*, 9234.
(10) Clausen, L.R.; Houbak, N.; Elmegaard, B., *Energy*, 2010, **35**, 2338.
(11) Hannula, I., *Biomass and Bioenergy*, **2015**, **74**, 26.
(12) De Klerk, A. *Energy Sci. Eng.*, **2015**, **3**, 60.
(13) Miglio, R.; Zennaro, R.; de Klerk, A., In *Greener Fischer—Tropsch processes for fuels and feedstocks*, P.M. Maitlis and A. de Klerk Eds., Wiley-VCH: Weinheim, **2013**, 311.
(14) A. de Klerk, *Prepr. Pap.-Am. Chem. Soc., Div. Energy Fuels*, **2014**, *59* (2), 823.
(15) Elliott, J.R.; Lira, C.T. *Introductory Chemical Engineering Thermodynamics;* Prentice Hall: Upper Saddle River, NJ, **1999**.
(16) Lwin, Y. Chemical equilibrium by Gibbs energy minimization on spreadsheets*, *International Journal of Engineering Education*, **2000**, *16*, 335-339.
(17) Ulrich, G.D.; Vasudevan, P.T. *Chemical engineering process design and economics: a practical guide*, Process Publishing: Durham, New Hampshire, **2004**.
(18) Kidnay, A.J.; Parrish, W.R., *Fundamentals of natural gas processing*, Taylor & Francis: Boca Raton, **2006**.
(19) Newman, S.A., *Acid and sour gas treating processes*, Gulf Publishing Company, Houston Texas, **1985**.
(20) Kohl, A.L.; Nielsen, R.B. *Gas Purification* 5ed, Gulf Publishing Company, Houston Texas, **1997**.

Chapter 5 – The thermodynamics of phase equilibria.

Introduction

It is necessary to go over the thermodynamics of phase equilibria before beginning Chapters 9 and 10, which is the modelling of Fischer—Tropsch products in VLLE, with the inclusion of oxygenates. This is therefore a review of the necessary literature to understand the fundamentals of phase equilibria. Two textbooks are used as references throughout the entire discussion: Elliott and Lira[(1)], and Matsoukas[(2)]. While direction has been added to the following discussion on phase equilibria, the concepts have been around for over 100 years and are not new. They are however necessary to understand the work that is done in Chapters 9 and 10, and they also provide valuable insight into the models discussed in Chapters 6 to 8.

It is the inclusion of oxygenates in the modelling of Fischer—Tropsch synthesis products that makes Chapter 10 a unique contribution to literature, and the inclusion of oxygenates and water is also what makes it the largest chapter. Oxygenates in Fischer—Tropsch are relatively dilute (Table 2.1) and are usually by-products of Fischer—Tropsch synthesis. However, being dilute does not mean that oxygenates are not problematic, or easily modelled. As mentioned earlier, if the carboxylic acids partition into the hydrocarbon phase, they lead to corrosion issues in downstream processing units. Figure 5.1 shows the areas of VLE and VLLE in the Fischer—Tropsch reactor and syncrude recovery sections of a Fischer—Tropsch process.

Figure 5.1 Vapor—liquid equilibrium (VLE) and vapor—liquid—liquid equilibrium (VLLE) of Fischer–Tropsch reaction products as illustrated by a typical low temperature Fischer–Tropsch process.

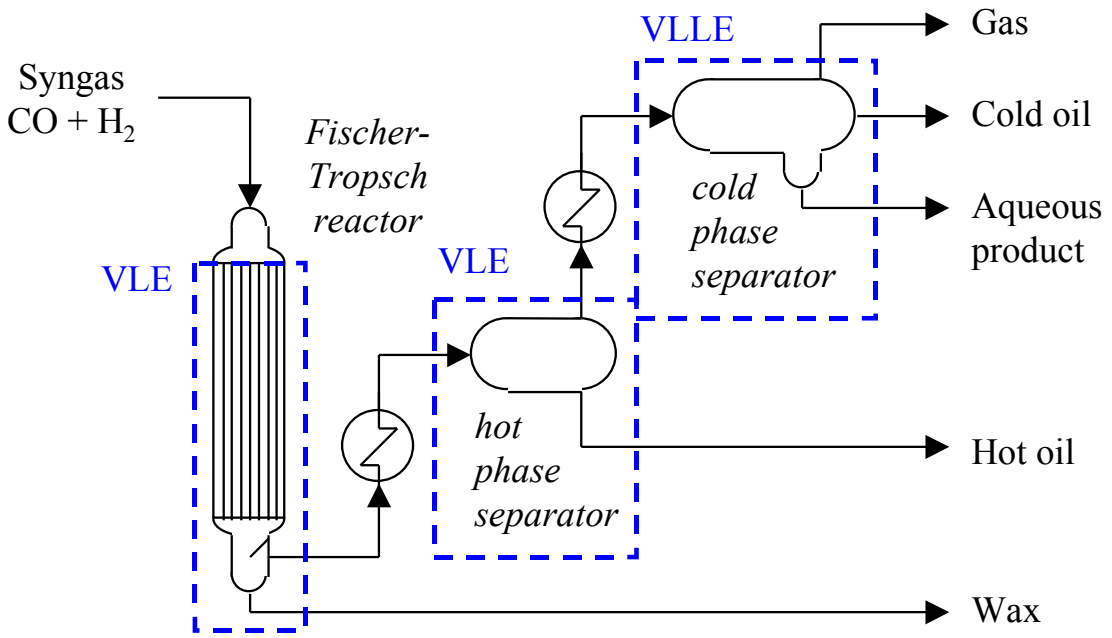

The most common classes of oxygenates found in Fischer—Tropsch are alcohols and carboxylic acids. Ethanol and acetic acid make up the majority of Fischer—Tropsch oxygenates. Ethanol is a polar molecule, meaning that the electrical charges are not equal at all points surrounding the atoms, some areas are more negative and others are more positive. The impact of this is that the negative dipoles are attracted to positive dipoles on other molecules. This complicates modelling, because a model must be capable of accounting for these polarized interactions. Figure 5.2 shows the different areas of polarity in a water molecule, although in the case of water the phenomena that occurs from the imbalance of charges is known as association or hydrogen bonding. Acetic acid is also an associating molecule and is problematic in Fischer—Tropsch products. Hydrogen bonding forms strong but not permanent bonds with other molecules. Hydrogen bonding between pure components is called association, hydrogen bonding between different molecules is known as solvation.[5] Acetic acid dimerizes, which is the result

of the positively charged hydrogen in one molecule bonding with the negatively charged electrons around the oxygen on another molecule, while the same effect is had from the perspective of the other molecule, i.e., two hydrogen-electron pair bonds are formed. In essence, two molecules begin behaving as one molecule. The simplest way to understand the influence this has is with the ideal gas law (i.e., PV = nRT).

Figure 5.2 Polarity in a water molecule. Blue dots indicate negatively charged electron pairs, "H" indicates positively charged hydrogen atoms.

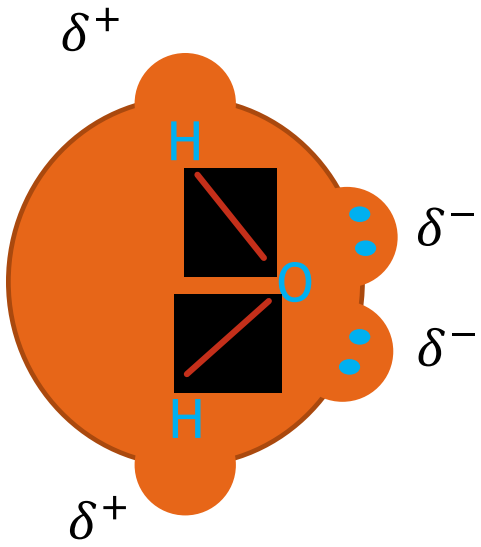

For example, if 100 molecules of acetic acid are contained in a given volume V at a given temperature T, and 40 of them dimerize, the system now acts as if there is only 80 molecules. However, the scientist or engineer is going to use n = 100 mol, rather than n = 80 mol in the ideal gas equation P = nRT/V, and this leads to an overestimation in pressure by 20 %. The error in the ideal gas equation was discovered early on, and hundreds of more advanced models have been proposed to describe different phenomena such as polarity, association, ionization, dipole moments, etc… in phase equilibria. They generally fall into a few classes of models. The model classes and specific models within each class chosen to represent the phase equilibria of

Fischer—Tropsch will be described in Chapters 6 to 8. The remainder of Chapter 5 will go over fundamentals required for understanding how models predict phase equilibria.

Criteria for phase equilibrium

The derivations for the conditions at equilibrium for a VLLE system are shown in Appendix A and can be modified with little work to that of VLE or LLE. The result is the same for all cases and is shown below:

$$\mu_i^I = \mu_i^{II} =, \dots, = \mu_i^{NP} \; for \; i = 1,2, \dots, NC \tag{5.1}$$

$$T^I = T^{II} =, \dots, = T^{NP} \tag{5.2}$$

$$P^I = P^{II} =, \dots, = P^{NP} \tag{5.3}$$

Where NC stands for number of components and NP stands for number of phases. This is the starting place for nearly all descriptions of phase equilibria in literature, and is somewhat presumptuous without the derivations which lead to these conditions. It is important to realize that entropy is the controlling factor of phase equilibrium, and at equilibrium entropy is at a maximum. The derivation in Appendix A is meant to show how it is necessary to begin with entropy and the fundamental equation (Equation 5.4), and work out the conditions for equilibrium from that point according to system specific constraints (i.e., isolated closed system, etc…).

Gibbs energy is the thermodynamic potential that is most naturally used during phase equilibrium conditions since it requires constant temperature and pressure, which are the conditions found in phase equilibria calculations. However, thermodynamics potentials such as Gibbs energy, Helmholtz energy, and enthalpy, are the result of Legendre transforms on the fundamental equation (Equation 5.4), and as such are results that follows from the fundamental

equation, and are not a beginning themselves. To summarize: Equations 5.1 to 5.3 are true, however, they are the result of understanding entropy and Equation 5.4, and respect should be paid to the derivations that lead to Equations 5.1 to 5.3. This is not typically done, and is not done in the first three reference textbooks.[1-3] This is largely due to the textbooks cited being used as introductory level instruction to thermodynamics, albeit, very thorough introductions. Callen provides good instruction on phase equilibrium from a more advanced level in which he begins with the fundamental equation shown below, and proceeds as explained above.[4]

$$dU = TdS - PdV + \sum_{i=1}^{NC} \mu_i dN_i \qquad 5.4$$

Phase equilibria for pure components

There are several good textbooks for understanding the fundamental thermodynamics of phase equilibrium. Elliott and Lira and Matsoukas were found to be the best resource and are used throughout Chapter 5 to explain phase equilibria. According to Elliott and Lira, and Matsoukas, the starting point for phase equilibrium (they begin with VLE) is as follows in Equation 5.5:

$$G^L = G^V \qquad 5.5$$

In Equation 5.5 the Gibbs energy of the liquid and vapor phases is given in terms of molar amounts. For a pure component it is equivalent to say that the chemical potential of the liquid phase is equal to the chemical potential of the vapor since the chemical potential is known as the molar Gibbs free energy of a pure component.[2] Equation 5.5 in terms of chemical potential is the pure component version of Equation 5.1, but applied to VLE. The molar Gibbs energy is the only thermodynamics potential that is the same in both phases.

In thermodynamics the whole can be broken down into the parts and added together. For instance, the Gibbs energy can be broken into all of its contributions such as polarity, association, dipole moments etc. A simple form of this is the following:

$$G = G^{ig} + G^{R} \qquad 5.6$$

The superscript R stands for residual, and accounts for all phenomena that is not ideal (i.e., all interactions between molecules such as polarity, association, dipole moments etc..). The ideal Gibbs energy is often available at standard reference points (pressure = 1 bar, temperature = 298 K), and can then be scaled to a systems given temperature and pressure. This is somewhat of an inconvenience since every calculation first requires a reference point and then the subsequent scaling of the ideal gas contribution to the Gibbs energy.

G.N. Lewis overcame this by developing a term called fugacity. Fugacity comes from the Latin term "fugere" ("to flee") and refers to the tendency of a specie to escape one phase for a more stable phase.[2] Fugacity has the advantage over Gibbs energy due to how it is defined in two aspects: first it does not require a reference state[2] and second, fugacity of a vapor is equal to pressure in the ideal gas state, and the fugacity of a liquid equals the vapor pressure of a liquid under common conditions (vapor pressure was the original property used for the characterization of phase equilibria by experimentalists).[1]

The differential equation for Gibbs energy (Equation 5.7) leads to the relation of fugacity and Gibbs energy. For a pure component at constant temperature the differential equation is given as:

$$d\mathrm{G} = VdP \qquad 5.7$$

Assuming the pressure is low (i.e., the molecules are far apart and do not interact (are ideal), V = RT/P), allows Equation 5.7 to become Equation 5.8:

$$d\mathrm{G}^{ig} = \frac{RT}{P}dP = RTd\ln P \qquad 5.8$$

The superscript *ig* denotes that Equation 5.8 refers to an ideal gas. As pressure approaches zero both Equations 5.7 and 5.8 become infinite. Elliott and Lira point out that in this case as a real fluid state approaches zero pressure, the compressibility factor, Z, approaches the ideal gas limit, and *d*G approaches $d\mathrm{G}^{ig}$. With this observation the following becomes true:

$$d\mathrm{G} - d\mathrm{G}^{ig} = \mathrm{d}(\mathrm{G} - G^{ig}) \qquad 5.9$$

The difference between the real Gibbs energy and the ideal Gibbs energy is what Elliott and Lira refer to as the departure function. It is how much the gas "departs" from ideal behavior. From Equation 5.6, the departure function is defined as the residual contribution. At equilibrium the residual Gibbs energies are defined by Matsoukas as being equivalent, as shown in Equation 5.10:

$$G_L^R = G_V^R \qquad 5.10$$

This is a powerful statement. It means that there are now conditions for phase equilibrium that do not require a reference state (as discussed above, the ideal Gibbs energy contribution required a reference state). Equations 5.7 to 5.10 can now be tied into the concept of fugacity.

G.N. Lewis was responsible for the original definition of fugacity and he defined it as follows:

$$d\mathrm{G} = VdP = RTd\ln f \quad \text{at constant T} \qquad 5.11$$

Subtracting Equation 5.8 from Equation 5.11 results in:

$$\frac{d\left(\mathrm{G} - G^{ig}\right)}{\mathrm{RT}} = RTd\ln\left(\frac{f}{P}\right) \qquad 5.12$$

From Equation 5.6 the residual contribution for the Gibbs energy can be inserted into Equation 5.12 and the differential equation can be integrated to yield:

$$\frac{d\left(\mathrm{G}-G^{ig}\right)}{\mathrm{RT}}=\frac{1}{RT}\int_{0}^{P} d(G^{R})=\left.\ln\left(\frac{f}{P}\right)\right|_{P}-\left.\ln\left(\frac{f}{P}\right)\right|_{P=0}=RTd\ln(\frac{f}{P}) \qquad 5.13$$

In the first step of integration low pressure and constant temperature has continued to be assumed. Finishing the integration results in what can arguably be considered the most powerful equation in phase equilibria:

$$\frac{G^{R}}{RT}=\ln\left(\frac{f}{P}\right)=\ln\varphi \qquad 5.14$$

The conditions for phase equilibria as given by Equation 5.10 can now be satisfied provided the fugacity coefficient, which is defined in Equation 5.14 as $\varphi=\left(\frac{f}{P}\right)$, is known (or capable of being predicted) in all phases. Replacing the residual Gibbs energies in Equation 5.10 with the result in Equation 5.14 provides a new condition for phase equilibrium that is based on fugacity:

$$f^{V}=f^{L} \qquad 5.15$$

To repeat what was said above about the utility of using fugacity as a condition for equilibrium, Equation 5.15 does not require a reference point which makes is much simpler to use than Equations 5.1 or 5.5.

Equations of state such as the virial and cubic equations of state solve for the fugacity coefficient, thus solving the conditions for equilibrium. This is necessary for ensuring the phases are in equilibrium; however the fugacity coefficient also enables the calculation of thermodynamic properties, which is the real reason for using an Equation of State. Determining that a phase is in equilibrium is a necessary task, but does not provide any information about the system other than that the system is in equilibrium.

Next an alternative method to using fugacity coefficients in the liquid phase will be discussed, and then using fugacity for mixtures along with a few of the properties that can be calculated with fugacity coefficients will follow before beginning ideal solution theory.

Fugacity in the liquid phase

When using an equation of state to calculate the fugacity in the liquid phase, it is a simple matter of using the liquid root of either the volume or compressibility factor to calculate the fugacity coefficient. The fugacity is then the fugacity coefficient multiplied by the pressure, which is the relation given in 5.14. If an equation of state is not being used to solve for the fugacity, then the Poynting method must be used to solve for the liquid fugacity. The Poynting method is derived as follows:

$$RT \ln \frac{f^L}{f^{sat}} = \int_{P^{sat}}^{P} V dP \qquad 5.16$$

The superscript "sat" stands for saturation. The fugacity *f* and pressure P represent the state the system is at. By assuming that the liquid is incompressible, the volume may be taken out of the integral, and then the integral can be solved leading to:

$$\frac{f^L}{f^{sat}} = exp\left(\frac{V^L(P - P^{sat})}{RT}\right) \qquad 5.17$$

From equation 5.14 we know that $f = \varphi P$, which means that $f^{sat} = \varphi^{sat} P^{sat}$. Equation 5.17 becomes:

$$f^L = \varphi^{sat} P^{sat} exp\left(\frac{V^L(P - P^{sat})}{RT}\right) \qquad 5.18$$

The exponential term is known as the Poynting correction. Using this relation the fugacity of compressed liquids can be calculated. An equation of state or correlation must be used to

calculate the saturated fugacity coefficient if it is not assumed unity. In the case of Raoult's law and activity coefficient models, both of which are examined further below, the saturated fugacity coefficient is assumed to be equal to 1 (ideal).

Fugacity coefficient and mixtures

The above derivations were demonstrated for a pure component in vapor—liquid equilibrium. As can be found in Appendix A, conditions for equilibrium can be determined for multiple components and multiple phases. The conditions for multi-component, multiphase systems are given below in terms of fugacity and only require changing Equation 5.1 to be in terms of fugacity rather than chemical potential, the temperature and pressure conditions at equilibrium are the same as Equations 5.2 and 5.3. Fugacity for mixtures can be generalized from Equation 5.11 to be:

$$d\mu_i = RTd\ln\hat{f}_i \tag{5.19}$$

The accent denotes that $\hat{f}_i$ is the fugacity of component i in a mixture. Choosing to define equilibrium for a mixture in terms of μ_i (i.e., Equation 5.1) is a valid choice, but using $\hat{f}_i$ is a more user friendly choice since a reference state is not required. In terms of a mixture, equilibrium can be defined as Equations 5.3, 5.3, and 5.16 given below:

$$\hat{f}_i^V = \hat{f}_i^L \tag{5.20}$$

Given below in Table 5.1 are several thermodynamic properties with their fugacity coefficient based calculation. They are given in terms of mixture properties since that applies to the later work more than pure component properties.

To this point the calculation of non-ideal thermodynamic properties has been shown for models which are based on the fugacity coefficient, and in the case of the liquid phase another method for estimating fugacity has been shown: the Poynting method. There is another class of

models which calculates non-ideality based on the activity coefficient, and utilizes the Poynting method. These models stem from an entirely different theoretical derivation which will begin in the next section of Chapter 5. First an introduction to the ideal solution theory is necessary.

Table 5.1 Thermodynamic properties calculated by the fugacity coefficient.[6]

Property	Fugacity Coefficient Relation
$\frac{G^R}{RT} =$	$\sum_i x_i \ln \hat{\varphi}_i$
$\frac{A^R}{RT} =$	$\sum_i x_i \ln \hat{\varphi}_i - (Z-1) + \ln(Z)$
$\frac{H^R}{RT} =$	$-T \sum_i x_i \left(\frac{\partial \ln \hat{\varphi}_i}{\partial T}\right)_P$
$\frac{V^R}{RT} =$	$\sum_i x_i \left(\frac{\partial \ln \hat{\varphi}_i}{\partial P}\right)_T$
$\frac{S^R}{RT} =$	$-\left(\frac{\partial A^R}{\partial T}\right)_{V,n} - \frac{A^R}{RT^2}$
P =	$-\left(\frac{\partial A^R}{\partial V}\right)_{T,n} + \frac{RT}{V}$
$\frac{C_V^R}{RT} =$	$-T\left(\frac{\partial^2 \left(\frac{A^R}{RT}\right)}{\partial T^2}\right)_{V,n} - 2\left(\frac{\partial \left(\frac{A^R}{RT}\right)}{\partial T}\right)_{V,n}$

Ideal solution theory

In an ideal gas it is assumed that there are no interactions between molecules (i.e., they are oblivious to the presence of other molecules). An ideal solution is the liquid counterpart to the ideal gas; except it does not negate the presence of interactions, because without interactions a liquid could not form. Instead it assumes that all interactions between molecules are of the same type and strength.[2] This means that self and cross interactions are identical, non-ideal molecules such as polar molecules have the same effect on their neighbors as non-polar molecules.

Realistically this only happens when molecules are very similar in size and chemical nature. When this occurs, the molecules form an ideal solution.

For the average molecule in the bulk of a phase, all of the forces sum to zero because it is surrounded equally on all sides by equal forces. However for molecules on the outside perimeter of the bulk phase, other molecules are only on one side, so there is an imbalance of forces which pulls these molecules back towards the bulk. Theories involving interactive forces are important for phases other than gases to exist, and the ideal solution provides the first theoretical framework for liquids.

In an ideal solution like molecules interact between themselves the same as with other species. This results in there being no change in volume or enthalpy when pure components are mixed to form a solution.[(2)] Entropy does change upon mixing, but that has to do with there being a greater number of ways to arrange the components after mixing compared to before mixing (i.e., 100! is larger than 50!+50!, where "!" represents factorial) and requires statistical mechanics to explain. That is outside of the scope of this chapter but is available in several textbooks on thermodynamics.[(1)(2)(7)(8)]

The chemical potential is important in solution theories. As given in Equation 5.1, equality of chemical potentials is sufficient condition for equilibrium, along with the temperature and pressure equality conditions.

It is necessary to be able to calculate the change in ideal solution Gibbs energy of mixing since this is used later in explaining activity coefficient models. Gibbs energy is related to enthalpy and entropy by the following relation: G = H-TS. Therefore $\Delta G_{mix}^{is} = \Delta H_{mix}^{is} - T\Delta S_{mix}^{is}$. In an ideal solution the enthalpy of mixing is zero. The entropy of mixing is given by Elliott and Lira as:

$$\frac{\Delta S_{mix}^{is}}{R} = -\sum_i x_i \ln(x_i) \tag{5.21}$$

By inserting zero for the enthalpy of mixing and Equation 5.21 into the definition given for the ideal solution Gibbs energy of mixing, the final relation is:

$$\frac{\Delta G_{mix}^{is}}{RT} = \frac{\Delta S_{mix}^{is}}{R} = \sum_i x_i \ln(x_i) \tag{5.22}$$

The Gibbs energy of mixing can also be calculated (a useful relation is $G = \sum_i x_i \mu_i$):

$$\Delta G_{mix} = G - \sum_i x_i G_i = \sum_i x_i(\mu_i - G_i) = RT \sum_i x_i \ln\left(\frac{\hat{f}_i}{f_i}\right) \tag{5.23}$$

According to Elliott and Lira, the Lewis/Randall rule is obtained by comparing the relations between Equation 5.22 and 5.23:

$$\Longrightarrow \frac{\hat{f}_i^{\,is}}{f_i} = x_i \implies \hat{f}_i^{\,is} = x_i f_i \tag{5.24}$$

This is a convenient relation that is used for VLE calculations based on the ideal solution. It also shows the relation between pure component fugacity and the fugacity of component *i* in a mixture. By implementing Equation 5.24 into Equation 5.20 the conditions for equilibrium becomes:

$$y_i f_i^{\,V} = x_i f_i^{\,L} \tag{5.25}$$

Substituting in the relation for fugacity given in Equation 5.14 with respect to vapor into the left hand side of Equation 5.25, and Equation 5.18 into the right hand side of Equation 5.25:

$$y_i \varphi_i^{\,V} P = x_i \varphi_i^{\,sat} P^{sat} exp\left(\frac{V^L(P - P^{sat})}{RT}\right) \tag{5.26}$$

Raoults Law is derived by assuming the system is ideal enough that $\varphi^V = \varphi^{sat} = 1$ and $exp\left(\frac{V^L(P-P^{sat})}{RT}\right) = 1$. From above it should be clear that the purpose of fugacity coefficients is

to measure and correct for non-ideality due to the fugacity coefficient having its roots in the residual Gibbs energy. Therefore, Raoult's law is removed from any method of accounting for non-ideality and is given as:

$$y_i P = x_i P^{sat} \qquad 5.27$$

Raoult's law is essentially a simplified version of the ideal solution theory. Hence, Raoult's law should never be used for complicated systems. This is important in Chapters 9 and 10 when highly non-ideal mixtures are modeled.

Activity coefficient

The foundation has now been laid for the last part of the necessary fundamentals for phase equilibria that will be used in the following chapters. The ideal solution provides the first theory into liquids interacting and this will be taken further into account for non-idealities through the activity coefficient. The activity coefficient is analogous to the fugacity coefficient; the activity coefficient accounts for deviation from the ideal solution, just as the fugacity coefficient accounted for deviation from ideal gas and liquids. The main difference, aside from the derivation, is that the activity coefficient is only for the liquid phase, whereas fugacity coefficients can be calculated for vapor or liquid (although not all equations of state can calculate the fugacity coefficient in both phases). Models that use activity coefficients are popular because of their ability to handle highly non-ideal fluids, which is something that many fugacity coefficient equations of state, such as cubic equations of state and the virial equation of state struggle with.

A good introduction to activity coefficients is to start with the definition of activity and then apply it to the ideal solution approximation. Activity is defined as

$$a_i = \frac{\hat{f}_i}{f_i^0} \tag{5.28}$$

The accent over the fugacity term in $\hat{f}_i$ simply means that it is the fugacity of component *i* in a mixture (as discussed above) and f_i^0 is the value of the fugacity of pure component *i* at standard state. The activity coefficient is defined as:

$$\gamma_i = \frac{\hat{f}_i}{x_i f_i^0} \tag{5.29}$$

Equation 5.14 related the fugacity and fugacity coefficient to the residual Gibbs energy contribution (Equation 5.6). The residual Gibbs energy is the non-ideal Gibbs energy and is the difference between the actual Gibbs energy and the ideal Gibbs energy. In the case of activity coefficients the non-ideal Gibbs energy is referred to as the excess Gibbs energy and is the difference between the Gibbs energy (real Gibbs energy) and the ideal solution Gibbs energy.

$$G^E = G - G^{is} = \left(G - \sum_i x_i G_i\right) - \left(G^{is} - \sum_i x_i G_i\right) \tag{5.30}$$

$$= \Delta G_{mix} - \Delta G_{mix}^{is} = \Delta G_{mix} - RT \sum_i x_i \ln(x_i)$$

ΔG_{mix}^{is} was solved for above in Equation 5.22, however at this point there is not an expression for ΔG_{mix} that incorporates the activity coefficient. This can be found by incorporating Equation 5.29 with Equation 5.23:

$$\Delta G_{mix} = G - \sum_i x_i G_i = \sum_i x_i(\mu_i - G_i) = RT \sum_i x_i \ln\left(\frac{\hat{f}_i}{f_i^0}\right) = RT \sum_i x_i \ln(x_i \gamma_i) \tag{5.31}$$

We now have an expression for ΔG_{mix} which can be substituted into Equation 5.30 to get the relation between activity coefficients and excess Gibbs energy. The end result is that

$$G^E = RT \sum_i x_i \ln(\gamma_i) \tag{5.32}$$

An expression has now been formulated which links the non-ideal or "excess" Gibbs energy of a solution to the activity coefficient. This relation is important because activity coefficient models predict the activity coefficient based on their calculations of the excess Gibbs energy of the solution. As "ideal" as it would be for models to calculate the real Gibbs energy, there are currently no models capable of doing this. Theory has only been able to develop models capable of predicting the non-ideal contributions. Fortunately thermodynamic properties can be calculated from the non-ideal contributions. If the real Gibbs energy is required then the ideal and non-ideal contributions must be added together. The ideal contribution is essentially entirely empirical, requiring experimental standard states or correlations based on experimental data.

Once the activity coefficient has been calculated by an appropriate model, the conditions for phase equilibrium given in Equation 5.27 can be improved by accounting for non-ideality through the activity coefficient. The "modified" Raoult's law for phase equilibrium then becomes:

$$y_i P = x_i \gamma_i P^{sat} \tag{5.33}$$

This assumes the Poynting correction is unity, which is not a necessary assumption, but rather a typical one. Similar to Raoult's law, the vapor and saturated fugacity coefficients must be set to unity since any model which supplies the activity coefficient, is not capable of supplying fugacity coefficients. This can lead to poor vapor phase estimates when using activity coefficient models. If the vapor phase is significantly non-ideal and an equation of state or correlation is available, then the fugacity coefficients can be implemented as shown in Equation 5.34:

$$y_i {\varphi_i}^V P = x_i \gamma_i {\varphi_i}^{sat} P^{sat} exp\left(\frac{V^L(P - P^{sat})}{RT}\right) \tag{5.34}$$

Equation 5.33 is the method used by activity coefficient models on their own. In Chapters 9 and 10 an equation of state was paired with the NRTL and UNIQUAC models allowing Equation 5.34 to be used for phase equilibrium. The NRTL and UNIQUAC models are covered in Chapter 7. Given below in Table 5.2 are a few of the properties that can be calculated once the activity coefficients are known.

Table 5.2 Thermodynamic properties calculated by the activity coefficient.[6]

Property	Fugacity Coefficient Relation
$\frac{G^E}{RT} =$	$\sum_i x_i \ln \gamma_i$
$\frac{A^E}{RT} =$	$\frac{1}{RT}(G^E + PV^E)$
$\frac{H^E}{RT} =$	$-T\sum_i x_i \left(\frac{\partial \ln \gamma_i}{\partial T}\right)_P$
$\frac{V^E}{RT} =$	$\sum_i x_i \left(\frac{\partial \ln \gamma_i}{\partial P}\right)_T$

Summary

The following background into phase equilibria is necessary for understanding what thermodynamic models contribute to chemical engineering. They are powerful tools that are frequently relied upon for making process design calculations. In doing calculations it is first necessary to ensure they are being done at conditions that correspond to equilibrium, and this has been shown for pure components and mixtures, for equations of state, and the necessary theory has been supplied for calculating equilibrium and thermodynamic properties with activity coefficient models. This represents all of the models found in industrial simulators and provides a thorough base for proceeding to Chapters 6 through 8, and finally Chapters 9 and 10.

References

(1) Elliott, J.R.; Lira, C.T. *Introductory Chemical Engineering Thermodynamics* (2ed.); Prentice Hall: Upper Saddle River, NJ, **1999.**

(2) Matsoukas, T. *Fundamentals of chemical engineering thermodynamics;* Prentice-Hall: Upper Saddle River, NJ, **2013**.

(3) Walas, S.M. *Phase Equilibria in Chemical Engineering*; Butterworth: Boston, **1985**.

(4) Callen, H.B., *Thermodynamics and an introduction to thermostatistics* 2ed; John Wiley & Sons: New York, **1985**.

(5) Kontogeorgis, G.M.; Folas, G.K. *Thermodynamic models for industrial applications;* John Wiley & Sons Ltd.: West Sussex, United Kingdom, **2010**.

(6) Michelsen, M.L.; Mollerup, J.M. *Thermodynamic Models: Fundamentals & Computational Aspect;* Tie-Line Productions: Denmark, **2007.**

(7) Sandler, S.I., *Chemical and Engineering thermodynamics*; John Wiley & Sons: New York, **1989**.

(8) Prausnitz, J.M.; Lichtenthaler, R.N.; Gomes de Azevedo, E., *Molecular thermodynamics of fluid phase equilibria* 3ed; Prentice hall PTR: Upper Saddle River, New Jersey, **1999**.

Chapter 6 - Thermodynamic modelling using Equations of State.

Introduction

The following chapter goes over the classes of equations of state used in Chapters 9 and 10. It does not represent novel work, but rather provides working knowledge of the equations used, their reasons for being used, strengths, and also weaknesses. The following Chapter is a review of literature on equations of state, with increased focus on the pertinent equations of state used in later chapters.

History of the cubic Equation of State:

The petroleum and chemical industry heavily relies on cubic equations of state because they are simple, fast, and for non-polar molecules (i.e., hydrocarbons) quite accurate. They are also capable of high pressure phase equilibrium calculations.[1] For this reason many reservoir simulations use cubic equations of state. Only a few of the equations of state available are shown below. A detailed list is provided by Poling, Prausnitz, and O'Connell.[2] The use of a single binary interaction parameter is often satisfactory and makes the models easy to optimize. Even in the event that temperature dependant binary interaction parameters are used, or a second binary interaction parameter, the cubic equations are still the simplest and fastest. In simulations where high amounts of iteration are required, speed is a necessity and for the foreseeable future cubic equations will be favored in petroleum simulation due to their speed. There are also large databases of parameters built up over time that makes cubic equations easy to apply for almost every practical hydrocarbon mixture of interest.

The very first equation of state was the ideal gas law, which is entirely empirical. In the year 1873 van der Waals published the first cubic equation of state, which is semi-empirical.[3] Van

der Waals' equation (and the class) is cubic because when either the volume or compressibility factor is solved for, three roots are found. This has proven to be incredibly valuable since the largest root corresponds to the volume of the gas phase, and the smallest volume root corresponds to the liquid root. The third (middle) root is classed as non-physical but has its place in calculating saturation pressures for isotherms. While the ideal gas law is a simple equation relating P-V-T properties (PV= nRT), van der Waals recognized that it was too simple. He understood that molecules interact, attracting and repulsing each other, and also that there was a hard-core volume which a real system could not go below (the volume if you pushed all of the molecules together so that there was no space between them. In the limit of infinite pressure the ideal gas law predicts a volume of zero exists, which is impossible).

Van der Waals (vdW)

As a result he expanded the ideal gas equation into Equation 6.1:

$$P = \frac{RT}{V-b} - \frac{a}{V^2} \qquad 6.1$$

The "a" term (Equation 6.2) represents the first attempt at quantifying the attraction of molecules, and is calculated with the critical properties of temperature and pressure, which is very convenient. Once the critical properties of a molecule have been calculated, they are available forever (i.e., are unchanging), allowing rapid calculation of thermodynamic properties at a variety of pressures and temperatures. The "b" term (Equation 6.3) represents the hard-core volume.

$$a = \frac{27}{64}\frac{(RT_c)^2}{P_c} \qquad 6.2$$

$$b = \frac{1}{8}\frac{RT_c}{P_c} \tag{6.3}$$

The van der Waals equation is accurate for several simple molecules and qualitatively good for many non-polar molecules.

Redlich—Kwong (RK)

Cubic equations of state had to wait until Redlich and Kwong (RK)[4] in 1949 modified the repulsion term in Equation 6.1, to make a leap in accuracy and robustness. The RK cubic equation of state is given below in Equations 6.4 to 6.6. The RK equation of state is very similar to the van der Waals equation. According to Walas, Redlich and Kwong did not have any particular reason for making the changes to the van der Waals equation that they did, and they were not the first to try changing the attraction term; however, they were the first to make changes that significantly improved the van der Waals equation of state.[5] The RK equation is given as:

$$P = \frac{RT}{V-b} - \frac{a}{V(V+b)\sqrt{T}} \tag{6.4}$$

$$a = 0.42748\frac{R^2T_c^{2.5}}{P_c} \tag{6.5}$$

$$b = 0.08664\frac{RT_c}{P_c} \tag{6.6}$$

The RK equation of state is mostly of historical value. The RK as well as van der Waals equations are known for having unsatisfactory vapor pressures away from the critical point.[1]

Soave—Redlich—Kwong (SRK)

It was the 1970's that brought classical cubic equations of state to their near final elevation as far as accuracy, speed and usability are concerned. In 1972 Soave[6] coupled the Pitzer acentric

factor "ω" with the "a" term forming the SRK equation of state below in Equations 6.7 to 6.12. Soave calculated the constants in Equation 6.12 by evaluating the reduced vapor pressure at a reduced temperature of 0.7 (Equation 6.7), over a range of ω= 0 to 0.5.[7] No experimental data is required to calculate the constants this way.

$$P_r^{sat} = 10^{-1-\omega} \text{ at } T_r = 0.7, \text{ where } P_r = {}^{P}/_{P_c} \quad 6.7$$

$$P = \frac{RT}{V-b} - \frac{a(T)}{V(V+b)} \quad 6.8$$

$$a = 0.42748 \frac{(RT_c)^2}{P_c} \quad 6.9$$

$$b = 0.08664 \frac{RT_c}{P_c} \quad 6.10$$

$$a(T) = a\left[1 + m\left(1 - \sqrt{T_r}\right)\right]^2 \quad 6.11$$

$$m = 0.48 + 1.574\omega - 0.176\omega^2 \quad 6.12$$

Peng—Robinson (PR)

In 1976 Peng and Robinson[8] (PR) made what is probably the most well-known equation of state. The Peng—Robinson equation of state is very similar to the SRK equation of state as can be seen in Equations 6.13 to 6.17. The main difference is that Peng and Robinson calculated the three constants in Equation 6.17 using residual sum of the squares to reduce the difference between experimental and predicted vapor pressures from the boiling point to critical point.[7] The PR has improved liquid densities over the SRK, however the differences are small in VLE.[7]

$$P = \frac{RT}{V-b} - \frac{a(T)}{V(V+b)+b(V-b)} \quad 6.13$$

$$a = 0.45724 \frac{(RT_c)^2}{P_c} \quad 6.14$$

$$b = 0.07780\frac{RT_c}{P_c} \quad 6.15$$

$$a(T) = a\left[1 + m\left(1 - \sqrt{T_r}\right)\right]^2 \quad 6.16$$

$$m = 0.37464 + 1.54226\omega - 0.26992\omega^2 \quad 6.17$$

The Peng—Robinson equation of state was made specifically for the oil and gas industry and the data used to regress the parameters in equation 6.17 were for lighter hydrocarbons. For this reason, the Peng—Robinson equation loses accuracy when calculating polar components and higher boiling hydrocarbons.(7) Several correlations have been created to increase the accuracy in liquid density. The Mathias—Copeman volume translation is used in several major commercial simulators to increase prediction capabilities for polar compounds.(9) The Peng—Robinson equation of state was chosen to represent cubic equations of state in Chapters 9 and 10, and was used as the sole equation of state for the hydrocarbon systems in Chapters 3 and 4 because of its speed, accuracy, and ease of programming for hydrocarbons.

Multi-component mixing rules

Cubic equations of state have an intrinsic assumption to them that must be understood: they calculate properties based on the input for a single fluid. Therefore, if a mixture is being investigated, mixing rules must be used to "mix" all of the properties of the pure fluids into that of a single hypothetical component, and then this single "mixed" component is input into the cubic equation of state. The most common mixing rules are the van der Waals one fluid (vdW1f), also known as classical mixing rules for the "a" term, and a simple combining rule is used for the "b" term.(9)

$$a = \sum_i^n \sum_j^n x_i x_j a_{ij} \; ; \quad 6.18$$

$$b = \sum_{i}^{n}\sum_{j}^{n} x_i x_j b_{ij} \tag{6.19}$$

$$a_{ij} = \sqrt{a_i a_j}(1 - k_{ij}); \tag{6.20}$$

$$b_{ij} = \frac{b_i + b_j}{2}(1 - l_{ij}) \tag{6.21}$$

However generally $l_{ij} = 0$ and b simplifies to

$$b = \sum_{i=1}^{n} x_i b_i \tag{6.22}$$

The terms k_{ij} and l_{ij} are empirical fitting parameters fit to experimental data to provide better accuracy. These parameters can greatly increase the accuracy of cubic equations of state. Parameter fitting is a very important to accurately calculate phase equilibria.

Virial Equation of State

The virial equation of state is a power series with respect to volume that is useable at low to medium pressures. It was developed by Thiesen in 1885. The compressibility factor can be written as[9]:

$$Z = 1 + \frac{B}{V} + \frac{C}{V^2} + \frac{D}{V^3} + \cdots \tag{6.23}$$

where B, C, D and so forth are the second, third, and fourth virial coefficients and represent intermolecular forces between two, three, four and so on molecules. Virial coefficients are dependant only on temperature; they are independent of pressure (or density) and composition.[12] Virial coefficients above C are not available since theoretical and experimental methods are not sufficient to provide qualitative results. Determining the B and C virial

coefficients is calculated by evaluating low pressure P-V-T data. By plotting the data in the form of isotherms, the intercept gives B and the slope is used to determine the C coefficient.[12] Not much is known about virial coefficients above C, and C is very seldom used itself. The virial equation is usually used in truncated form since accurate results have been found for low to medium pressures and experimental results for the third and higher coefficients are poor.[13]

$$Z = 1 + \frac{B}{V} = 1 + \frac{BP}{RT} \qquad 6.24$$

Virial equations of state have two major weaknesses: the first is that they can only be used for vapor phase calculations, and the second is that the virial equation cannot be used at high pressures.[9][12] This makes them ideal for pairing with activity coefficient models provided pressures are not high. The virial equation has been expanded to account for different phenomena over time, and one very important modification to it was done by Hayden and O'Connell when they applied the chemical theory to account for association, specifically the dimerization of carboxylic acids.

Extension of the virial equation of state to mixtures

The extension to mixtures is straight forward. For the second virial coefficient, the extension needs to account for the interactions between two molecules. The simplest case is that of a binary system. In this system there are three types of interaction. Each molecule can interact with other molecules of the same type i.e., *i*-*i*, and *j*-*j* interactions can occur for molecule *i* and molecule *j*. The third type of interaction is when molecule *i* and molecule *j* interact, i.e., *i*-*j*. The second virial coefficient for the three types of interactions are respectively as follows: B_{ii}, B_{jj}, and B_{ij}. The pure component second virial coefficient is calculated by evaluating an integral which incorporates the molecular interaction potential between pure component molecules, Γ_{ii}:

$$B_{ii} = 2\pi N_A \int_0^\infty \left[1 - e^{-\Gamma_{ii}(r)/kT}\right] r^2 dr \qquad 6.25$$

The extension to Bij is the same except the integral is evaluated using the intermolecular potential between unlike molecules, Γ_{ij}.

$$B_{ij} = 2\pi N_A \int_0^\infty \left[1 - e^{-\Gamma_{ij}(r)/kT}\right] r^2 dr \qquad 6.26$$

According to Prausnitz, it can be shown that the second virial coefficient of a mixture is a quadratic function of the mole fractions y_i and y_j. For a binary mixture the B_{mix} is:

$$B_{mix} = y_i^2 B_{ii} + 2y_i y_j B_{ij} + y_j^2 B_{jj} \qquad 6.27$$

The virial equation of state is often used for multicomponent systems in which case the mixing rule for the second virial coefficient is shown below:

$$B_{mix} = \sum_{i=1}^{NC} \sum_{j=1}^{NC} y_i y_j B_{ij} \qquad 6.28$$

Similar derivations can be used for higher order virial coefficients, however, this requires knowledge of their intermolecular potentials which is not as widely known as second virial coefficients. When the virial equation is truncated it is possible to calculate the second order coefficients from theory if experimental P-V-T data is not available.

In the next section the chemical theory is applied to the virial equation to make it usable for associating mixtures.

Hayden O'Connell equation of state

Hayden and O'Connell took the virial equation above (Eqn. 6.23) and used statistical mechanics to derive the second virial coefficient B.[14] In doing so they created an equation that could correlate polar and associating compounds with very good accuracy. Many properties in thermodynamics can be broken into a sum of the parts, the Helmholtz and Gibbs energy are two

common examples, but the second virial coefficient is another. Dividing the whole into parts is also a common approach taken in other models that are derived partly or entirely from statistical mechanics, for example the UNIQUAC equation and statistical associating fluid theory (SAFT). The second virial coefficient can be broken up as follows:

$$B_{total} = B_{Free} + B_{Metastable} + B_{Bound} + B_{Chem} \quad 6.29$$

The four terms on the right hand side of Equation 6.29 refer to the different intermolecular forces which contribute to the second virial coefficient. The first three terms on the right hand side of Equation 6.29 represent the nonpolar repulsion and attraction, and classical electrostatic interactions that are separate from chemical interactions such as the charge-transfer complexing of hydrogen bonding.[14] The fourth term accounts for chemical interactions such as polarity and association which at the time of publication of the Hayden O'Connell were considered non-classical contributions.

Hayden and O'Connell through the previous work of others,[12] assumptions, and empirical correlations, arrived at the following results for each of the terms:

$$B_{Free} = B_{Free-nonpolar} - b_o\mu^{*\prime}\left(0.75 - \frac{3}{T^{*\prime}} + \frac{2.1}{T^{*\prime 2}} + \frac{2.1}{T^{*\prime 3}}\right) \quad 6.30$$

$$B_{Free-nonpolar} = b_o\left(0.94 - \frac{1.47}{T^{*\prime}} - \frac{0.85}{T^{*\prime 2}} + \frac{1.015}{T^{*\prime 3}}\right) \quad 6.31$$

$$\frac{1}{T^{*\prime}} = \frac{\epsilon}{kT} - 1.6\omega' \quad 6.32$$

$$B_{Metastable} + B_{Bound} = b_o A\left[\frac{\Delta H}{kT/\epsilon}\right] \quad 6.33$$

Where:

$$b_o = \frac{2\pi}{3}N_0\sigma^3 \quad 6.34$$

$$A = -0.3 - 0.05\mu^* \quad 6.35$$

$$\Delta H = 1.99 + 0.2\mu^{*2} \quad 6.36$$

$$\mu^* = \frac{\mu^2}{\epsilon\sigma^3} \quad 6.37$$

And:

$$B_{chem} = b_o exp\left\{\eta\left[\frac{650}{\left(\epsilon/k + 300\right)} - 4.27\right]\right\}\left\{1 - exp\left[\frac{1500\eta}{T}\right]\right\} \quad 6.38$$

The theory is quite in depth and for a full understanding the original paper should be read. This however gives an over view of the main points to the equation of state. A Master's thesis by Walpot has an explanation from a programming point of view as well as MATLAB code for the Hayden O'Connell equation's (as well as UNIQUAC).[14]

Conclusion

Cubic equations of state have been proven reliable for hydrocarbon calculations and have many strengths and weaknesses. Their major strengths are that they are fast, easy to use and efficient for programming. They are also very fast to optimize. They can handle high pressures and can calculate vapor pressures up to the critical point. They are accurate for the VLE of hydrocarbons and non-polar molecules. There are large databases with interaction parameters to save time on optimizing. There are also group contribution methods available for predicting interaction parameters.[10] Their weaknesses are that they depend on critical properties which are not available for many heavy hydrocarbons. They suffer from an inability to properly predict polar molecules such as glycols, alcohols and associating molecules such as carboxylic acids. [1] Cubic equations struggle with LLE and VLLE; they also often require volume translation modifications to improve liquid density accuracies in VLE as well as LLE and VLLE. They often poorly represent Gibbs excess properties.[1]

The Hayden O'Connell equation's strength lies in its ability to fully describe intermolecular forces and use these to generate phase equilibria results. The short coming is that experimental techniques are not sophisticated enough to measure the required intermolecular potentials above

the third coefficient, and the theory is also not developed to a usable extent above the third viral coefficient. At low to medium pressures the truncated viral equation of state gives good representation of the compressibility factor to about one half the critical density and fair representation to nearly the critical density.[11] The virial and Hayden O'Connell equations cannot be used for any calculations other than the vapor phase. The ability to break the second virial coefficient into a sum of the contributing parts means that any phenomena, such as hydrogen bonding, can be included in the virial equation of state. Also, so long as the virial equation of state is truncated, theory can calculate second virial coefficients if experimental P-V-T data is not available. As with all equations of state, parameters regressed from quality experimental data is superior to theory, and this is true for the virial and Hayden O'Connell equations of state. When possible, second virial coefficients should be estimated from P-V-T data.

References

(1) Kontogeorgis, G.M.; Folas, G.K. *Thermodynamic models for industrial applications;* John Wiley & Sons Ltd.: West Sussex, United Kingdom, **2010**.

(2) Poling, B.E.; Prausnitz, J.M.; O'Connell, J.P. *Properties of gases and liquids*, 5ed; McGraw-Hill Education: New York, **2001**.

(3) Van der Waals, J.D. On the continuity of the gas and liquid state. Doctoral Dissertation, Leiden, **1873**.

(4) Redlich, O.; Kwong, J.N.S.; On the thermodynamics of solutions: V. an equation of state: fugacities of gaseous solutions. *Chem. Rev.***1949**, *44*, 233-244.

(5) Walas, S.M., *Phase equilibria in chemical engineering;* Butterworth Publishers: Boston, **1985**.

(6) Soave, G. Equilibrium constants from a modified Redlich-Kwong equation of state. *Chem. Eng. Sci.* **1972**, *27*, 1197-1203.

(7) Michelsen, M.L.; Mollerup, J.M., *Thermodynamic models: fundamentals & computational aspects*, 2ed; Tie-Line Publications: Denmark, **2007**, 81-82.

(8) Peng, D.Y.; Robinson, D.B.; A new two constant equation of state. *Ind. Eng. Chem. Fundam.,* **1976**, *15*, 59-64.

(9) Mathias, P. M.; Copeman, T. W. Extension of the Peng—Robinson equation-of-state to complex mixtures: Evaluation of the Various Forms of the Local Composition Concept. *Fluid Phase Equil.* **1983***, 13*, 91.

(10) Elliott, J.R.; Lira, C.T. *Introductory Chemical Engineering Thermodynamics;* Prentice Hall: Upper Saddle River, NJ, **1999**.
(11) Jaubert, J.N.; Mutelet, F., VLE predictions with the Peng—Robinson equation of state and temperature dependant kij calculated through a group contribution method, *Fluid Phase Equilibria*, **2004**, 224, 285.
(12) Prausnitz, J.M.; Lichtenthaler, R.N.; Gomes de Azevedo, E., *Molecular thermodynamics of fluid phase equilibria* 3ed; Prentice hall PTR: Upper Saddle River, New Jersey, **1999**.
(13) Hayden, J.G.; O'Connell, J.P. A generalized method for predicting second Virial coefficients. *Industrial Engineering and Chemistry Process Design and Development* **1975**, *Vol 14*, 209-216.
(14) Walpot, Henk. *Theoretical modelling of residue curve maps for a reactive distillation concept for the production of n-propyl propionate*; Master's Thesis, Technical University of Delft*;* **2011**

Chapter 7 - Thermodynamic Modelling using activity coefficient models

Introduction

Similar to Chapter 6, the content in Chapter 7 is a literature review of activity coefficient models. This includes their history, uses, strengths, and weaknesses. Activity coefficient models are an important class of models used frequently in industry, academia, and Chapters 9 and 10. The following descriptions are taken from literature.

History of the activity coefficient models

This section will begin by going over the history and equations of the activity coefficient models used in this work. Activity coefficient models are as old as the fugacity coefficient models, and actually progressed a little faster. Similar to the van der Waals initial cubic equation of state, van Laar and Margules came up with early and relatively simple activity coefficient models that were capable of handling non-ideal VLE mixtures quite accurately. Regular solution theory was the next step up from the van Laar and Margules type models and is still in use today in some niche areas.

As with the cubic equations of state, major advances came after the 1950s, but for activity coefficient models the 1960's was the decade of great progress when the theory of local compositions was introduced. Local composition models do not assume the mixture is completely randomly mixed. Wilson paved the way for local composition activity coefficient models with his publication in 1964.[(1)] While good at VLE calculations, Wilson's equation was unable to predict LLE. New models following Wilson's steps were created to overcome the shortfalls of the Wilson equation. The prolific John M. Prausnitz had a hand in the two most significant local composition models to follow Wilson's equation: the Non-Random-Two-Liquid

(NRTL) model and the Unified Quasi-Chemical (UNIQUAC) model. Both the NRTL and UNIQUAC are shown in detail later in this section, and both are used to calculate LLE and VLLE for the ternary systems designed to model Fischer—Tropsch synthesis products.

Activity coefficient models, regardless of the theoretical derivation, are also known as Gibbs Excess energy models because the activity coefficients are calculated from the excess Gibbs energy of the fluid mixture.

Random mixing models

Random mixing models such as the van Laar and Margules have largely been replaced by models whose derivations come from the local composition theory.(1) For this reason, only a short review is done on random mixing models, and no models are shown in equation form since they were not used for phase equilibria predictions in any of the previous or following chapters. The Margules equation was the first random mixing model and often gives good VLE results, even for highly non-ideal systems. The parameters in the Margules equation are regressed from binary VLE data. The Margules has not been used very much for multicomponent systems beyond ternaries.(1)

Van Laar was a student of van der Waals, and based his work on Equation 7.1, which is the van der Waals cubic equation manipulated to calculate excess Gibbs energy. It is possible to estimate activity coefficients from Equation 7.1. Kontogeorgis and Folas give the van der Waals equation in terms of excess Gibbs energy as:

$$\frac{G^{E,vdW}}{RT} = \left[\sum_i x_i \ln\left(\frac{V_i - b_i}{V - b}\right)\right] + \left[\frac{1}{RT}\left(\sum_i x_i \frac{a_i}{V_i} - \frac{a}{V}\right)\right] \qquad 7.1$$

The excess Gibbs energy for the van der Waals equation was shown here because it relates to random mixing models and led to the van Laar equation. More importantly, the excess Gibbs

form of the van der Waals cubic equation forms a link between cubic equations of state and activity coefficient models, which is the topic of Chapter 8. Until now equations of state were kept separate from activity coefficient models, with the exception of mentioning the use of an equation of state to model the vapor phase while separately using an activity coefficient to model the liquid phase.

The last aspect of the random mixing models is relevant in today's industries - the regular solution theory. Regular solution theory assumes that mixture interactions are independent of one another such that quadratic mixing rules provide reasonable approximations.[2] This theory is still in use for low pressure VLE and LLE, in pharmaceuticals for solid-liquid equilibria (SLE), polymer solutions in combination with Flory—Huggins mixing rules, and studies of drug release in polymers.[1]

The Margules, van Laar, and regular solution theories all struggle with complex systems such as alcohol-hydrocarbons and while capable of VLE, are significantly less capable of LLE.[3] For these reasons they were not considered for use in modelling Fischer—Tropsch products since alcohol-hydrocarbons and LLE are present.

Local composition theory

Unlike the van der Waals class of activity coefficient models, the random mixing models, the local composition theory does not assume everything is randomly mixed. By assuming that molecules can form local compositions the assumption that mixture interactions are independent of each other, as in the regular solution theory, is broken down. Local composition theory is an improvement on the regular solution theory, much like the activity coefficient is a correction to Raoult's law to account for deviations from ideality.

There are three well used and applied models based on local composition theory worth discussing. They are the Wilson equation, the NRTL, and the UNIQUAC equations. The Wilson equation was the first local composition equation, but is only capable of VLE. The Wilson equation was tested against the Margules and van Laar equations for over 100 components and was found to be as good as or better than both random mixing models for nearly all systems.[4] Despite its accuracy in VLE the Wilson equation is not capable of LLE and was therefore not considered for use in modelling Fischer—Tropsch products.

Non—Random—Two—Liquids (NRTL)

The NRTL model was designed to be an improvement to the Wilson equation and to also be capable of LLE prediction. In many equations of state, cubic equations of state being a good example, mixing rules are used to mix the pure component properties into a hypothetical pure fluid with average properties of the components in the mixture. The non-random part of the NRTL comes from the local composition theory assuming that mixing is not entirely random, and the two-liquids comes from extending the fundamental idea that properties can be mixed into not one hypothetical pure fluid, but two hypothetical pure fluids.[4]

According to Kontogeorgis and Folas, the excess Gibbs energy of a mixture can be calculated by the NRTL model as follows

$$\frac{G^E}{RT} = \sum_i x_i \frac{s_i}{r_i} \tag{7.2}$$

$$r_i = \sum_j x_j G_{ji} \tag{7.3}$$

$$s_i = \sum_j x_j \tau_{ji} G_{ji} \tag{7.4}$$

$$G_{ji} = exp(-a_{ij}\tau_{ji}) and\ a_{ij}=a_{ji} \tag{7.5}$$

$$\tau_{ji} = (g_{ji} - g_{ii})/RT \tag{7.6}$$

$$\tau_{ij} = (g_{ij} - g_{jj})/RT \quad (7.7)$$

Activity coefficients for mixtures can be calculated by the NRTL according to the following expression

$$ln\gamma_i = \frac{s_i}{r_i} + \sum_j \frac{x_j G_{ij}}{r_j}\left(\tau_{ij} - \frac{s_j}{r_j}\right) \quad (7.8)$$

In Equations 7.6 and 7.7, the g_{ji} parameters represent energy of interactions between molecule *i* and *j*. These parameters are not explicitly determined, but rather the differences as shown in Equations 7.5 and 7.6, which are represented by τ_{ji} and τ_{ij}, are determined from binary experimental data; usually from VLE data for miscible components, and LLE data for immiscible pairs. While the NRTL is listed as an excess Gibbs energy model, it does not have an entropic contribution and more formally could be called an excess enthalpy energy model.

Unified Quasi Chemical (UNIQUAC)

At the time of the derivation of UNIQUAC, data was quite scarce and often there was not enough to regress three meaningful parameters.[6] The UNIQUAC was an attempt to both improve the NRTL, as well as use only two parameters in order to make its parameters easier to regress. According to Kontogeorgis and Folas the excess Gibbs energy of a mixture can be calculated by UNIQUAC as follows:

$$\frac{G^E}{RT} = \sum_i x_i ln\frac{\Phi_i}{x_i} - \frac{Z}{2}\sum_i q_i x_i \, ln\frac{\Phi_i}{\vartheta_i} - \sum_i q_i x_i \, lnS_i \quad \text{where Z = 10} \quad (7.8)$$

$$S_i = \sum_j \vartheta_j \tau_{ji} \quad (7.9)$$

$$\Phi_i = \frac{r_i x_i}{\sum_j r_j x_j} \quad (7.10)$$

$$\vartheta_i = \frac{q_i x_i}{\sum_j q_j x_j} \quad (7.11)$$

Activity coefficients for mixtures can be calculated by UNIQUAC according to the following expressions

$$ln\gamma_i = ln\gamma_i{}^{comb} + ln\gamma_i{}^{res} \quad 7.12$$

$$ln\gamma_i{}^{comb} = ln\left(\frac{\Phi_i}{x_i}\right) + 1 - \left(\frac{\Phi_i}{x_i}\right) - \frac{Z}{2} q_i \left(ln\left(\frac{\Phi_i}{\vartheta_i}\right) + 1 - \frac{\Phi_i}{\vartheta_i}\right) \quad 7.13$$

$$ln\gamma_i{}^{res} = q_i \left(1 - lnS_i - \sum_j \frac{\tau_{ji}\vartheta_j}{S_i}\right) \quad 7.14$$

The UNIQUAC model differs from the NRTL model in its derivation, using a combinatorial and residual contribution part, shown for activity coefficients in Equation 7.12. The combinatorial part is determined by composition, and size and shapes of the molecules. There are no intermolecular forces included in the combinatorial part. Intermolecular interactions are included only in the residual term, thus the two adjustable binary parameters are found in the residual contribution (Equation 7.9).

Conclusion

Activity coefficient models have been in use for over 100 years and are often highly adept at modelling multicomponent VLE with high accuracy using only two or three adjustable binary interaction parameters. The oldest models assumed that mixtures were entirely randomly mixed which is not always true. Polar and associating molecules will tend to form around each other excluding non-polar molecules. As such, these models using what has been called the van der Waals type approach have been largely left to history, although the regular solution theory is still practiced in some applications. Since the development of local composition theory, models based on non-random mixing have taken prevalence in VLE, LLE and VLLE modelling of both ideal and highly non-ideal mixtures.

There are three widely used local composition models: the Wilson equation, NRTL and UNIQUAC. The Wilson equation, while being the first local composition model, is incapable of LLE behavior, rendering it unusable for any prediction in Fischer—Tropsch VLLE. The NRTL and UNIQUAC equations are both highly popular models for multicomponent VLE, and are also capable of LLE and VLLE, although they have been found to require careful parameter fitting.[5] They have both been found to exhibit serious problems representing LLE and VLLE well, especially in the presence of highly polar and hydrogen bonding compounds (water, acids, etc.).[1] A note on issues regarding the representation of water and acetic acid is that all models have issues, even advanced models like SAFT and cubic-plus-association (CPA) equations of state.[6][7]

References

(1) Kontogeorgis, G.M.; Folas, G.K. *Thermodynamic models for industrial applications;* John Wiley & Sons Ltd.: West Sussex, United Kingdom, **2010**.

(2) Elliott, J.R.; Lira, C.T. *Introductory Chemical Engineering Thermodynamics;* Prentice Hall: Upper Saddle River, NJ, **1999**.

(3) Matsoukis, T. *Fundamentals of chemical engineering thermodynamics;* Prentice-Hall: Upper Saddle River, NJ, **2013**.

(4) Prausnitz, J.M.; Lichtenthaler, R.N.; Gomes de Azevedo, E., *Molecular thermodynamics of fluid phase equilibria* 3ed; Prentice hall PTR: Upper Saddle River, New Jersey, **1999**.

(5) Prausnitz, J.M.; Anderson, T.F.; Grens, E.A.; Eckert, C.A.; Hsieh, R.; O'Connell, J.P., *Computer calculations for multicomponent vapor—liquid and liquid—liquid equilibria;* Prentice-Hall, Inc., Engelwood Cliffs, New Jersey, **1980**.

(6) Breil, M.P.; Kontogeorgis, G.M.; Behrens, P.K.; Michelsen, M.L., Modelling of the thermodynamics of the Acetic Acid-water mixture using the cubic-plus-association equation of state, *Industrial & Engineering Chemistry Research* **2011** *50* (9), 5795-5805

(7) Yushu, C.; Afef, A.; Fabrice, M.; Roland, S.; Jeday, M.R., Thermodynamics modelling of mixtures containing carboxylic acids using the PC-SAFT equation of state. *Industrial & Engineering Chemistry Research* **2012** *51*, 13846-13852.

Chapter 8 - Thermodynamic modelling using advanced excess Gibbs energy cubic equations of state.

Introduction

The following chapter provides a literature review on a hybrid class of models known as excess Gibbs energy cubic equations of state. These models combine the activity coefficient models in Chapter 7 with the cubic equations of state in Chapter 6. They are often used in industry and are used in Chapters 9 and 10 to predict VLE, LLE and VLLE. It is therefore worthwhile to review their development, uses, strengths, and weaknesses.

Development of EOS/G^E models

In Chapter 6 equations of state were discussed and in Chapter 7 activity models were discussed. In Chapter 8 a class of hybrid models is discussed that incorporates activity coefficient models inside cubic equations of state mixing rules. There are several forms of mixing rules which include excess Gibbs energy models into the energy parameter mixing rules of a cubic equations of state. The most common three are the infinite pressure Huron—Vidal, zero pressure modified Huron—Vidal, and Wong—Sandler derivations. In chapters 9 and 10, results for the excess Gibbs energy equation of state are based on the original Huron—Vidal[(1)] mixing rules and are used with the advanced Peng—Robinson cubic equation of state in VMGSim. The reason for choosing the Huron—Vidal mixing rules out of the most common three was simple: VMGSim only offers the Huron—Vidal mixing rules. This chapter will not go into extensive details of the derivation of advanced mixing rules, however derivations are provided by Michelsen and Mollerup[(2)] as well by Kontogeorgis and Folas for the SRK[(3)]. As was shown in Chapter 7 for the van der Waals equation of state, cubic equations of state can be put in terms of excess Gibbs

energy. Shown below in Equation 8.1 is a generalized equation. For the Peng—Robinson $\delta_1 = 1 + \sqrt{2}$, and $\delta_2 = 1 - \sqrt{2}$. For the Soave—Redlich—Kwong $\delta_1 = 1$, and $\delta_2 = 0$.[2]

$$\frac{G^E}{RT} = \frac{P}{RT}\left(V_i - \sum_i z_i V_i\right) - \left(\ln(V-b) - \sum_i z_i \ln(V_i - b_i)\right) - \frac{1}{\delta_2 - \delta_1}\left(a \ln\left(\frac{V + \delta_2 b}{V + \delta_1 b}\right) - \sum_i z_i a_i \ln\left(\frac{V_i + \delta_2 b_i}{V_i + \delta_1 b_i}\right)\right) \quad 8.1$$

This can be rearranged (with a lot of algebra) so that Equation 8.1 is given in terms of the "a" mixing parameter (Equation 6.11 and 6.16):

$$a = \sum_i z_i a_i - \frac{1}{\Delta}\frac{G^E_\infty}{RT} \quad 8.2$$

The infinity symbol (∞) in the excess Gibbs energy terms means that infinite pressure was assumed for this derivation. $\Delta = \frac{1}{\delta_2 - \delta_1} \ln \frac{1+\delta_2}{1+\delta_1}$. From Chapter 7 the excess Gibbs energy of any activity coefficient model can be inserted into equation 8.2, and then Equation 8.2 can be used in a cubic equation of state instead of the traditional Equations 6.11 and 6.16. Huron and Vidal chose to use a modified NRTL[2]:

$$\frac{G^E_\infty}{RT} = \sum_i z_i \frac{\sum_j z_i b_j \exp\left(-\alpha_{ij}\frac{C_{ij}}{RT}\right) C_{ji}}{\sum_j z_j b_j \exp\left(-\alpha_{ji}\frac{C_{ji}}{RT}\right)} \quad 8.3$$

Where C_{ij} and C_{ji} are the interaction energies similar to those given in Equations 7.6 and 7.7 and α_{ij} is the non-randomness parameter. This is very similar to the expression derived in chapter 7 for the NRTL.

There are several advantages to using an activity coefficient model inside of a cubic equations mixing rules. Cubic equations can be used at high pressures, near critical points and for vapor and liquid phases. What they lack is accuracy with polar components. By combining activity

coefficients with cubic equations of state, the cubic equation loses none of its utility but gains the ability to be used for polar molecules, which was the largest weakness of the cubic equation class. When a cubic equation is used separately for the vapor phase, and an activity coefficient model is used for the liquid phase, rather than the two being combined via mixing rules, the liquid phase can calculate non-ideality, however the vapor phase is limited to the cubic equation of states accuracy, which is low for polar components. There is also the issue of phase envelopes not converging at the critical points when Gamma—Phi modelling is used (when two separate models are used for specific phases).[2] In Fischer—Tropsch product modelling the use of Gamma—Phi modelling is acceptable since no critical phase boundaries are approached. However, for reservoir simulations that can be at very high pressures and temperatures, the issue of a phase boundary not converging would be more likely to be encountered. The Huron—Vidal excess Gibbs energy model has been used successfully for several water—oxygenate—hydrocarbon systems in which the oxygenate was glycol or methanol.[4-6]

Conclusion

From a theory perspective there is a lot to gain by using an activity coefficient model inside cubic equation of state mixing rules. The cubic equation gains the ability to model polar components without losing its appeal for high pressure calculations. Anywhere a cubic equation could be used, an advanced mixing rule cubic equation should also be capable of being used, and also, anywhere an activity coefficient model would be valid, and advanced mixing rule cubic equation of state should also be valid.

One issue is that depending on the derivation for the advanced mixing rule cubic equation of state, databases with interaction parameters may no longer be useable for the activity coefficient once it is inside the mixing rules. For example, as was developed in Chapter 5, the excess Gibbs

energies are often derived at low pressure. The low pressure assumption is often the case for local composition models.[3] If the advanced mixing rule equation of state was derived at high pressures, such as was the Huron—Vidal (infinite pressure assumption), any interaction parameters estimated for activity coefficient models derived for low pressure excess Gibbs energy are no longer usable. In the case of VMGSim, which uses the Huron—Vidal with the NRTL, the Huron—Vidal being derived at infinite pressure, the NRTL at low pressure, all interaction parameters for the NRTL are not valid and are assigned zero by default. Regressing the parameters for a model can consume a lot of time. In VMGSim, activity coefficient models can often spend hours trying to converge on optimized parameters, only to fail and need to be restarted with new initial guesses. It is possible to calculate interaction parameters using the UNIFAC group contribution method, however in VMGSim, this is not enabled for the Huron—Vidal. UNIFAC is used in VMGSim for the NRTL on its own, and the UNIQUAC model, and possibly others which were not of interest for the modelling of Fischer—Tropsch synthesis products.

References

(1) Huron, V.J.; Vidal, J. New mixing rules in simple equations of state for representing vapor-liquid of strongly non-ideal mixtures. *Fluid Phase Equilibria* **1979**, *Vol. 3*, pp 255-271.

(2) Michelsen, M.L.; Mollerup, J.M., *Thermodynamic Models: Fundamentals & Computational Aspect;* Tie-Line Productions: Denmark, **2007.**

(3) Kontogeorgis, G.M.; Folas, G.K. *Thermodynamic models for industrial applications;* John Wiley & Sons Ltd.: West Sussex, United Kingdom, **2010**.

(4) Pedersen, K.S.; Michelsen, M.L.; Fredheim, A.O. Phase equilibrium calculations for unprocessed well streams containing hydrate inhibitors. *Fluid Phase Equilibria*, **1996**, *126*, 13-26.

(5) Neau, E.; Nicolas, C.; Jaubert, J. N.; Mutelet, F. The generalized NRTL model associated with the Peng—Robinson equation of state to predict liquid—liquid equilibria between hydrocarbons, water, and ethylene glycol. *Polish Journal of Chemistry,* **2006**, *80*, 27

(6) Pedersen, K. S.; Milter, J.; Rasmussen, C. P. Mutual solubility of water and a reservoir fluid at high temperatures and pressures – experimental and simulated data. *Fluid Phase Equilibria*. **2001**, *189*, 85-97.

Chapter 9 - Binary parameter optimization for classical to advanced mixing rule models.

Introduction

Previously in Chapters 6-8 the theoretical origins of several different types of models were reviewed and their abilities for phase equilibria were discussed. In Chapter 9 the semi-empirical nature of these models will be explored. Parameter optimization is as important as model selection. Phase equilibria modelling cannot take place without careful consideration of the best suitable model (Chapters 6-8), as well as the often tedious but necessary optimization and fitting of binary interaction parameters to experimental data. As has been said in previous chapters, the VLLE behaviour of Fischer—Tropsch synthesis products is modelled in Chapter 10. The following sections in Chapter 9 will go over the methodology used in selecting the models used in Chapter 10, the types of data used to optimize each models binary interaction parameters, as well as the results given in figure form for each of the data sets evaluated, showing the fitting of each model. This provides easy comparison between each models ability at predicting VLE and mutual solubility. Modelling VLE is not however any indication of a models capabilities for LLE and VLLE modelling. These more difficult types of phase behavior are handled solely in Chapter 10. The Figures 9.1 to 9.6 were plotted by asking VMGSim to predict bubble and dew pressures or temperatures, depending on the data type, at composition intervals of 0.01. These points were then plotted in Microsoft Excel.

Methodology

Thermodynamic models for the description of the VLLE of water—oxygenate—hydrocarbon systems were evaluated. The following methodology was employed:

(a) Representative thermodynamic models of each class of model description were selected for evaluation. In order to make the work as generally useful as possible, the models that were selected, were models typically found in commercial process simulation software.

(b) The next step was to gather published experimental liquid—liquid equilibrium (LLE)/VLLE data on representative ternary systems, and the necessary VLE and mutual solubility data for the constituent binary systems of each ternary. These ternary systems are simpler than the mixtures produced during Fischer—Tropsch synthesis, which is a shortcoming. Being simpler, the ternary systems made it easier to analyze the results to determine why thermodynamic models provided an adequate description, or not.

(c) The selected thermodynamic models were employed to predict the LLE/VLLE data. The calculations were performed using the implementation of the different thermodynamic models in the VMGSim process modelling software. In principle other software implementations should give the same results, although in practice there are sometimes differences. The difference in the calculated values (x_{calc}) from the experimental values ($x_{\exp}$) were expressed as an absolute average percentage difference (AAPD) of the number of data points (n) by Equation 1.

$$AAPD = \frac{100}{n}\sum_{i=1}^{n}\left|\frac{(x_{\exp})_i - (x_{calc})_i}{(x_{\exp})_i}\right| \qquad 9.1$$

(d) The performance of each of the thermodynamic models was evaluated. The objective was not a numeric analysis (that is included irrespective), but an analysis of the underlying reasons for the performance of the model. By doing so more generalized statements could be made about the suitability of classes of thermodynamic model descriptions.

Thermodynamic model selection

At equilibrium it is a necessary and true condition for each component in a mixture to have equal chemical potentials in each phase. It is equivalent to say that each component in a mixture must have the same fugacity in each phase.

As applied in process simulation software, thermodynamic models are used to calculate the fugacities of each component in each phase. Appropriate algorithms are applied to ensure that mole and energy balance constraints, as well as stability requirements are also met.

The degree to which the equilibrium calculation matches the reality, depends on how accurately the thermodynamic model describes the fugacity of each component in each phase. This is not an easy task for non-ideal mixtures. Many models poorly predict equilibrium compositions. The reason for poor predictions can often be found in the theoretical derivation of the model that included simplifications and assumptions that are invalid for non-ideal mixtures. Many models in process simulation software are therefore at least semi-empirical in nature.

There are four types of commonly used models: (a) classical cubic equations of state, (b) advanced mixing rule cubic equations of state, (c) activity coefficient models, and (d) virial equations of state. Advanced mixing rule cubic equations of state are cubic equations of state that incorporate activity coefficient models in their mixing rules.

Newer models, such as the statistical associating fluid theory (SAFT), and cubic-plus-association (CPA), are slowly gaining acceptance. These models are more complex, but in principle offer better predictive capability.[1] However, SAFT and CPA models are not yet widely found in major process simulation software. Part of the reason is the computation effort required, since these models are quite complicated compared to cubic, virial, or activity coefficient models.

One model of each type was selected for evaluation (Table 9.1).[2][3] The Peng—Robinson equation was chosen to represent cubic equations of state. In literature the Peng—Robinson model is commonly used for hydrocarbons, as well as for VLE calculations in Fischer—Tropsch reactors. The implementation of the Peng—Robinson model that was used included a correction for liquid volume estimation.[4] The Huron—Vidal Peng—Robinson equation plus non-random two liquid description was chosen as the advanced mixing rule model to show the influence modification of mixing rules can have on cubic equation of state phase equilibria predictions. The description of association is important for compounds such as carboxylic acids (acetic acid in the data sets employed for this study). The non - random two liquid (NRTL) and universal quasi-chemical (UNIQUAC) activity coefficient models are the two most common models used for non-ideal liquid calculations.[2] The Hayden—O'Connell equation was chosen as the vapor phase virial equation of state, because it combines the virial equation with chemical theory to account for association.

VLLE of water—oxygenate—hydrocarbon systems

Equilibrium data selection

In general the models used in process simulators are either semi-empirical or entirely empirical, there are no models that are entirely theoretical. All of the chosen models (Table 9.1) were semi-empirical and ideally required empirical optimizing prior to being used for ternary LLE and VLLE calculations.

Table 9.1 Thermodynamic models and model types evaluated.

Model	Model Type	Reference
Peng—Robinson	Cubic Equation of State	(2)
Huron—Vidal Peng—Robinson	Advanced mixing rule Cubic Equation of State	(2)
NRTL	Activity Coefficient	(2)
UNIQUAC	Activity Coefficient	(2)
Hayden O'Connell	Virial + Chemical Theory	(3)

Despite Fischer—Tropsch technology being a mature and significant industry, published data that involves hydrocarbons—oxygenates—water is limited. What data is available and relevant, is at ambient pressure. This is an unfortunate limitation of the current evaluation, since the intended application of the work is for VLLE calculations at elevated pressure. Furthermore, in an actual Fischer—Tropsch reaction product there are many components and it is impractical to obtain equilibrium data for each possible binary pair. Out of necessity, and to make this a practical endeavor, only the types of data likely to be available in a larger context was used, i.e. VLE data for miscible pairs and mutual solubility data for immiscible pairs.

VLE data was employed to fit binary interaction parameters for the miscible pairs of components (Table 9.2),[5-12] and mutual solubility data was used for the water—hydrocarbon (immiscible) pairs (Table 9.2).[13][14] The ternary data sets that were employed for model evaluation are summarized in (Table 9.2).[15-17] The data was used as published.

T**able 9.2** Origin of experimental data employed for optimizing and modelling.

Compounds	Measurement range covered		Reference
	temperature (K)	pressure (kPa)	
Binary systems			
water—acetic acid	373.15 to 391.65	101.325	(5-8)
water—ethanol	351.26 to 373.15	101.325	(12) (DECHEMA) [a]
water—hexane	273.15 to 313.15	101.325	(13)(IUPAC-NIST) [a]
water—heptane	273.15 to 318.15	101.325	(14)(IUPAC-NIST) [a]
acetic acid-hexane	313.2 to 391.25	10.5 to 101.325	(9)(11)(DECHEMA)
Ethanol—heptane	344.15 to 371.15	101.325	(10)(DECHEMA) [a]
Ternary Systems			
water—acetic acid—hexane	298.15 and 304.15	101.325	(15)(16)
water—ethanol—heptane	341.87 to 352.39	101.325	(17)

[a] Multiple sources included in each data collection. Data from NIST was smoothed data from multiple sources provided by NIST. Data from DECHEMA was all sources at the temperatures and pressure listed.

Regression of fitting parameters

Optimizing models can become very time consuming and gets more complicated with each component added to the mixture. The very basic necessity is VLE data for the miscible pairs, followed by mutual solubility data for the immiscible pairs (typically the water—hydrocarbon pairs in the case of Fischer—Tropsch reaction products). In addition to these basic requirements for fitting, binary interaction parameters can also have experimental tie-lines from other ternaries that include their pair added into the regression routine. When available, experimental ternary tie-lines help increase the accuracy of binary interaction parameters significantly. While in the case of the selected ternaries it would be possible to increase accuracy by including experimental tie-lines into the regression routine, too few are available for the vast majority of components.

The quality, type, and conditions of the available data (Table 9.2) affected the quality of fitting parameters that were regressed. The binary interaction parameters for the energy of interaction of component *i* with component *j* were optimized for all of the models. The optimized values for the fitting parameters and the default values in the process simulator are

given for the Peng—Robinson (Table 9.3), Huron—Vidal Peng—Robinson (Table 9.3), NRTL (Table 9.3), UNIQUAC (Table 9.3), and Hayden O'Connell (Table 9.3) thermodynamic models.

There are theoretical bounds in which some parameters should be limited during optimization, such as the Peng—Robinson interaction parameter being between negative one and positive one. In the NRTL model a third parameter, the nonrandomness parameter (α_{ij}) is supposed to be equal to $2/Z$, where Z is the coordination number, and is generally between 8 and 12. The α_{ij} parameter is typically set to a constant value of 0.2 or 0.3, thus making the NRTL a two parameter model, rather than a three parameter model.[2]

It was found that by allowing the nonrandomness parameter value to be free to take on any value (i.e., be entirely empirical), better fits were predicted. The NRTL model was therefore treated as a three parameter model in this work. Whenever possible the value of the nonrandomness parameter was kept positive to retain physical meaning, as originally designed by Renon and Prausnitz. However, Marina and Tassios[18] found that by allowing this parameter to be treated as purely empirical, improved fits could sometimes be found by allowing the nonrandomness parameter to have a negative value. They further found that $\alpha_{ij} = -1$ has nearly the same effect as $\alpha_{ij} = 0.3$ and that with $\alpha_{ij} = -1$, better predictions were made for immiscible binary components. In this work for hexane-water, allowing a negative value for the NRTL α_{ij} (Table 9.3) led to the best fit when dealing with the LLE ternary system of acetic acid—water—hexane.

Table 9.3 Default and optimized parameters for all thermodynamic models.

Peng—Robinson		
Binary systems	Optimized	Default [a]
	k_{12}	k_{12}
water (1) – acetic acid (2)	-0.1521	0
water (1) – ethanol (2)	-0.0875	-0.0911
water (1) – hexane (2)	0.4479	0.4669
water (1) – heptane (2)	0.4491	0.4606
heptane (1) – ethanol (2)	0.0600	0
hexane (1) – acetic acid (2)	0.0760	0

Huron—Vidal Peng—Robinson (Huron-Vidal)						
Binary systems	Optimized			Default a		
	b_{12} [b]	b_{21} [b]	α_{12}	b_{12} [b]	b_{21} [b]	α_{12}
water (1) – acetic acid (2)	465.780	298.770	0.7371	0	0	0
water (1) – ethanol (2)	765.948	161.814	0.3100	0	0	0
water (1) – hexane (2)	631.4449	1535.499	-0.3388	0	0	0
water (1) – heptane (2)	5899.55	2501.18	0.1527	0	0	0
heptane (1) – ethanol (2)	897.665	811.418	0.3583	0	0	0
hexane (1) – acetic acid (2)	-774.570	1668.11	0.0175	0	0	0

NRTL						
Binary systems	Optimized			Default [a]		
	b_{12} [b]	b_{21} [b]	α_{12}	b_{12} [b]	b_{21} [b]	α_{12}
water (1) – acetic acid (2)	588.870	-269.100	0.2000	575.678	-434.089	0.0077
water (1) – ethanol (2)	704.435	-85.009	0.2637	683.406	-71.3683	0.2981
water (1) – hexane (2)	300.920	392.948	-1.7827	1955.30	1552.14	0.3
water (1) – heptane (2)	5891.68	2031.30	0.2054	2158.74	1519.13	0.3
heptane (1) – ethanol (2)	716.773	615.327	0.4965	719.492	-566.693	0.3
hexane (1) – acetic acid (2)	639.220	631.090	0.5054	470.965	-470.965	0.3616

UNIQUAC				
Binary systems	Optimized		Default [a]	
	b_{12} [c]	b_{21} [c]	b_{12} [c]	b_{21} [c]
water (1) – acetic acid (2)	-387.953	347.839	-307.772	288.142
water (1) – ethanol (2)	-114.651	-35.1894	-114.386	-25.0915
water (1) – hexane (2)	-571.384	-1246.53	-300.026	-1318.01
water (1) – heptane (2)	-461.143	-1304.15	-300.031	-1308.01
heptane (1) – ethanol (2)	-586.574	77.4075	-601.794	93.2960
hexane (1) – acetic acid (2)	-284.317	-38.6999	-354.661	-0.2408

Hayden O'Connell[d]				
Binary systems	Optimized		Default [a]	
	a_{12} (NRTL)	a_{12} (UNIQUAC)	a_{12} (NRTL)	a_{12} (UNIQUAC)
water (1) – acetic acid (2)	3.06	3.47	2.5	2.5
water (1) – ethanol (2)	1.129	0	1.55	1.55

[a]Parameters provided by VMGSim using default settings.[b] $\tau_{ij} = b_{ij}/T$. [c] $\ln(\tau_{ij}) = b_{ij}/T$.[d]Binaries not shown for Hayden O'Connell were zero optimized and default.

The importance of optimization, as well as knowing the capabilities of a model, is illustrated below in Figure 9.1. A binary system of ethanol and heptane is modeled by the Peng—Robinson equation of state using several different binary parameter values. The optimized value has a significantly better fit to the experimental data.

Figure 9.1 VLE of ethanol (1)-heptane (2) at 101.325 kPa. Comparison of optimized Peng—Robinson (kij=0.059) with two un-optimized values. Experimental data from Table 9.2.

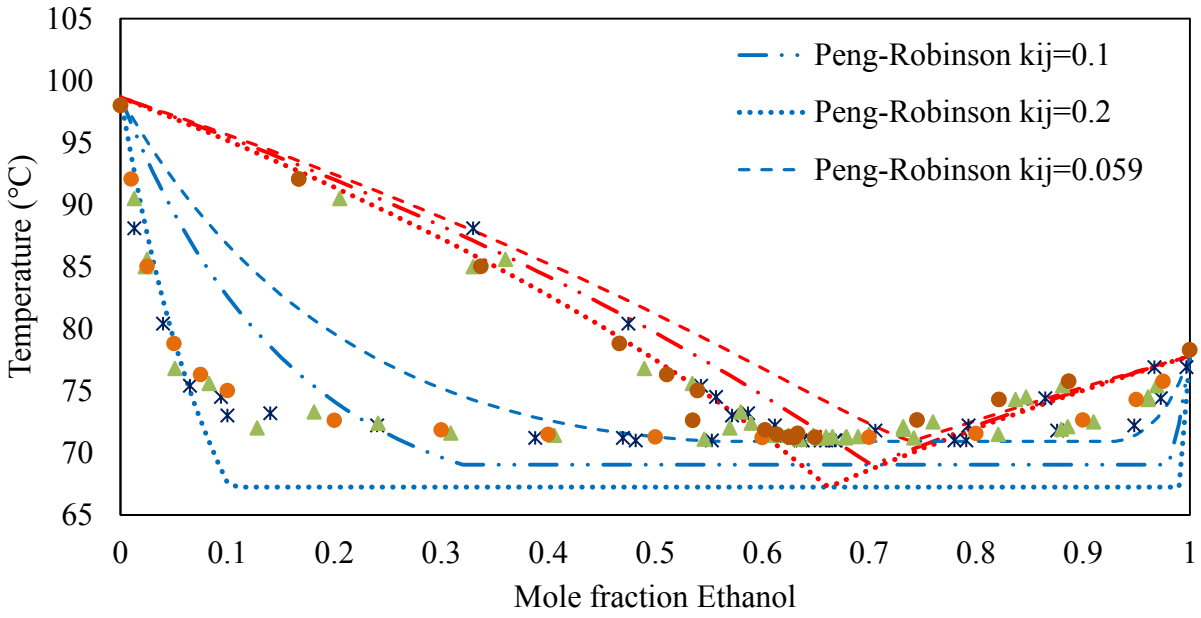

The results in Figure 9.1 have several significant messages. Firstly, optimization has significant influence on a models prediction capabilities. Secondly, even after optimization the fit may still be poor. This is the case with the Peng—Robinson in Figure 9.1. Despite being optimized, the accuracy is not satisfactory. This can be compared with Figure 9.2 which shows rest of the models fit to the same data as in Figure 9.1. All of the other models have better predictions for ethanol-heptane than the Peng—Robinson. Modelling is therefore not a matter of selecting a model, or optimizing, but is the combination of both. The best results require careful model selection as well as careful parameter optimization.

A third result of Figure 9.1 is that at times, depending on the range of conditions of the system of interest, it may be necessary to optimize to a very specific range. For example, in Figure 9.1 using interaction parameter of k_{ij} = 0.2 the bubble point temperature has significant error at ethanol concentrations higher than 5 mol %. However, using k_{ij} = 0.2 at concentrations less than 5 mol % ethanol would provide the best binary VLE bubble temperature predictions in the 0 to 5 mol % ethanol range. Due to the availability and accuracy of activity coefficient models, as is shown in Figure 9.2, it is not necessary to optimize based on specific composition ranges.

Results for VLE

Previously Figure 9.1 was shown to demonstrate the necessity of optimizing models. Figures 9.2 to 9.6 show the optimized fits of all of the models for each respective binary required for modelling the ternary LLE system water—acetic acid—hexane, and the VLLE ternary water—ethanol—heptane. VMGSim has built in model regression function for fitting binary parameters. This function was used with the absolute error minimisation option. VMGSim has several local minimum search algorithms available. The Nelder—Mead simplex algorithm was chosen to minimize the objective function. Once the minimum has been found VMG reports the value(s) of the binary interaction points which resulted in the minimum (Table 9.3). One issue with this method is that the true minimum represents a global minimum, but the search method is a local search method. As has been discussed by Kontogeorgis and Folas, there are often many sets of binary parameters which result in similar minimums.[2]

Table 9.4 VLE and MS error analysis.

Binary systems	Peng—Robinson	Gibbs Excess—Peng Robinson
	AAPD (%)	AAPD (%)
water—acetic acid	1.0	0.2
water—ethanol	0.8	0.6
water—hexane	26	25
water—heptane	26	25
heptane—ethanol	5	0.5
hexane—acetic acid	9	0.8[a]
Binary systems	NRTL + Hayden O'Connell	UNIQUAC + Hayden O'Connell
	AAPD (%)	AAPD (%)
water—acetic acid	0.2	0.2
water—ethanol	0.2	0.6
water—hexane	21	18
water—heptane	35	113
heptane—ethanol	0.5	1.0
hexane—acetic acid	1	6

[a]Does not include data by Arai et al. in regression. This modification resulted in better LLE accuracy.

These two factors make optimizing a tedious task. There is no guarentee that a minimum has truly been found, and it is likely that there is an alternative set of parameters that yield similar results in VLE, but could possibly yield different LLE or VLLE results. Table 9.4 below shows the error analysis for the VLE and mutual solubility optimization.

Ethanol—heptane VLE optimization

Shown below in Figure 9.2 are the results for the parameter estimation of the ethanol-heptane binary parameters. The optimized parameters are available in Table 9.3. Error analysis is provided above in Table 9.4. The Peng—Robinson equation had the largest error and this is clearly visible in the bubble and dew point predictions at concentrations below 0.7 mole fraction ethanol. The NRTL + Hayden O'Connell and Huron—Vidal Peng—Robinson both had the lowest errors at only 0.5 % AAPD. The UNIQUAC + Hayden O'Connell had a low error at 1.0 %.

Figure 9.2 VLE of ethanol—heptane at P = 101.325 kPa. Red is dew point temperature, blue is bubble point temperature. Experimental data is from Table 9.2.

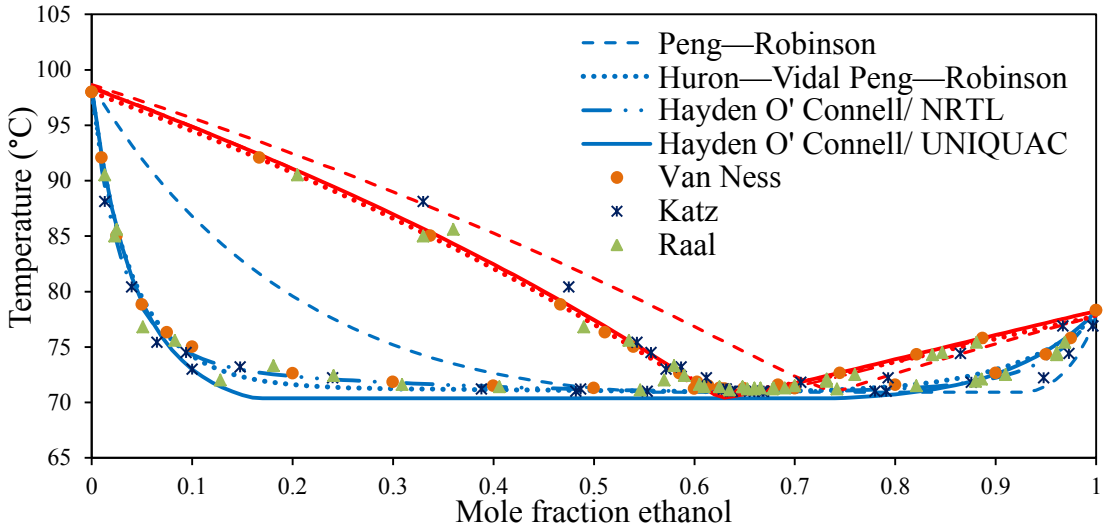

Hexane—acetic acid VLE optimization

Only one system was available that had bubble and dew point temperatures for acetic acid with hexane (Figure 9.3). Unfortunately this system was at reduced pressure (40 kPa). Two systems were found which allowed the calculation of the bubble temperature and were at atmospheric conditions, but the experimenters did not report any dew temperature points (Figure 9.4), thus limiting the quality of data available for optimizing the hexane—acetic acid binary interaction parameters. The optimized parameters are available in Table 9.3. Error analysis is available in Table 9.4. With the exception of the Huron—Vidal Peng—Robinson equation, all of the models were fit to all three data sets. The Huron—Vidal Peng—Robinson equation was found to exhibit better LLE predictions by excluding the data in Figure 9.4. While not shown, when regression for the Huron—Vidal Peng—Robinson equation included all sets, it was significantly better at capturing the association of acetic acid in the vapor phase in Figure 9.3 than the Peng—Robinson equation, however it was significantly worse than the Hayden O'Connell equation.

A second unfortunate lacking in experimental data was that no relevant data was found in which acetic acid was in a ternary with water and a hydrocarbon in VLLE conditions. Therefore, the VLE plot at reduced pressure (Fig 9.3) gives the only meaningful insight into the benefit of using the Hayden O'Connell model for associating mixtures. As can be seen in Figure 9.3, when the Hayden O'Connell model is used for the vapor phase with both the NRTL and UNIQUAC models it provides significantly better fits than the Peng—Robinson model, and as mentioned above, is significantly better than the Huron—Vidal Peng—Robinson model. Most of the error comes from predicting bubble and dew pressures at lower than 20 % acetic acid. This is unfortunate for Fischer—Tropsch synthesis products since acetic acid is always lower than 10 % of the product mixture.

Figure 9.3 VLE of hexane—acetic acid at T = 40.05 °C. Red is dew point pressure curve, blue is bubble point pressure curve. Experimental data is available from Table 9.2.

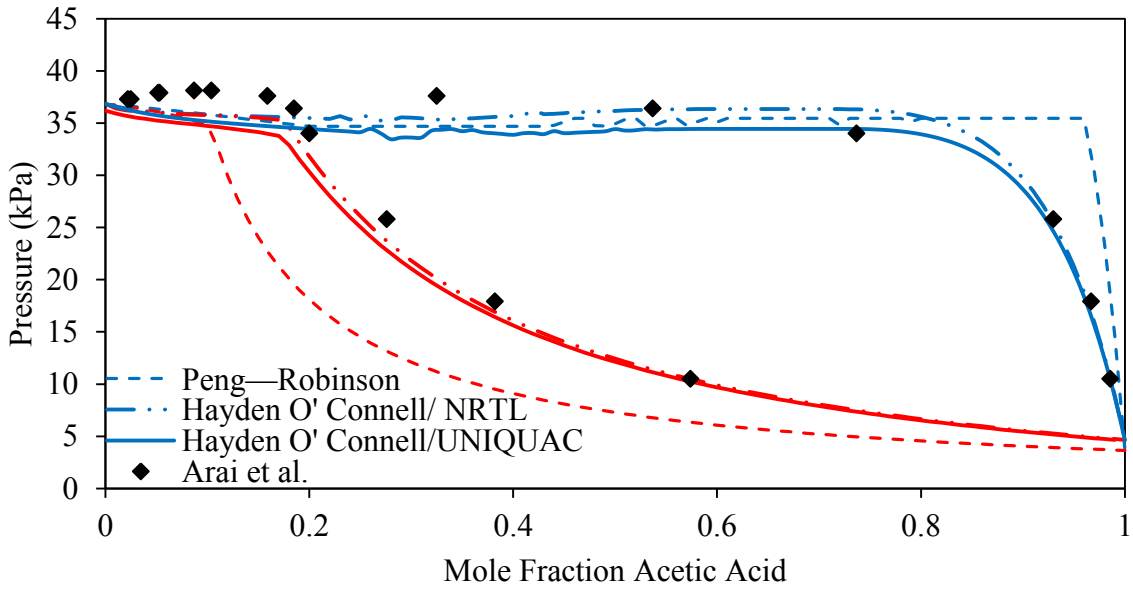

Figure 9.4 VLE of hexane—acetic acid at P = 101.325 kPa. Blue is bubble point temperature. Experimental data is from Table 9.2.

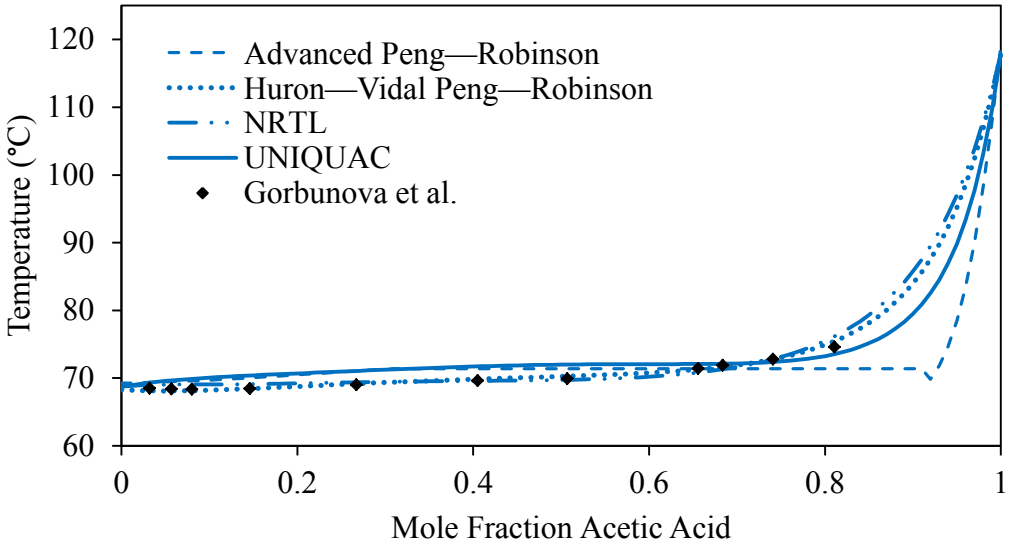

Water—ethanol VLE optimization.

Shown in Figure 9.5 is the water—ethanol atmospheric VLE binary system. Optimised parameters are available in Table 9.3 and error analysis is available in Table 9.4. The water—ethanol and water acetic acid systems are both well studied systems available at higher pressures. However, the LLE and VLLE systems studied in Chapter 10 are only available at atmospheric conditions so data was limited to atmospheric conditions for optimizing the water—ethanol and water—acetic acid binary interaction parameters. All of the models predicted the experimental data well. The Peng—Robinson had the largest error at 0.8 % AAPD, and the NRTL+ Hayden O'Connell and UNIQUAC + Hayden O'Connell had the smallest error at 0.2 % AAPD.

Figure 9.5 VLE of water—ethanol at P = 101.325 kPa.. Red is dew point temperature, blue is bubble point temperature. Experimental data from Table 9.2.

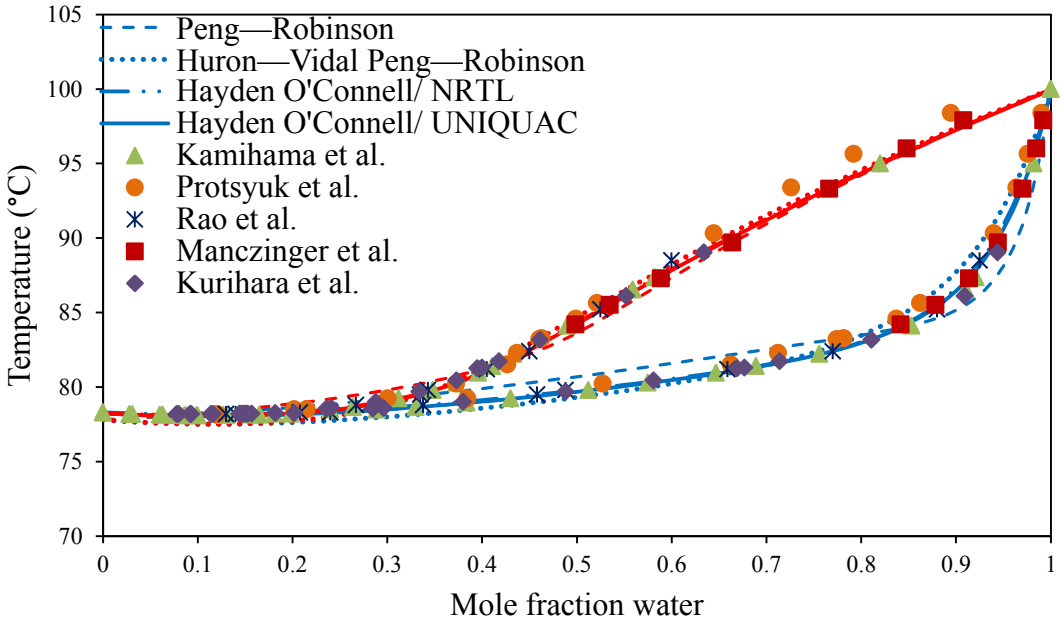

Water- acetic acid VLE optimization

The results for the water—acetic acid optimization is shown below in Figure 9.6 and comparison is made with the PC-SAFT equation of state using the same data in Figure 9.7. Optimized parameters are available in Table 9.3 and error analysis is shown in Table 9.4. The water—acetic acid binary VLE system is a well studied system in literature because all models struggle with accurately modelling it. It is particularly popular among SAFT modelling groups.[19][20] As can be seen, the activity coefficient models show comparable fits, even slightly better fits at rich concentrations of acetic acid. The PC-SAFT group reported 3.79 % absolute average deviation (AAD) for the water—acetic acid VLE. They do not show how they calculate their AAD. If it is the same as the AAPD reported in this work, then PC-SAFT offers no benefit to the VLE for water—acetic acid. In Figure 9.5 only the Peng—Robinson is clearly a worse choice of model for the water—acetic acid VLE modelling. All three models using activity coefficients had 0.2 % AAPD. Theoretically then all three are equally well suited for predicting water—acetic acid

VLE. These models should also represent acetic acid in the aqueous phase as well, or better than PC-SAFT.

Figure 9.6 VLE of water—acetic acid at P = 101.325 kPa. Red is dew point temperature, blue is bubble point temperature. Experimental data is from Table 9.2.

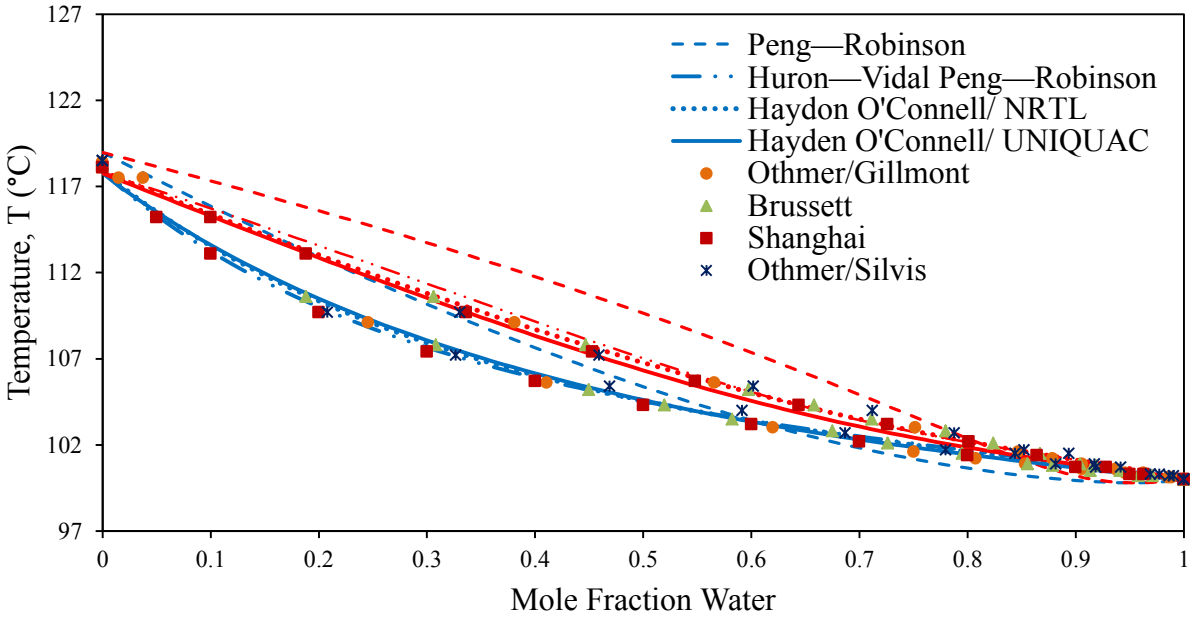

Figure 9.7 Literature PC-SAFT results for atmospheric water—acetic acid VLE, k_{ij} = -0.111. Reproduced with permission.[19]

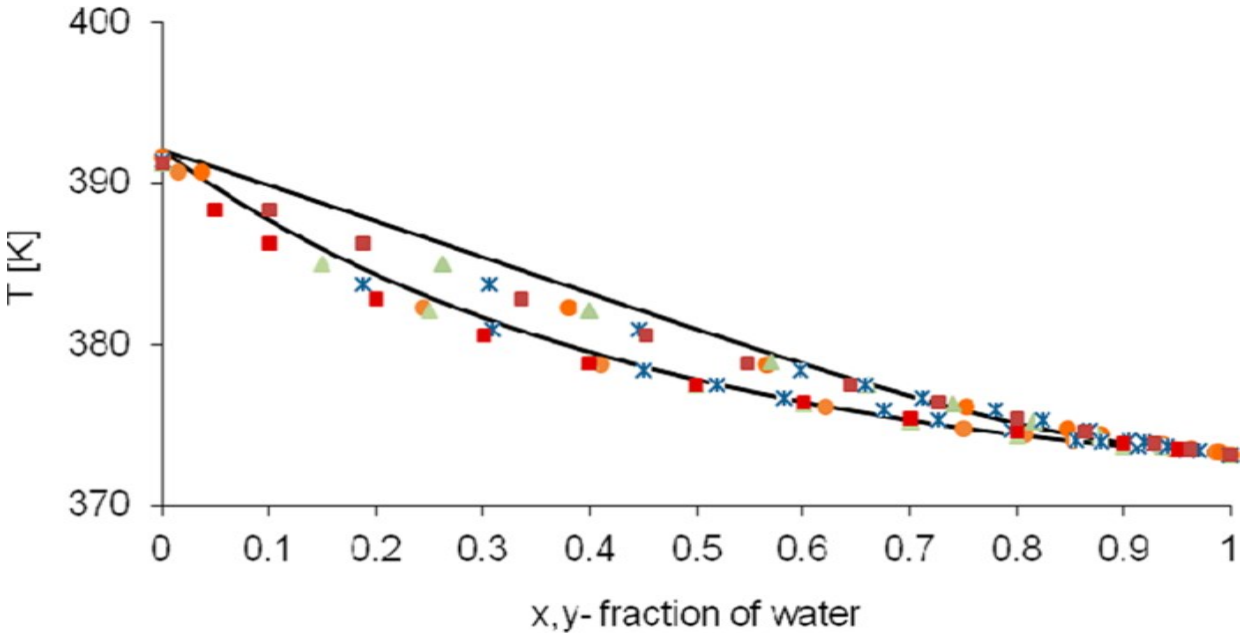

Results for mutual solubility

For miscible components VLE data is used for regression. In the case of immiscible components such as water—hydrocarbon mixtures VLE data is incredibly rare, and actually not very useful since it is quite likely that in multicomponent, multiphase systems water and hydrocarbons will form their own liquid phases (i.e. be in LLE). It is therefore necessary to make use of mutual solubility data which is available in a fairly wide range of temperatures. Pressure does not have as significant effect on mutual solubility so atmospheric conditions should generally be acceptable if data at the pressure of the system of interest are not available. Shown below in Figures 9.7 and 9.8 are the optimized results for the models tested (except there is no Hayden O'Connell since it only does vapor and this is LLE) on the water—hexane and water—heptane solubility data. Optimized parameters are available in Table 9.3 and error analysis is available in Table 9.4.

Figure 9.7 Mutual solubility for water—hexane at P = 101.325. Diamonds are experimental hexane in aqueous phase; squares are experimental data of water in hydrocarbon phase. Experimental data is from Table 9.2.

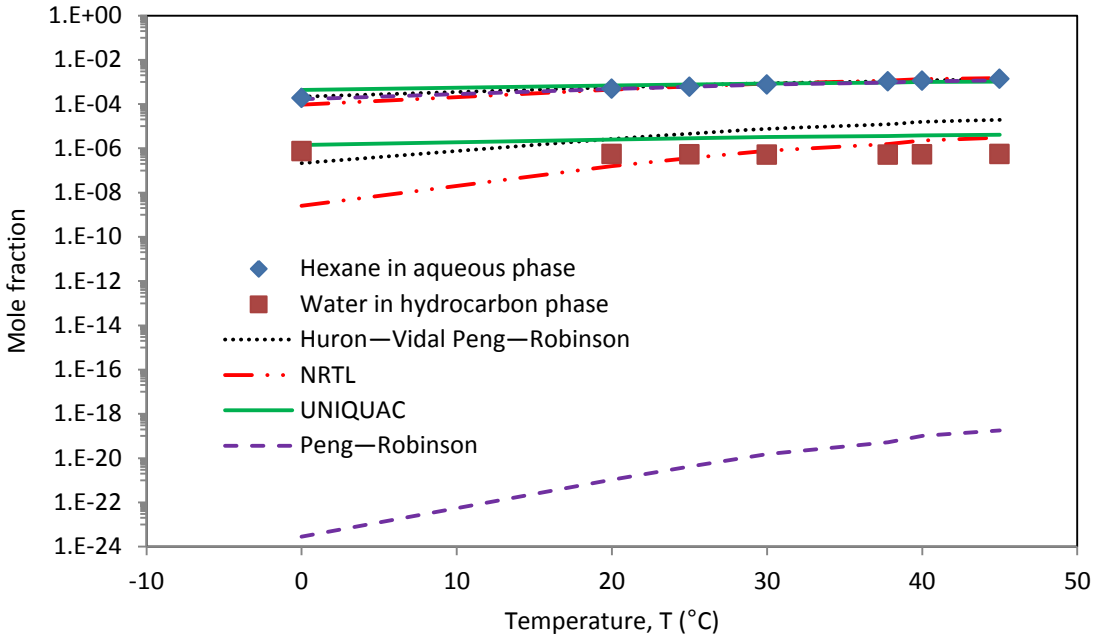

Figure 9.8 Mutual solubility for water—heptane at P = 101.325. Diamonds are experimental heptane in aqueous phase; squares are experimental data of water in hydrocarbon phase. Experimental data is from Table 9.2.

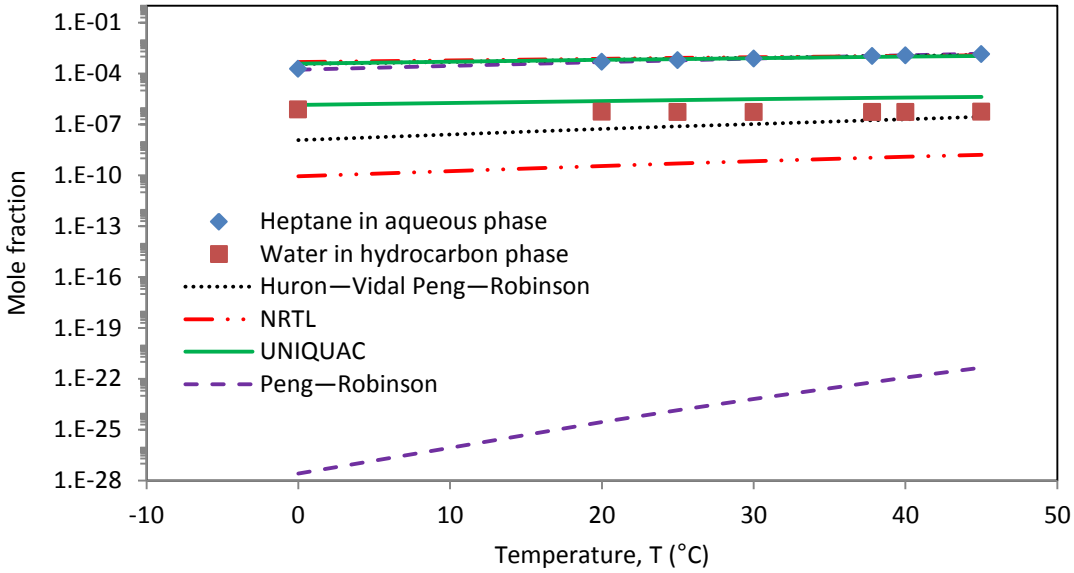

Figures 9.7 and 9.8 shows the extent to which all of the models struggled with compositional accuracy of water in the hydrocarbon phases. There are many orders of magnitude of error for several of the models and over 14 orders of magnitude for the Peng—Robinson. Even in predicting hydrocarbon composition in the water phase the models struggle considerably, the results are merely overshadowed by worse aptitudes for water in the hydrocarbon phase. In terms of error analysis the Peng—Robinson has the largest error in Figure 9.7 at 26 %. However in Figure 9.8 the UNIQUAC has the worst results at 113 % error.

The use of figures is key to a true understanding of the errors in mutual solubility. Looking at Figures 9.7 and 9.8 it is obvious that the Peng—Robinson model is the worst fit, especially for predicting water in hydrocarbons. This does not show up in the AAPD calculation simply because the predicted value of Peng—Robinson is so small, in the numerator of Equation 9.1, it only very slightly has an effect. Thus, the Peng—Robinson models errors, despite being orders of magnitudes worse than the rest of the models, always come out at 100 % AAPD for the water

in hydrocarbons. Using AAPD as it is currently defined is the wrong method for judging the error in water—hydrocarbon mutual solubility. The logarithmic figures provide much better comparisons.

Conclusion

Beginning first with Figure 9.1, it should be clear that parameter optimization is a necessity. It should also be clear that selecting the correct model is as important as parameter optimization. Optimization can take a long time, so doing it for the correct model is crucial. Quality data is an issue with Fischer—Tropsch synthesis products, notably the hexane—acetic acid which only has VLE data with bubble and dew point experimental data available at reduced pressures. The Huron—Vidal Peng—Robinson equation seems very sensitive to data types when it comes to regressing parameters. The hexane—acetic acid binary parameter provided a good fit for the high temperature bubble point data, however it did not provide a good fit for the reduced pressure VLE. The Huron—Vidal Peng—Robinson equation was also the most time consuming to get convergence in optimizing parameters.

In the case of water—acetic acid VLE at atmospheric pressures there does not seem to be any advantage to using the advanced PC-SAFT model. The activity coefficient models all fit the same experimental data as the PC-SAFT model to significantly better error. This however does not translate into saying that the PC-SAFT model will have more error in multi-component, multiphase calculations.

References

(1) Nguyen-Huynh, D.; De Hemptinne, J-C.; Lugo, R.; Passarello, J-P.; Tobaly, P. Simultaneous liquid—liquid and vapor-liquid equilibria predictions of selected oxygenated aromatic molecules in mixtures with alkanes, alcohols, water, using the polar GC-PC-SAFT. *Chem. Eng. Res. Des.* **2014**, *92*, 2912-2935.

(2) Kontogeorgis, G. M.; Folas, G. K. *Thermodynamic models for industrial applications: From classical and advanced mixing rules to associations theories*; John Wiley & Sons: West Sussex, **2010**.
(3) Hayden, G. J.; O'Connell, J. P. A generalized method for predicting second Virial coefficients. *Ind. Eng. Chem. Process Des. Dev.* **1975***, 1,* 209-216.
(4) Mathias, P. M.; Copeman, T. W. Extension of the Peng—Robinson equation-of-state to complex mixtures: Evaluation of the Various Forms of the Local Composition Concept. *Fluid Phase Equil.* **1983***, 13*, 91.
(5) Brusset, H.; Kaiser, L.; Hoquel, J. Présentation d'un nouvel ébulliomètre à recyclage. *Chim. Ind. Genie Chim.* **1968***, 99*, 220-224.
(6) Gilmont, R.; Othmer D. F. Composition of vapors from boiling binary solutions. *Ind. Eng. Chem.* **1944***, 36*, 1061-1064.
(7) Othmer, D. F.; Silvis, S. J.; Spiel, A. Composition of vapors from boiling binary solutions. Pressure equilibrium still for studying water—acetic acid system. *Ind. Eng. Chem.* **1952***, 36*, 1864-1872.
(8) Chemical Engineering Speciality, College of Shanghai Chemical Engineering Shanghai Instutute of Petrochemistry. I. Study on the vapor liquid equilibrium data for acetic acid-water-vinyl acetate ternary system. The mutually miscible liquid phase region (paper in Chinese, data in Roman numerals). *Acta Chim. Sinica* **1976**, *34*, 79-92.
(9) Arai, Y. Measurement of isothermal vapor—liquid equilibria for hydrocarbon + monocarboxylic acid binary systems by a flow-type apparatus. *J. Chem. Eng. Data* **2000***, 45*, 857-861.
(10) Gmehling, J.; Onken, U.; Rarey-Nies, J. R. *Vapor—liquid Equilibrium Data Collection: Organic Hydroxyl Compounds: Alcohols. Vol. I Part 2a*; DECHEMA: Frankfurt, **1977**.
(11) Gmehling, J.; Onken, U.; Grenzheuser, P. *Vapor—liquid Equilibrium Data Collection: Carboxylic Acids, Anhydrides, Esters. Vol. I Part 5*; DECHEMA: Frankfurt, **1982**.
(12) Gmehling, J.; Onken, U.; Rarey-Nies, J. R. *Vapor—liquid Equilibrium Data Collection: Aqueous Systems. Vols. I, Part 1b (Supplement 2)*; DECHEMA: Frankfurt, **1988**.
(13) Journal of Physical and Chemical Reference Data. AIP Publishing (NIST), **2005**, pp 1399.
(14) Journal of Physical and Chemical Reference Data. AIP Publishing (NIST), **2005**, pp 709.
(15) Arlt, W.; Sørenson, J. M. Liquid—liquid Equilibrium Data Collection: Ternary Systems. Vols. V Part 2; DECHEMA: Frankfurt, **1980**.
(16) Rao, M. R.; Rao, C. V. Ternary Liquid Equilibria. IV. Various Systems. *J. Appl. Chem.* **1957***, 7*, 659-666.
(17) Gomis, V.; Font, A.; Saquete, M. D. Vapor—liquid—liquid and vapor liquid equilibrium of the system water + ethanol + heptane at 101.3 kPa. *Fluid Phase Equil.* **2006***, 248*, 206-210.
(18) Marina, J. M.; Tassios, D. P. Effective local compositions in phase equilibrium correlations. *Ind. Eng. Chem. Process Des. Dev.* **1973***., 12*, 67-71.
(19) Yushu, C.; Afef, A.; Fabrice, M.; Roland, S.; Jeday, M.R. Thermodynamics modelling of mixtures containing carboxylic acids using the PC-SAFT equation of state. *Industrial & Engineering Chemistry Research*. **2012**, *51*, 13846-13852.
(20) Breil, M.P.; Kontogeorgis, G.M.; Behrens, P.K.; Michelsen, M.L. Modelling of the thermodynamics of the acetic acid-water mixture using the cubic-plus-association equation of state. *Industrial & Engineering Chemistry Research*. **2011**, *50*, 5795-5805.

Chapter 10 – Modelling vapor—liquid—liquid phase equilibria in Fischer—Tropsch syncrude

Introduction

Fischer—Tropsch synthesis is an indirect liquefaction technology that is industrially applied for the conversion of synthesis gas to syncrude. The composition of the syncrude depends on the Fischer—Tropsch technology and its operation, but in all cases the syncrude contains a mixture of hydrocarbons, oxygenates, and water. Cooling and condensation of the hot gaseous syncrude leaving the reactor after Fischer—Tropsch synthesis produces a three-phase mixture consisting of an organic phase, an aqueous phase and a gas phase product (Figure 5.1). The impact of phase separation on downstream processing is far reaching, and it can be the origin of unrecoverable product loss, corrosion problems, refining challenges and increased wastewater treatment cost.[1]

Design engineers that want to improve the design of syncrude cooling and phase separation require an accurate thermodynamic description of the phase equilibria. A similar problem is encountered in the design of phase separation for biomass conversion processes.[2][3] There is little guidance in literature on what thermodynamic description to employ and that is available in process simulation software, in order to accurately predict the vapor—liquid—liquid equilibrium (VLLE) resulting from the condensation of mixed hydrocarbons, oxygenates, and water.

Modelling of phase equilibria related to Fischer—Tropsch synthesis is discussed in the literature, but usually in a more limited context. There is a body of phase equilibrium modelling work published on the vapor—liquid equilibrium (VLE) in the Fischer—Tropsch reactor (Figure 5.1) under typical low temperature Fischer—Tropsch synthesis conditions.[4-8] In related

investigations, the VLE of synthesis gas in the liquid phase was studied.[9][10] All of these studies are concerned with describing the phase behavior in the synthesis reactor. Under low temperature Fischer—Tropsch synthesis conditions, with an operating temperature upwards of 170 °C and operating pressure below 3 MPa, water is a vapor phase product and there is no second liquid phase. Furthermore, the contribution of oxygenates is usually ignored in the VLE calculations, because the more polar short chain oxygenates are also vapor phase products under the synthesis conditions in the Fischer—Tropsch reactor.

Investigations that deal with VLLE of Fischer—Tropsch syncrude are less common. The need to have better descriptions of the VLLE was realized early on in the industrial development of the Fischer—Tropsch refining processes.[11] Considerable effort was expended to gather distillation and separation data experimentally, little of which was published. The same situation was faced decades later for the development for processes dealing with hydrocarbon, oxygenate and water separations.[12] For process development some piloting is inevitable, but this is not tenable for the development and evaluation of conceptual designs.

Previously the VLLE of syncrude during product cooling and separation after Fischer—Tropsch synthesis was considered, and a limited evaluation and validation of thermodynamic models was presented.[13] It highlighted the need for guidance in the selection of a credible thermodynamic description of the VLLE of water—oxygenate—hydrocarbon systems. It is the objective of this study to provide guidelines for the selection of suitable thermodynamic models for this purpose.

Modelling of water—oxygenate—hydrocarbon VLLE

The industrial process simulation software VMGSim was used to model the published experimental equilibrium data (Table 9.2) of two ternary LLE systems and one VLLE system. The evaluation was performed with the optimized fitting parameters, as well as the VMGSim

default fitting parameters, because it is not always practical to optimize fitting parameters for complex systems, such as the Fischer—Tropsch reaction product (Table 9.3). The evaluation using default fitting parameters is an indication of the quality of predictions that can typically be anticipated. The evaluation with optimized parameters is a measure of how well the thermodynamic model can predict non-ideal systems. In these evaluations a systematic deviation from the experimental data indicates a fundamental shortcoming of the model.

Both LLE systems and the VLLE system modelled exhibited classical ternary behavior based on reported experimental results i.e., the water—hydrocarbons formed an immiscible boundary and the oxygenate was miscible with both water and the hydrocarbon of interest along the entirety of both binary boundaries.

Peng—Robinson

The phase equilibria calculated by the Peng—Robinson cubic equation of state are shown for the water—acetic acid—hexane[14][15] (Figure 10.2 and 10.3) and water—ethanol—heptane[15] (Figure 10.4) systems. Additional figures which show only the Peng—Robinson model are included in Appendix B (Figures B.1, and B.2). Error analysis is shown below in Table 10.1.

Large errors of prediction were found using both default and optimized values in each phase of every system. Two things are immediately clear: firstly that the Peng—Robinson equation is vastly improved with parameter optimization, showing its importance, and second that even after parameter optimization the Peng—Robinson equation is still a very poor model for systems containing water and oxygenates in addition to hydrocarbons, showing the importance of a models theoretical foundation.

Table 10.1 Error analysis of calculated compared to experimental equilibrium data of ternary systems using the Peng—Robinson equation of state with default and optimized parameters.

Description	AAPD (%)		Maximum error (%)	
	default	optimized	default	optimized
Water—acetic acid—hexane (25 °C)				
organic phase	107	53	785	99
aqueous phase	198	37	1606	100
Water—acetic acid—hexane (31 °C)				
organic phase	316	42	1313	293
aqueous phase	83	34	166	100
Water—ethanol—heptane				
organic phase	98	70	400	327
aqueous phase	78	46	709	100
vapor phase	18	9	57	24

The Peng—Robinson equation was developed specifically for the oil and gas sector and is not designed for polar components. Using the Peng—Robinson equation of state with default settings led to spectacular failure in predictions for all liquid—liquid equilibria. The absolute average percentage difference (AAPD), as well as the maximum deviation between the calculated and experimental data is shown above in Table 10.1. While not as bad, the calculated multicomponent vapor phase compositions involving oxygenates were still poor.

While it is a simple model and quick to optimize, not enough was gained through optimization in these systems to make it viable for use as thermodynamic model to calculate VLLE data for water—oxygenate—hydrocarbon systems.

Huron—Vidal Peng—Robinson

The addition of the NRTL model into the mixing rules of the Peng—Robinson cubic equation of state greatly increases its ability to predict the phase behavior of oxygenates. The calculated phase equilibria using the Huron—Vidal Peng—Robinson model with optimized parameters is shown for the water—acetic acid—hexane[14][15] (Figure 10.2 and 10.3), and water—ethanol—

heptane[15] (Figure 10.4) systems. Additional figures which show only the Huron—Vidal Peng—Robinson are included in Appendix B (Figures B.3 and B.4).

The Huron—Vidal Peng—Robinson model with default parameters failed to predict LLE. This was a consequence of the default parameters that were all zero in the process simulation software employed for this study (Table 9.2). Zero values for the interaction parameters are not realistic for the NRTL model. The specific implementation in the process modelling software did not implement an estimation of the NRTL parameters. The poor performance of the Huron—Vidal Peng—Robinson with default parameters was not an inherent shortcoming of the model.

Table 10.2 Error analysis of calculated compared to experimental equilibrium data of ternary systems using the Huron—Vidal Peng—Robinson model with default and optimized parameters.

Description	AAPD (%)		Maximum error (%)	
	default	optimized	default	optimized
Water—acetic acid—hexane (25 °C)				
organic phase	- [a]	39	- [a]	93
aqueous phase	- [a]	36	- [a]	100
Water—acetic acid—hexane (31 °C)				
organic phase	- [a]	27	- [a]	160
aqueous phase	- [a]	33	- [a]	100
Water—ethanol—heptane				
organic phase	- [a]	32	- [a]	81
aqueous phase	- [a]	97	- [a]	1349
vapor phase	32	6	74	16

[a] Failed to predict liquid—liquid equilibrium.

The optimized Gibbs Excess mixing rules improved the performance of the Peng—Robinson to predict the aqueous and organic phase for every component in the LLE systems (Table 10.2). Both the average error and the maximum error decreased significantly compared to that of the Peng—Robinson equation of state on its own (Table 10.1).

While showing great improvement in the LLE systems, the Gibbs excess calculation failed even qualitatively at providing reasonable results for the VLLE (Figures 10.3 and B.4). The quality and type of data used to regress parameters have a significant role in the accuracy of a model, and the Gibbs excess model seems to be the most sensitive of the models tested in this regard.

NRTL and Hayden O'Connell

Similar to the application of the NRTL as mixing rule in the Huron—Vidal Peng—Robinson model, the NRTL requires non-zero interaction parameters to function with the Hayden–O'Connell virial equation of state. The main difference in the application with the virial equation of state is that the unknown default parameters of the NRTL were automatically estimated using the UNIFAC model, whereas this was not the case for the software implementation of NRTL in the Gibbs excess function. The default settings for the NRTL used UNIFAC for the water—hexane, water—heptane and heptane—ethanol pairs. The rest were calculated by VMGSim using VLE data.

The comparison of the experimental and calculated LLE of the water—acetic acid—hexane systems using NRTL and Hayden–O'Connell are shown in Figure 10.2 and 10.3 and Figures B.5 (in Appendix B). Error analysis is available below in Table 10.3. In both default LLE systems the NRTL failed to predict LLE at high concentrations of acetic acid. As a general consideration this is a major error. The VLLE comparison for the water—ethanol—heptane system[15] is shown in Figures 10.4 and B.6.

Table 10.3 Error analysis of calculated compared to experimental equilibrium data of ternary systems using the NRTL with Hayden O'Connell with default and optimized parameters.

Description	AAPD (%)		Maximum error (%)	
	default	optimized	default	optimized
Water—acetic acid—hexane (25 °C)				
organic phase	554	34	- [a]	92
aqueous phase	521	30	- [a]	100
Water—acetic acid—hexane (31 °C)				
organic phase	434	18	- [a]	74
aqueous phase	407	32	- [a]	100
Water—ethanol—heptane				
organic phase	63	43	- [a]	- [a]
aqueous phase	428	89	- [a]	- [a]
vapor phase	8	3	22	7

[a] Failed to predict some liquid—liquid equilibrium tie-lines.

There was a general improvement in the prediction of the phase equilibria when optimized parameters were employed (Table 10.3). The NRTL predicted each tie-line's existence using default settings in the water—ethanol—heptane ternary system, with good fits at low concentration of ethanol and large errors at high concentrations of ethanol shown in Figures 10.4 and B.6. Optimizing the NRTL led to increased accuracy in the low concentration tie-lines but did not help at high concentrations, even failing to predict the last two tie-lines entirely. The Hayden O'Connell improved after optimization.

UNIQUAC and Hayden O'Connell

Modelling of the two water—acetic acid—hexane ternary systems[14][15] using the Hayden–O'Connell virial equation of state with UNIQUAC as mixing rule are shown in Figure 10.2 and 10.3 and Figure B.8in Appendix B. The modelling of the VLLE data of the water—ethanol—heptane system[15] is shown in Figure 10.4 and B.8. Error analysis is shown below in Table 10.4.

The development of UNIQUAC led to the group contribution method known as UNIFAC and it is of no surprise that by default several parameters for UNIQUAC are estimated using UNIFAC. In the present evaluation the process modelling software, VMGSim, used UNIFAC to

estimate the water—hexane, water—heptane and hexane—acetic acid binary pairs. VLE data sets were used for the rest of the parameters. Surprisingly, in the case of UNIQUAC, there was little difference in the accuracy of LLE and VLLE results (Table 10.4) in the organic phase when using default parameters compared to using optimized parameters. There was however significant improvement in prediction in the aqueous phases.

Table 10.4 Error analysis of calculated compared to experimental equilibrium data of ternary systems using the UNIQUAC with Hayden O'Connell with default and optimized parameters.

Description	AAPD (%)		Maximum error (%)	
	default	optimized	default	optimized
Water—acetic acid—hexane (25 °C)				
organic phase	40	38	164	197
aqueous phase	79	38	776	253
Water—acetic acid—hexane (31 °C)				
organic phase	27	27	424	487
aqueous phase	42	22	249	147
Water—ethanol—heptane				
organic phase	37	37	136	90
aqueous phase	63	34	1349	447
vapor phase	3	3	12	14

Another difference between UNIQUAC predictions and the other models was that while the most dilute tie-line had the highest error using default UNIQUAC and the other models, this was not the case for the optimized UNIQUAC. For UNIQUAC with optimized parameters the highest deviation from the experimental occurred for more oxygenate-rich mixtures. Regardless of whether default or optimized UNIQUAC was used, both results were more accurate than the other models for the water—acetic acid—hexane systems with respect to the entire system. UNIQUAC also always predicted the correct number of tie-lines in LLE and VLLE.

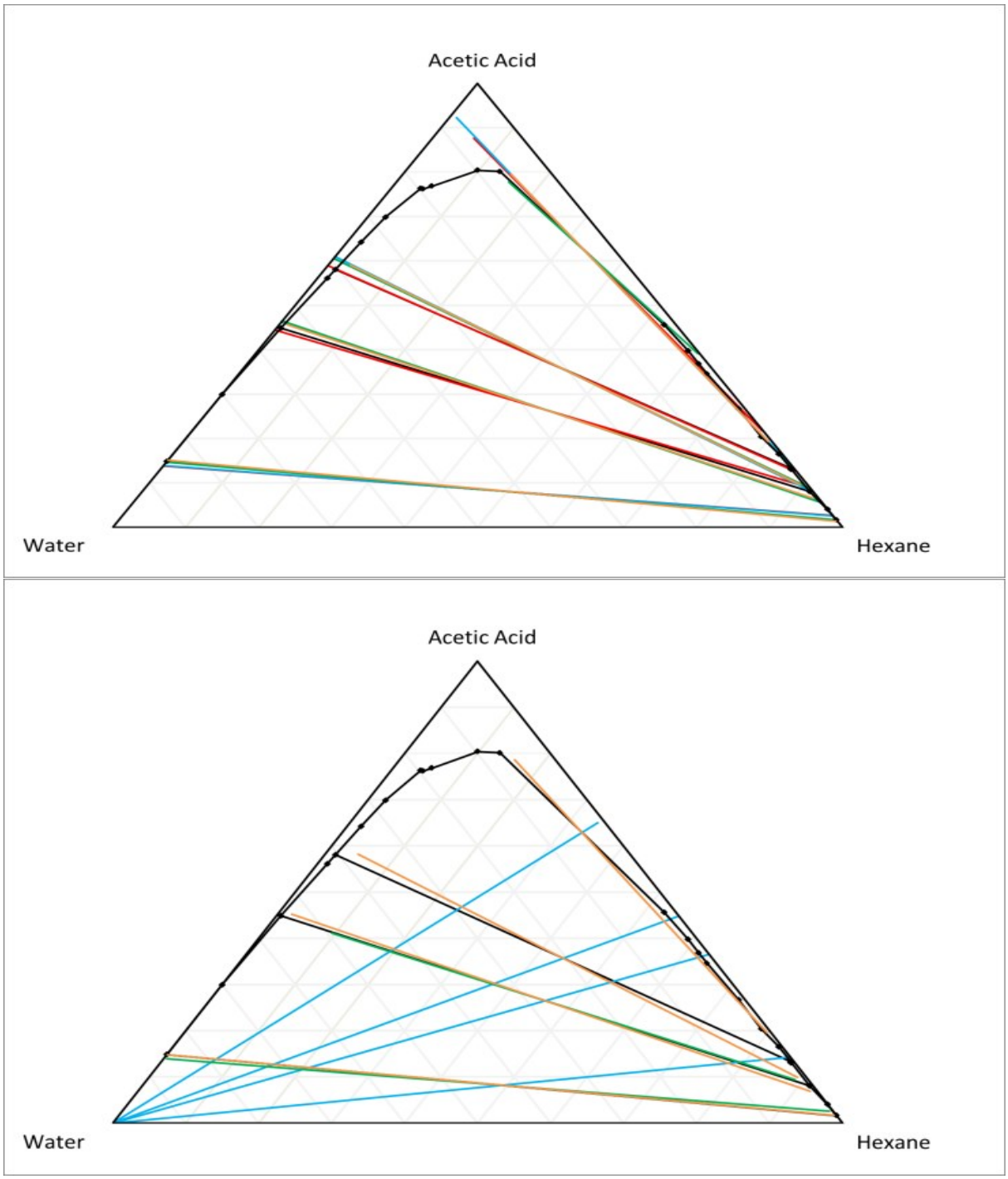

Figure 10.2: Modelling is with optimized parameters (top) and default parameters (bottom). Experimental data is modelled by the Peng—Robinson (blue), Huron-Vidal Peng—Robinson (red), NRTL (green) and UNIQUAC (orange). Data taken at 25 ° C and 101.325 kPa. Note: the Huron-Vidal Peng—Robinson failed to predict any tie-lines with default parameters.

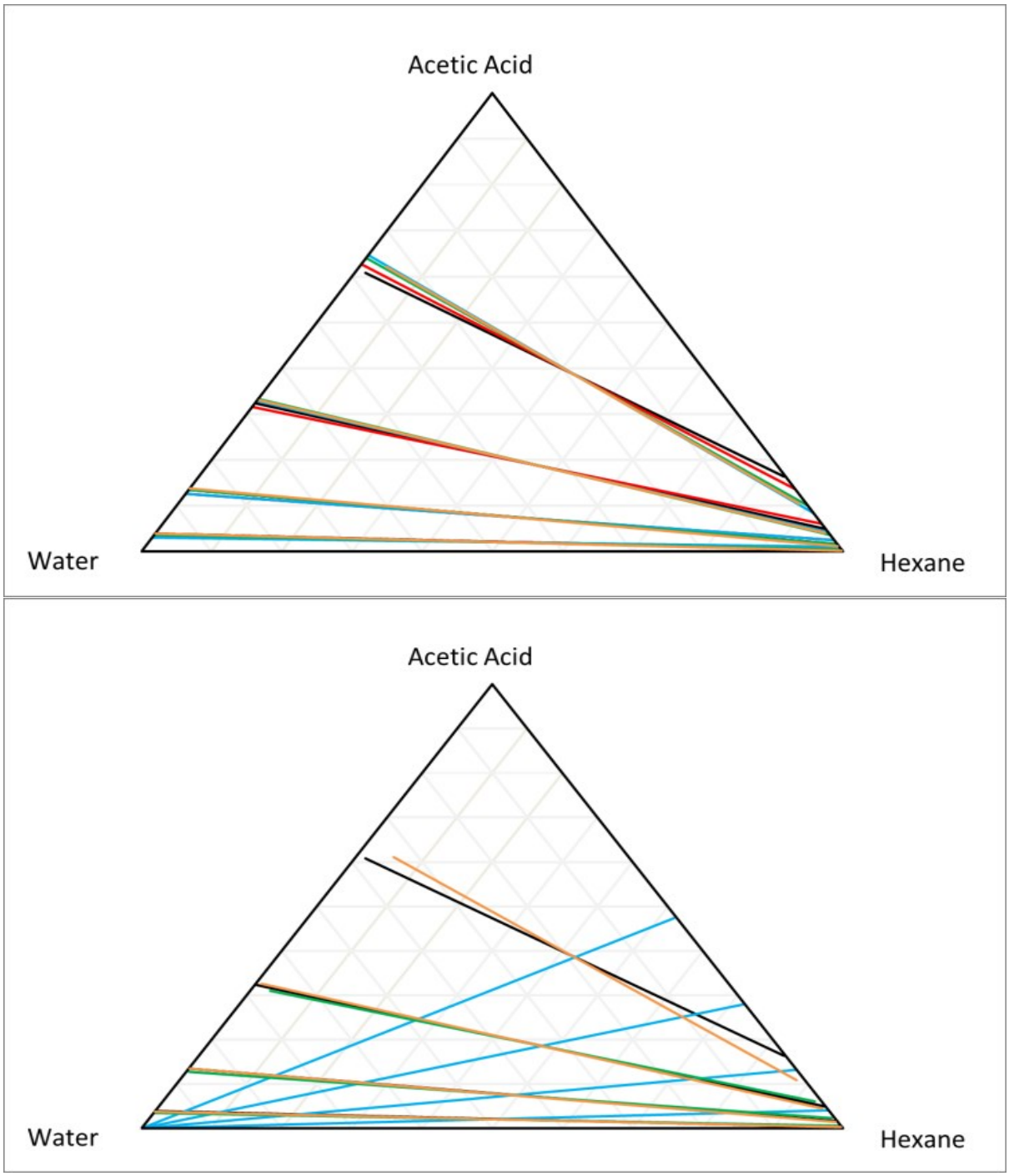

Figure 10.1: Modelling is with optimized parameters (top) and default parameters (bottom). Experimental data is modelled by the Peng—Robinson (blue), Huron-Vidal Peng—Robinson (red), NRTL (green) and UNIQUAC (orange). Data taken at 31 ° C and 101.325 kPa. Note: Huron-Vidal Peng—Robinson failed to predict any tie-lines with default parameters.

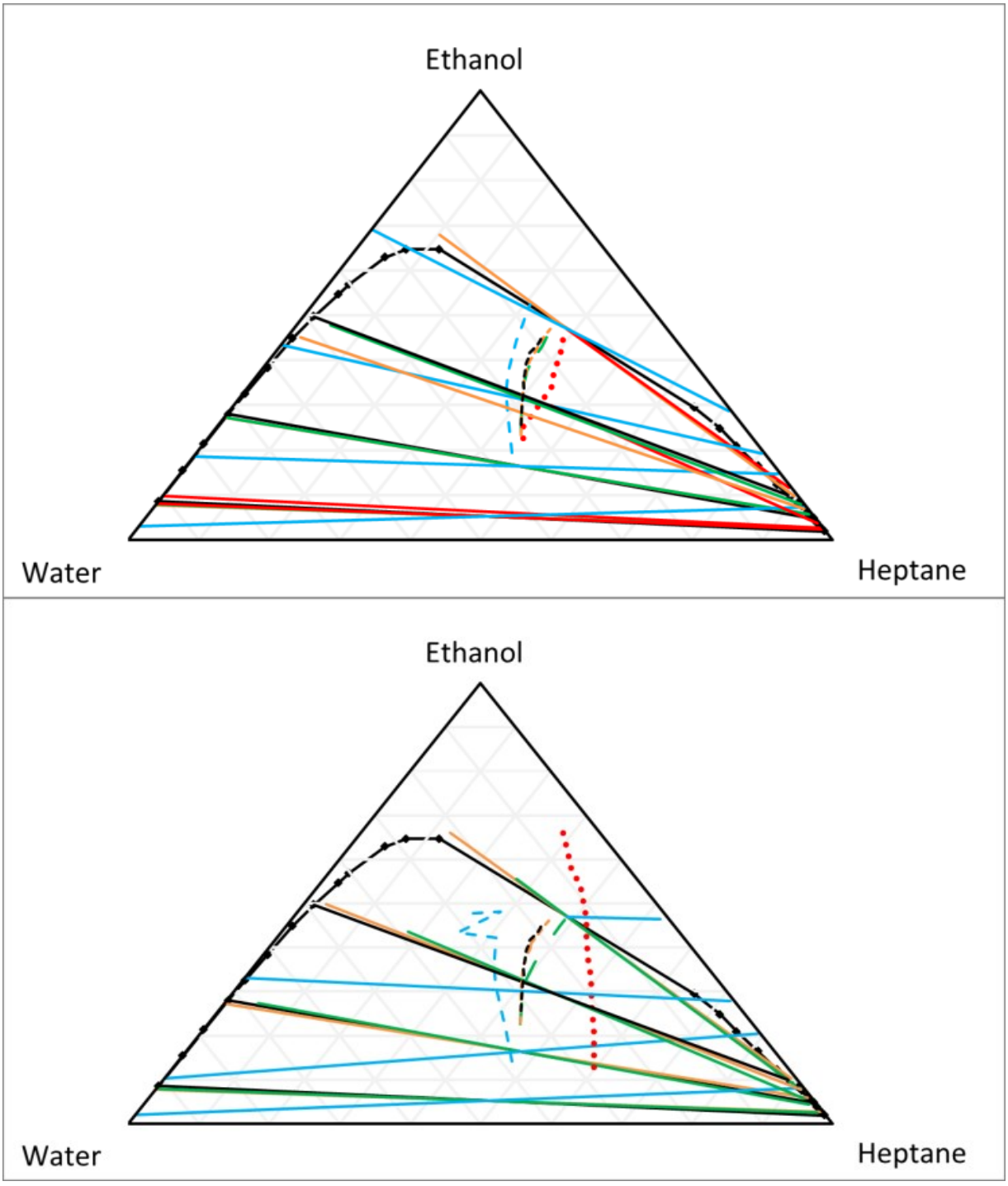

Figure 10.3: Modelling is with optimized parameters (top) and default parameters (bottom). Modelling is done with the Peng—Robinson (blue), Huron-Vidal Peng—Robinson (red), HC+NRTL (green), HC+UNIQUAC (orange). Data taken at 68.72 – 79.24 °C and 101.325 kPa. Note: Huron-Vidal Peng—Robinson failed to predict any tie-lines with default parameters.

Suitability of models for water—oxygenate—hydrocarbon VLLE in Fischer—Tropsch .

Aqueous phase solutions with 0 to 10 % oxygenates

The evaluation of the selected models over the entire composition space is not an application specific evaluation, but provides a general assessment of the performance of the models for water—oxygenate—hydrocarbon mixtures. In reality, Fischer—Tropsch mixtures are not oxygenate rich, and nearly always contain less than 10 % oxygenates. Of the industrial processes, high temperature Fischer—Tropsch synthesis contains the highest concentration of oxygenates. The syncrude contains around 12 wt. % oxygenates,[1] and the liquid phase concentration during VLLE (Figure 10.1) is around 8 wt. % oxygenates, with 25 to 30 wt. % hydrocarbons, the remainder being water.

The selection of appropriate thermodynamic models for the description of VLLE of Fischer—Tropsch syncrude should therefore focus on the performance of the model on the more limited composition range 0 to 10 % oxygenates. For this reason, the accuracy of the models for tie-lines containing less than 10 % oxygenates were investigated so that a recommendation specifically for Fischer—Tropsch could be made.

As could be seen from Tables 10.1, 10.2, 10.3, and 10.4 the errors for all of the models were quite high when basing the results on the entire composition space. This is caused mainly by the loss in accuracy in the oxygenate-rich zones (Figures 10.2, 10.3, and 10.4), which are outside the Fischer—Tropsch synthesis composition range, as well as inherent difficulties in calculating water—hydrocarbon compositions, an issue that effects all models. By excluding the tie-lines with high oxygenate concentrations from the analysis and focusing on the prediction of oxygenates composition in the aqueous and organic phases (liquid phase partitioning), lower errors were found.

Accuracy in predicting carboxylic acid concentration in the hydrocarbon phase is viewed as a high priority, since insufficient partitioning to the aqueous phase at separation could lead to corrosion issues downstream from separation. The AAPD and maximum error results for tie-lines with less than 10 % oxygenates were calculated for the different thermodynamic models.

Peng—Robinson

Error analysis for oxygenates in the organic and aqueous phases for the Peng—Robinson is provided in Table 10.5, as well as Tables B1 to B5 in the Appendix B. The Peng—Robinson equation of state was capable of predicting the correct number of tie-lines in the LLE and VLLE systems, however, its accuracy was poor. Optimization of interaction parameters improved the prediction capabilities of the Peng—Robinson in all phases and all ternaries investigated. Unfortunately, even after significant improvement, as can be seen in Table 10.5, the AAPD and maximum errors were still large.

Table 10.5 Error analysis of oxygenates in organic and aqueous phases for ternary equilibrium data of 10% or lower oxygenate concentration using the Peng—Robinson equation of state.

Description	AAPD (%)		Maximum error (%)	
	default	optimized	default	optimized
Water—acetic acid—hexane		*Acetic acid in…*		
organic phase	935	135	1313	293
aqueous phase	100	11	100	21
Water—ethanol—heptane		*Ethanol in…*		
organic phase	362	303	400	327
aqueous phase	76	61	77	64
vapor phase	38	19	44	24

Huron—Vidal Peng—Robinson

Error analysis for oxygenates in the organic and aqueous phases for the Huron—Vidal Peng—Robinson is provided in Table 10.6 and in Tables B1 to B5 in Appendix B. Only the optimized results are shown for the Huron—Vidal Peng—Robinson . It is impractical to compare with

results taken without the use of interaction parameters. Once the interaction parameters were optimized, the Gibbs excess modification was an improvement over the Peng—Robinson for the prediction of the LLE. However, it failed quantitatively and qualitatively for the prediction of VLLE as can be seen in Figure 10.4.

Table 10.6 Error analysis of oxygenates in organic and aqueous phases for ternary equilibrium data of 10% or lower oxygenate concentration using the Huron—Vidal Peng—Robinson equation of state.

Description	AAPD (%)		Maximum error (%)	
	default	optimized	default	optimized
Water—acetic acid—hexane		*Acetic acid in…*		
organic phase	-[a]	91	-[a]	160
aqueous phase	-[a]	7.8	-[a]	11.3
Water—ethanol—heptane		*Ethanol in…*		
organic phase	-[a]	35	-[a]	45
aqueous phase	-[a]	6	-[a]	7
vapor phase	-[a]	9	-[a]	12

[a] Failed to predict tie-lines.

In the LLE systems all of the results were a significant improvement over the Peng—Robinson using classical Van der Waals one fluid mixing rules. In the VLLE system the Huron—Vidal Peng—Robinson was only accurate at very low concentration and as a result, would not be preferable over the Peng—Robinson , since it cannot be trusted to predict the equilibrium even qualitatively.

NRTL and Hayden O'Connell

Error analysis for oxygenate concentration in the organic and aqueous phases for the NRTL and Hayden–O'Connell is provided in Table 10.7 and in Appendix B in Tables B1 to B5. It was found that the NRTL model failed to predict LLE at high concentrations of acetic acid, as illustrated by Figures 10.2 and 10.3. Optimizing the interaction parameters boosted the NRTL model's accuracy significantly in both the organic and aqueous phases. The maximum error was also significantly reduced in both phases. It is worth noting that the maximum error occurred in

the lowest tie-line, which is unexpected, since the overall trend is to lose accuracy with increasing oxygenate concentration as can be seen in Figures 10.2 to 10.4.

Table 10.7 Error analysis of oxygenates in organic and aqueous phases for ternary equilibrium data of 10% or lower oxygenate concentration using the NRTL and Hayden O'Connell equation of state.

Description	AAPD (%)		Maximum error (%)	
	default	optimized	default	optimized
Water—acetic acid—hexane		*Acetic acid in…*		
organic phase	75	26	126	72
aqueous phase	6	2	8	5
Water—ethanol—heptane		*Ethanol in…*		
organic phase	35	43	38	52
aqueous phase	6	7	7	8
vapor phase	11	5	12	7

Model prediction in the VLLE system for all components in all phases had high overall AAPD with the default parameters for NRTL having an AAPD of more than 200 %, mainly due to errors in predicting water/heptane compositions. When optimized interaction parameters were used this error was reduced to 21 %. The error in the predicted ethanol composition in the organic phase rose after optimization. The error also increased slightly in the aqueous phase predictions of ethanol concentration.

The reduction in overall error can be attributed to the optimization of the water—heptane pair using mutual solubility data. The increase in error in the oxygenate pairs likely stems from the replacement of the UNIFAC parameter for heptane—ethanol with one optimized from the published[15] VLE heptane—ethanol data.

UNIQUAC and Hayden O'Connell

Error analysis for oxygenates in the organic and aqueous phases for the UNIQUAC and Hayden—O'Connell is provided (Table 10.8). Additional information on the error analysis can be found in Appendix B (Tables B1 to B5). For the water—acetic acid—hexane ternary tie-lines

optimizing parameters for the UNIQUAC model reduced the error in acetic acid prediction in the organic phase, however, changes in the aqueous phase were negligible. The maximum error decreased significantly in the organic phase after optimization, but the maximum error increased slightly in the prediction of the aqueous phase composition.

Table 10.8 Error analysis of oxygenates in organic and aqueous phases for ternary equilibrium data of 10% or lower oxygenate concentration using the UNIQUAC and Hayden O'Connell equation of state.

Description	AAPD (%)		Maximum error (%)	
	default	optimized	default	optimized
Water—acetic acid—hexane		*Acetic acid in…*		
organic phase	9	7	21	16
aqueous phase	1	1	1	2
Water—ethanol—heptane		*Ethanol in…*		
organic phase	54	53	62	59
aqueous phase	9	9	10	10
vapor phase	9	7	12	9

As in the LLE systems, increased oxygenate (ethanol in this case) concentration was met with decreased composition accuracy, as can be seen in (Figures 10.3 and B.8); most notably in the organic phase. As seen in Table 10.8 the errors for ethanol composition were quite high even at low concentration. The overall AAPD for all components in all phases was 24 % for both default and optimized settings. A large part of the overall error was due to the contribution from the ethanol inaccuracy in the organic phase. Optimization increased the accuracy of ethanol prediction in the organic phase slightly. Likewise, there was only very slight improvement in the aqueous phase prediction of ethanol after optimization.

Recommendations for modelling of Fischer—Tropsch syncrude VLLE

For the purposes of Fischer—Tropsch product separation, as mentioned previously, partitioning of the oxygenates between the different phases is important. The results in Table 10.5 indicated that the Peng—Robinson equation of state is not capable of accounting for oxygenate

partitioning. This really is to be expected. The Peng—Robinson equation was designed for hydrocarbons, not polar and dimerizing molecules. In each of the ternaries investigated, the error was large, even after optimizing the interaction parameters. These observations can be generalized to recommend that cubic equations of state on their own should not be employed as thermodynamic models for VLLE of Fischer—Tropsch syncrude.

The addition of NRTL to the mixing rules using the Huron–Vidal method enhanced the accuracy of the Peng—Robinson equation of state, making it one of the better choices in the LLE systems. However, in the VLLE system the Huron—Vidal Peng—Robinson did very poorly for the water—ethanol—heptane ternary. The Gibbs excess model was found to be reliable in the literature for oxygenates.[17][18][19] It is possible that with better data, such as including tie-lines of other LLE systems that have each of the binary pairs, or even including some experimental tie-lines, the accuracy of the VLLE can be made comparable to that of the LLE systems. Taking this extra step takes a considerable amount of increased effort, especially if the system has more than 3 components, which Fischer—Tropsch syncrude certainly does. It is also possible that accuracy could be improved by the use of Wong—Sandler mixing rules, rather than Huron–Vidal, but this was not verified. The Wong—Sandler mixing rules have been used successfully for oxygenate VLLE before.[2] Since the additional effort to optimize the model is not justified for general conceptual studies, the Huron—Vidal Huron—Vidal Peng—Robinson is not recommended as a thermodynamic model for calculating VLLE of Fischer—Tropsch syncrude.

Both activity coefficient models were based on the theory of local composition. The NRTL model was initially an attempt to take the Wilson equation and make it work for LLE, and the UNIQUAC was an attempt to take the NRTL model and make it better. Whether the UNIQUAC model is actually a better model than the NRTL model, is an open debate. For the systems

employed in this investigation, it appears that the UNIQUAC model was better. The use of UNIFAC to estimate interaction parameters for hydrocarbon—oxygenate pairs did not significantly reduce accuracy, although it was beneficial to optimize the water—hydrocarbon pairs using mutual solubility data, and optimize the water-oxygenate pairs using VLE data. All of the thermodynamic models struggled to accurately predict oxygenates in the organic phase. UNIQUAC had the best performance for acetic acid in the hexane phase, with 9 % AAPD (Table 10.8) for default parameters and 7 % AAPD for optimized parameters. Although NRTL performed better than UNIQUAC at predicting ethanol partitioning between the liquid phases at low concentrations of ethanol, the failure to predict phase equilibria, even qualitatively, at higher oxygenate concentrations raised doubt about the general validity of NRTL for predictions of water—oxygenate—hydrocarbon systems without the use of experimental data and parameter fitting.

The modelling of various other water—oxygenate—hydrocarbon systems with NRTL and UNIQUAC were reported in literature. Gomis, et al.[20] found that the NRTL and UNIQUAC models accurately reproduced the VLE of the water, 1-butanol and *p*-xylene system, but that meaningful deviations were found for VLLE. Based on the mean deviations of water and 1-butanol in the organic and aqueous phases, NRTL was marginally better than UNIQUAC for the organic phase prediction, but considerably worse for the aqueous phase prediction. In another study by the same group,[22] the VLLE of water, 1-butanol and toluene was determined. Model predictions using NRTL and UNIQUAC found that UNIQUAC consistently had lower mean deviations for the prediction of water and 1-butanol in the organic and aqueous phases. It was found that the experimental LLE of the water, benzaldehyde and toluene system was also better predicted using UNIQUAC than NRTL.[23] Likewise, it was reported that the UNIQUAC was

better than NRTL for the prediction of the LLE of water, tetrahydrofuran and methylcyclohexane.[24]

The present evaluation and the reviewed literature does not prove the UNIQUAC model is superior to NRTL model for water—oxygenate—hydrocarbon systems, but it suggests that UNIQUAC is generally better. It is recommended that UNIQUAC in combination with an equation of state, such as Hayden–O'Connell, be selected as thermodynamic model for general conceptual studies involving VLLE of Fischer—Tropsch syncrude.

Conclusions

Different thermodynamic models were evaluated for the modelling of the VLLE of water—oxygenate—hydrocarbon systems in general, as well as VLLE of Fischer—Tropsch syncrude with < 10 % oxygenates in particular. Representative models from each type were evaluated, and where possible, more general conclusions were derived from the model performance based on the origin of deviations between experimental and predicted value for phase equilibria. The following were concluded:

(a) Cubic equations of state, such as Peng—Robinson, should not be used for multicomponent prediction of non-ideal mixtures, such as water—oxygenate—hydrocarbon systems.

(b) The performance of cubic equations of state can be improved by the use of advanced mixing rules, such as Huron–Vidal (Gibbs excess) mixing rules. When applying advanced mixing rules care must be taken in optimizing the binary interaction parameters. There is

risk of poor predictive performance when using a cubic equation of state with advanced mixing rules with default values.

(c) In literature the NRTL model is considered a go-to activity coefficient model for polar components, but the present investigation highlighted poor performance at moderate to high oxygenate concentration for the water—ethanol—heptane system. It was also found that the NRTL model performed worse at predicting carboxylic acid partitioning than UNIQUAC as evaluated with the water—acetic acid—hexane ternary. The limited evaluation suggested that the predictive performance of NRTL degraded as the non-ideality of the system increased.

(d) The UNIQUAC activity coefficient model was the best all-around model for predicting phase behavior of water—oxygenate—hydrocarbon systems. It was also the most accurate model when phase behavior was predicted with default settings.

(e) The use of the Hayden–O'Connell equation of state for vapor phase calculations is recommended whenever hydrogen bonding may be encountered, such as with carboxylic acids.

(f) It is recommended that UNIQUAC in tandem with the Hayden–O'Connell equation of state should be used for Fischer—Tropsch syncrude VLLE modelling when accuracy in the prediction of oxygenate partitioning between phases is important.

(g) The performance of thermodynamic models can be improved by optimizing the values of interaction parameters using experimental data. It appears best to optimize the water-oxygenate interaction parameters with VLE data. The best results for hydrocarbon-water interaction parameters were obtained through the use of mutual solubility data. Hydrocarbon—oxygenate interaction parameters in activity coefficient models were acceptably estimated by UNIFAC.

References

(1) De Klerk, A. *Fischer—Tropsch refining*; Wiley-VCH: Weinheim, **2010**.
(2) González Prieto, M.; Sánchez, F. A.; Pereda, S. Thermodynamic model for biomass processing in pressure intensified technologies. *J. Supercrit. Fluids* **2015**, *96*, 53-67.
(3) Nguyen-Huynh, D.; De Hemptinne, J-C.; Lugo, R.; Passarello, J-P.; Tobaly, P. Simultaneous liquid—liquid and vapor-liquid equilibria predictions of selected oxygenated aromatic molecules in mixtures with alkanes, alcohols, water, using the polar GC-PC-SAFT. *Chem. Eng. Res. Des.* **2014**, *92*, 2912-2935.
(4) Caldwell, L.; Van Vuuren, D. S. On the formation and composition of the liquid phase in Fischer—Tropsch reactors. *Chem. Eng. Sci.* **1986**, *41*, 89-96.
(5) Marano, J. J.; Holder, G. D. Characterization of Fischer—Tropsch liquids for vapor—liquid equilibria calculations. *Fluid Phase Equilibria.* **1997**, *138*, 1-21.
(6) Derevich, I. V.; Ermolaev, V. S.; Mordkovich, V. Z. Liquid-vapor thermodynamic equilibrium in Fischer—Tropsch synthesis products. *Theo. Found. Chem. Eng.* **2008**, *42*, 216-219.
(7) Karimi, Z.; Rahmani, M.; Moqadam, M. A study on the vapor-liquid equilibria in Fischer—Tropsch synthesis. *Procedia Eng.* **2012**, *42*, 25-33.
(8) Masuku, C. M.; Ma, W.; Hildebrandt, D.; Glasser, D.; Davis, B. H. A vapor—liquid equilibrium thermodynamic model for a Fischer—Tropsch reactor. *Fluid Phase Equilibria.* **2012**, *314*, 38-45.
(9) Huang, S. H.; Lin, H. M.; Tsai, F. N.; Chao, K. C. Solubility of synthesis gases in heavy n-paraffins and Fischer—Tropsch wax. *Ind. Eng. Chem. Res.* **1988**, *27*, 162-169.
(10) Chou, J. S.; Chao, K. C. Solubility of synthesis and product gases in a Fischer—Tropsch Sasol wax. *Ind. Eng. Chem. Res.* **1992**, *31*, 621-623.
(11) Eliot, T. Q.; Goddin, C. S. Jr; Pace, B. S. Chemicals from hydrocarbon synthesis. *Chem. Eng. Progr.* **1949**, *45*, 532-536.
(12) Diamond, D.; Hahn, T.; Becker, H.; Patterson, G. Improving the understanding of a novel complex azeotropic distillation process using a simplified graphical model and simulation. *Chem. Eng. Process.* **2004**, *43*, 483-493.
(13) Rodríguez Vallejo, D. F.; De Klerk, A. Improving the interface between Fischer—Tropsch synthesis and refining. *Energy Fuels* **2013**, *27*, 3137-3147.
(14) Arlt, W.; Sørenson, J. M. Liquid—liquid Equilibrium Data Collection: Ternary Systems. Vols. V Part 2; DECHEMA: Frankfurt, **1980**

(15) Rao, M. R.; Rao, C. V. Ternary Liquid Equilibria. IV. Various Systems. *J. Appl. Chem.* **1957***, 7*, 659-666
(16) Gomis, V.; Font, A.; Saquete, M. D. Vapor—liquid—liquid and vapor liquid equilibrium of the system water + ethanol + heptane at 101.3 kPa. *Fluid Phase Equil.* **2006***, 248*, 206-210.
(17) Pedersen, K. S.; Michelsen, M. L.; Fredheim, A. O. Phase equilibrium calculations for unprocessed well streams containing hydrate inhibitors. *Fluid Phase Equilibria.* **1996**, *126*, 13-28.
(18) Neau, E.; Nicolas, C.; Jaubert, J. N.; Mutelet, F. The generalized NRTL model associated with the Peng—Robinson equation of state to predict liquid—liquid equilibria between hydrocarbons, water and ethylene glycol. *Polish J. Chem.* **2006**, *80*, 27.
(19) Pedersen, K. S.; Milter, J.; Rasmussen, C. P. Mutual solubility of water and a reservoir fluid at high temperatures and pressures – experimental and simulated data. *Fluid Phase Equilibria.* **2001**, *189*, 85-97.
(20) Kontogeorgis, G. M.; Folas, G. K. Thermodynamic models for industrial applications: From classical and advanced mixing rules to associations theories; John Wiley & Sons: West Sussex, **2010**.
(21) Gomis, V.; Font, A.; Saquete, M. D.; García-Cano, J. Isothermal (liquid + liquid) equilibrium data at T = 313.15 K and isobaric (vapor + liquid + liquid) equilibrium data at 101.3 kPa for the ternary system (water + 1-butanol + p-xylene). *J. Chem. Thermodynamics* **2014**, *79*, 242-247.
(22) Gomis, V.; Font, A.; Saquete, M. D.; García-Cano, J. Phase equilibria of the water + 1-butanol + toluene ternary system at 101.3 kPa. *Fluid Phase Equilibria.* **2015**, *385*, 29-36.
(23) Wang, H.; Wang, Q.; Xiong, Z.; Chen, C. Liquid–liquid equilibria for ternary system water + toluene + benzaldehyde at (303.2–343.2) K. *Fluid Phase Equilibria.* **2014**, *383*, 43-48.
(24) García-Flores, B. E.; Justo-García, D. N.; Aquino-Olivos, M. A.; García-Sánchez, F. (Liquid + liquid) equilibria in the (water + tetrahydrofuran + methylcyclohexane) ternary system at temperatures between (278 and 343) K and atmospheric pressure: Experimental data and correlation. *Fluid Phase Equilibria.* **2015**, *385*, 166-174.

Chapter 11 - Conclusions

Introduction

The previous work had three major facets that were investigated and concluded upon in their respective chapters (3, 4, and 10). The main points from the three respective conclusions are summarized below, followed with suggestions for what can be done in the future to further these research areas.

Major conclusions

Objective 1:

In assessing the possible advantages of using Fischer—Tropsch technology to generate steam for SAGD bitumen recovery, two cases were compared with the traditional OTSG. One case produced steam for SAGD at low pressure and the other case produced steam for OTSG at high pressure.

a) Pairing Fischer—Tropsch with OTSG increased the utility requirements of the process, but reduced CO_2 emissions by a significant amount more than the additional utility requirements of the process.
b) Provided the Fischer—Tropsch synthesis produces less than 40 mol % methane, using Fischer—Tropsch technology to generate steam for SAGD will result in the same amount of steam generation as traditional OTSG, but have lower CO_2 emissions and increased bitumen/syncrude yield. Knowing at what temperature cobalt—based Fischer—Tropsch can be run and produce 40 mol % methane will require experimental testing in a lab.

c) The best results were from low pressure production of steam. Under these conditions the use of Fischer—Tropsch technology reduced CO_2 emissions by 29 % and increased bitumen/syncrude yield by 17.2 %.

Objective 2:

The use of a water electrolysis unit in a hydrogen gas loop as well as cobalt catalyst and iron catalyst based Fischer—Tropsch gas loops has been compared against the use of a traditional air separation unit in the gas loops for oxygen production. Several things were found that are of use for potential gas loop designs:

a) The use of water electrolysis led to significant gains in carbon efficiency in Fischer—Tropsch gas loops. In the case of cobalt Fischer—Tropsch the carbon efficiency was 86.9 % and for the iron Fischer—Tropsch gas loops the carbon efficiency was 97 %.
b) When using a WEU within a cobalt Fischer—Tropsch gas loop, the excess hydrogen can be used to generate the necessary power for the WEU, which is the main user of electricity. The WEU used 21.1 MJ/kg O_2 of electricity to electolyze water into oxygen and hydrogen. The WEU gas loop has a significantly lower CO_2 emission than the ASU gas loop provided the steam generated in the process provides power for the WEU as well as a portion of the excess hydrogen is converted into electricity in a gas turbine.
c) When using a WEU in a iron Fischer—Tropsch gas loop there is not enough excess hydrogen to supplement the power generation from steam, and either a renewable energy resource is needed to power the WEU, or natural gas can be used to generate the required electricity. Either way, the iron Fischer—Tropsch gas loop will still have a lower CO_2 emission than the ASU gas loop.

Objective 3:

Several guidelines for modelling Fischer—Tropsch oxygenate products as a result of the Chapter 10 have been determined:

(a) All models are not equal. In this work Gamma—Phi models were the best models. This can most likely be attributed to having several parameters focused on liquid phase accuracy and one parameter focused on the vapor phase. Whereas with classical and advanced cubic equations of state the parameters must capture vapor and liquid phase accuracy. The use of the Hayden O'Connell for vapor phase modelling with UNIQUAC for the liquid phase was the most reliable choice.

(b) Parameter optimization is as important as model selection. Models are not equipped by default for Fischer—Tropsch products. While time consuming, optimizing parameters greatly reduces error. If data is scarce, UNIFAC provided reasonable estimates for the hydrocarbon oxygenate pairs. Mutual solubility data improved the LLE and VLLE predictions of all models. The use of VLE data for optimizing water-oxygenate pairs also improved accuracy in models and these pairs should be regressed whenever data is available.

(c) The Huron—Vidal Peng—Robinson had difficulty with VLLE which was a surprise. Care should be taken when using these advanced mixing rule models for VLLE. When possible include experimental tie-lines into the regression routine.

Future work

Suggestion 1: The use of iron catalyzed Fischer—Tropsch should be investigated. Iron Fischer—Tropsch is run at temperatures that can naturally produce high pressure steam for SAGD.

Suggestion 2: An assessment of capital cost should also be evaluated for the use of using Fischer—Tropsch technology to produce steam for SAGD since the capital cost of Fischer—Tropsch may outweigh the benefits.

Suggestion 3: The cases in Chapter 4 were not optimized. There could be a greater benefit to WEU after optimization. This would require a sensitivity analysis to determine and model each variable (i.e., ratio of internal recycle, external recycle, purge etc.). The potential for other feed types, specifically hydrogen lean feeds like coal, could see even larger benefits to the use of a WEU in a Fischer—Tropsch gas loop.

Suggestion 3: Advanced mixing rule cubic equations of state had an unexpectedly poor performance for water—oxygenate—hydrocarbon VLLE. It is likely to be worth investigating other advanced mixing rules such as the Wong—Sandler mixing rules. There are newer models not included in this investigation that are derived from a statistical basis to account for association. The two broad classes are the statistical associating fluid theory (SAFT) and cubic-plus-association (CPA). These models should also be evaluated in the same fashion as the classical models done in this work. They may turn out to be particularly good at handling carboxylic acids.

Bibliography

Aika, K. I.; Christiansen, L. J.; Dybkjaer, I.; Hansen, J. B.; Nielsen, P. H.; Nielsen, A.; Tamaru, K. *Ammonia: catalysis and manufacture*. A. Nielsen (Ed.). Springer Science & Business Media, **2012**.

Arai, Y. Measurement of isothermal vapor—liquid equilibria for hydrocarbon + monocarboxylic acid binary systems by a flow-type apparatus. *J. Chem. Eng. Data* **2000***, 45*, 857-861.

Arlt, W.; Sørenson, J. M. Liquid—liquid Equilibrium Data Collection: Ternary Systems. Vols. V Part 2; DECHEMA: Frankfurt, **1980**.

Asia Industrial Gases Association. Reciprocating compressors for oxygen service, code of Practice AIGA 048/08; AIGA: Singapore, **2008**.

Babadagli, T.; Al-Bahlani, A.M.: Hydrocarbon Recovery Process for Fractured Reservoirs, Canadian Patent Application, Serial No: 2,639,997 filed in Oct. 6, **2008**.

Becker, W.L.; Braun, R.J.; Penev, M.; Melaina, M. Production of Fischer—Tropsch liquid fuels from high temperature solid oxide co-electrolysis units. *Energy* **2012**, *Vol.47*, 99-115.

Bertau, M.; Plass, H.O.L.; Wernicke, F.S.H-J. (Eds), *Methanol: The basic chemical and energy feedstock of the future: Asinger's vision today,* Springer-Verlag: Berlin, **2014**.

Brusset, H.; Kaiser, L.; Hoquel, J. Présentation d'un nouvel ébulliomètre à recyclage. *Chim. Ind. Genie Chim.* **1968***, 99*, 220-224.

Butler, R.M. *Horizontal wells for the recovery of oil, gas, and bitumen*, Petroleum Society, **1994.**

Butler, R.M. *Thermal recovery of oil and bitumen*, Prentice-Hall, **1991.**

Caldwell, L.; Van Vuuren, D. S. On the formation and composition of the liquid phase in Fischer—Tropsch reactors. *Chem. Eng. Sci.* **1986**, *41*, 89-96.

Canadian Oil Sands innovation Alliance, COSIA challenge: Down Hole Steam Generation, **2014**

Chemical Engineering Speciality, College of Shanghai Chemical Engineering Shanghai Instutute of Petrochemistry. I. Study on the vapor liquid equilibrium data for acetic acid-water-vinyl acetate ternary system. The mutually miscible liquid phase region (paper in Chinese, data in Roman numerals). *Acta Chim. Sinica* **1976**, *34*, 79-92.

Chou, J. S.; Chao, K. C. Solubility of synthesis and product gases in a Fischer—Tropsch Sasol wax. *Ind. Eng. Chem. Res.* **1992**, *31*, 621-623.

Chou, J.S.; Chao, K.C. Correlation of synthesis gas solubility in n-paraffin solvents and Fischer—Tropsch waxes. *Fluid Phase Equilibria* **1989**, *Vol. 46,* 179-195.

Chueh, W.C.; Falter, C.; Abbott, M.; Scipio, D.; Furler, P.; Haile, S.M.; Steinfeld, A., *Science*, **2010**, *330*, 1797.

Clausen, L.R.; Houbak, N.; Elmegaard, B., *Energy*, 2010, **35**, 2338.

De Klerk, A., *Prepr. Pap.-Am. Chem. Soc., Div. Energy Fuels*, **2014**, *59* (2), 823.

De Klerk, A. *Energy Sci. Eng.*, **2015**, **3**, 60.

De Klerk, A. Hydroprocessing peculiarities of Fischer—Tropsch syncrude. *Catalysis Today*, **2008,** *130*, 439-445.

De Klerk, Arno. *Fischer—Tropsch Refining*; Wiley-VCH: Germany, 2010.

Derevich, I.V.; Ermdaev, V.S.; Mordkovich, V.Z. Liquid-vapor thermodynamic equilibrium in Fischer—Tropsch synthesis products. *Theoretical Foundations of Chemical Engineering* **2008**, *Vol. 42*, 216-219.

Derevich, I.V.; Ermdaev, V.S.; Mordkovich, V.Z. Modelling the thermal and physical properties of liquid and gas mixtures of Fischer—Tropsch products. *Theoretical Foundations of*

Chemical Engineering **2011**, *Vol. 45*, 221-226.

Derevich, I.V.; Ermdaev, V.S.; Zol'nikova, N.V.; Mordkovich, V.Z. Thermodynamics of wax formation in the Fischer—Tropsch Synthesis products. *Theoretical Foundations of Chemical Engineering* **2013**, *Vol. 47*, 191-200.

Diamond, D.; Hahn, T.; Becker, H.; Patterson, G. Improving the understanding of a novel complex azeotropic distillation process using a simplified graphical model and simulation. *Chem. Eng. Process.* **2004**, *43*, 483-493.

Doscher, T.M. Factors influencing success in steam soak operations. *Proc. Pet. Ind.* Conference on thermal oil recovery. Los Angeles, **1966**, 70-80.

Dry, M. E.;Steynberg, A. P. Commercial FT process applications. *Studies in Surface Science and Catalysis*, **2004,** *152*, 406-481.

Dry, M.E.; The Fischer—Tropsch Process: 1950-2000. *Catalysis Today*, **2002**, 71, 227

Eliot, T. Q.; Goddin, C. S. Jr; Pace, B. S. Chemicals from hydrocarbon synthesis. *Chem. Eng. Progr.* **1949**, *45*, 532-536.

Elliott, J.R.; Lira, C.T. *Introductory Chemical Engineering Thermodynamics* (2ed.); Prentice Hall: Upper Saddle River, NJ, **1999.**

Falbe ed. *New synthyses with carbon monoxide*, Springer Verlag: Heildelberg, **1980**.

Farouq Ali, S.M. Canada's super strategy for oil sands. *Journal of Canadian Petroleum Technology*, **1994**, 16-19.

García-Flores, B. E.; Justo-García, D. N.; Aquino-Olivos, M. A.; García-Sánchez, F. (Liquid + liquid) equilibria in the (water + tetrahydrofuran + methylcyclohexane) ternary system at temperatures between (278 and 343) K and atmospheric pressure: Experimental data and correlation. *Fluid Phase Equilibria.* **2015**, *385*, 166-174.

Gilmont, R.; Othmer D. F. Composition of vapors from boiling binary solutions. *Ind. Eng. Chem.* **1944***, 36*, 1061-1064.

Gmehling, J.; Onken, U.; Grenzheuser, P. *Vapor—liquid Equilibrium Data Collection: Carboxylic Acids, Anhydrides, Esters. Vol. I Part 5*; DECHEMA: Frankfurt, **1982**.

Gmehling, J.; Onken, U.; Rarey-Nies, J. R. *Vapor—liquid Equilibrium Data Collection: Aqueous Systems. Vols. I, Part 1b (Supplement 2)*; DECHEMA: Frankfurt, **1988**.

Gmehling, J.; Onken, U.; Rarey-Nies, J. R. *Vapor—liquid Equilibrium Data Collection: Organic Hydroxyl Compounds: Alcohols. Vol. I Part 2a*; DECHEMA: Frankfurt, **1977**.

Gomis, V.; Font, A.; Saquete, M. D. Vapor—liquid—liquid and vapor liquid equilibrium of the system water + ethanol + heptane at 101.3 kPa. *Fluid Phase Equil.* **2006***, 248*, 206-210.

Gomis, V.; Font, A.; Saquete, M. D.; García-Cano, J. Isothermal (liquid + liquid) equilibrium data at T = 313.15 K and isobaric (vapor + liquid + liquid) equilibrium data at 101.3 kPa for the ternary system (water + 1-butanol + p-xylene). *J. Chem. Thermodynamics* **2014**, *79*, 242-247.

Gomis, V.; Font, A.; Saquete, M. D.; García-Cano, J. Phase equilibria of the water + 1-butanol + toluene ternary system at 101.3 kPa. *Fluid Phase Equilibria.* **2015**, *385*, 29-36.

González Prieto, M.; Sánchez, F. A.; Pereda, S. Thermodynamic model for biomass processing in pressure intensified technologies. *J. Supercrit. Fluids* **2015**, *96*, 53-67.

Graves, C.; Ebbesen, S.D.; Mogensen, M.; Lackner, K.S. Sustainable hydrocarbon fuels by recycling CO_2 and H_2O with renewable or nuclear energy. *Renewable and Sustainable energy Reviews* **2011**, *Vol. 15*, 1-23.

Graves, C.R. *Recycling CO_2 into sustainable hydrocarbon fuels: electrolysis of CO_2 and H_2O.* PhD Thesis, Columbia University, **2010.**

Gunardson, H. H. (Ed.). *Industrial gases in petrochemical processing: chemical industries*. CRC Press, **1997**.

Gupta, S.C.; Gittins, S.D.; Field implementation of solvent aided process "waxy" mixtures. Paper 2002-299 presented at the Canadian International Conference, Calgary, Alberta, Canada, June 11-13, **2002**.

Hannula, I., *Biomass and Bioenergy*, **2015**, **74**, 26.

Häring, H-W. ed. *Industrial gases processing*, Wiley-VCH: Weinheim, **2008**.

Hayden, J.G.; O'Connell, J.P. A generalized method for predicting second Virial coefficients. *Industrial Engineering and Chemistry Process Design and Development* **1975**, *Vol 14*, 209-216.

Higman, C.; van der Burgt, M., *Gasification*, 2ed, Elsevier: Amsterdam, **2008**.

Holladay, J. D.; Hu, J.; King, D. L.; Wang, Y. An overview of hydrogen production technologies. *Catalysis Today* ***2009***, *139*(4), 244-260.

Huang, S. H.; Lin, H. M.; Tsai, F. N.; Chao, K. C. Solubility of synthesis gases in heavy n-paraffins and Fischer—Tropsch wax. *Ind. Eng. Chem. Res.* **1988**, *27*, 162-169.

Huron, V.J.; Vidal, J. New mixing rules in simple equations of state for representing vapor-liquid of strongly non-ideal mixtures. *Fluid Phase Equilibria* **1979**, *Vol. 3*, pp 255-271.

Jager, B. Developments in Fischer—Tropsch Technology. *Studies in Surface Science and Catalysis* **1998**, *Vol. 119*, 25-34.

Jensen, S.H.; Larsen, P.H.; Mogensen, M. Hydrogen and synthetic fuel productions from renewable energy sources. *International Journal of Hydrogen Energy* **2007**, *Vol. 32*, 3253-3257.

Journal of Physical and Chemical Reference Data. AIP Publishing (NIST), **2005**, 1399.

Journal of Physical and Chemical Reference Data. AIP Publishing (NIST), **2005**, 709.

Karimi, Z.; Rahmani, M.; Mogadam, M. A study on the vapor—liquid equilibria in Fischer—Tropsch synthesis. *Procedia Engineering* **2012**, *Vol. 42*, 25-33.

Keshavarz, M. Mechanistic simulation study of steam-solvent co-injection for bitumen and heavy oil recovery; Masters. Thesis, University of Alberta, **2013**.

Kidnay, A.J.; Parrish, W.R., *Fundamentals of natural gas processing*, Taylor & Francis: Boca Raton, **2006**.

Kohl, A.L.; Nielsen, R.B. *Gas Purification* 5ed, Gulf Publishing Company, Houston Texas, **1997**.

Kontogeorgis, G. M.; Folas, G. K. *Thermodynamic models for industrial applications: From classical and advanced mixing rules to associations theories*; John Wiley & Sons: West Sussex, **2010**.

Kresnyak, S. Process for co-producing commercially valuable products from byproducts of heavy oil and bitumen upgrading process, US Patent # US20150038599, Feb 5, **2015**.

Lwin, Y. Chemical equilibrium by Gibbs energy minimization on spreadsheets*, *International Journal of Engineering Education*, **2000**, *16*, 335-339.

Marano, J. J.; Holder, G. D. Characterization of Fischer—Tropsch liquids for vapor—liquid equilibria calculations. *Fluid Phase Equilibria.* **1997**, *138*, 1-21.

Marina, J. M.; Tassios, D. P. Effective local compositions in phase equilibrium correlations. *Ind. Eng. Chem. Process Des. Dev.* **1973***., 12*, 67-71.

Masuku, C. M.; Ma, W.; Hildebrandt, D.; Glasser, D.; Davis, B. H. A vapor—liquid equilibrium thermodynamic model for a Fischer—Tropsch reactor. *Fluid Phase Equilibria.* **2012**, *314*, 38-45.

Mathias, P. M.; Copeman, T. W. Extension of the Peng—Robinson equation-of-state to complex mixtures: Evaluation of the Various Forms of the Local Composition Concept. *Fluid Phase Equil.* **1983***, 13*, 91.

Matsoukas, T. *Fundamentals of chemical engineering thermodynamics;* Prentice-Hall: Upper Saddle River, NJ, **2013**.

Michelsen, M.L.; Mollerup, J.M. *Thermodynamic Models: Fundamentals & Computational Aspect;* Tie-Line Productions: Denmark, **2007.**

Miglio, R.; Zennaro, R.; de Klerk, A., In *Greener Fischer—Tropsch processes for fuels and feedstocks*, P.M. Maitlis and A. de Klerk Eds., Wiley-VCH: Weinheim, **2013**, 311.

Nasr, T.N.; Beaulieu, G.; Golbeck, H.; Heck, G. Novel expanding solvent-SAGD process "ES-SAGD". *Journal of Canadian Petroleum Technology* **2003**, *Vol. 42*, 13-16.

Nasr, T.N.; Isaacs, E.E., Process for Enhancing Hydrocarbon Mobility Using a Steam Additive; US Patent # 6,230,814, May 15, **2001**.

Neau, E.; Nicolas, C.; Jaubert, J. N.; Mutelet, F. The generalized NRTL model associated with the Peng—Robinson equation of state to predict liquid—liquid equilibria between hydrocarbons, water, and ethylene glycol. *Polish Journal of Chemistry,* **2006**, *80*, 27

Newman, S.A., *Acid and sour gas treating processes*, Gulf Publishing Company, Houston Texas, **1985**.

Nguyen, V.N.; Blum, L. Syngas and synfuels from H_2O and CO_2: current status. *Chemie Ingenieur Technik* **2015**, *Vol. 87*, 354-375

Nguyen-Huynh, D.; De Hemptinne, J-C.; Lugo, R.; Passarello, J-P.; Tobaly, P. Simultaneous liquid—liquid and vapor-liquid equilibria predictions of selected oxygenated aromatic molecules in mixtures with alkanes, alcohols, water, using the polar GC-PC-SAFT. *Chem. Eng. Res. Des.* **2014**, *92*, 2912-2935.

Othmer, D. F.; Silvis, S. J.; Spiel, A. Composition of vapors from boiling binary solutions. Pressure equilibrium still for studying water—acetic acid system. *Ind. Eng. Chem.* **1952***, 36*, 1864-1872.

Ouellette, N.; Rogner, H-H.; Scott, D.S., *Int. J. Hydrogen Energy* **1995**, *20*, 873.

Pedersen, K. S.; Michelsen, M. L.; Fredheim, A. O. Phase equilibrium calculations for unprocessed well streams containing hydrate inhibitors. *Fluid Phase Equilibria.* **1996**, *126*, 13-28.

Pedersen, K. S.; Milter, J.; Rasmussen, C. P. Mutual solubility of water and a reservoir fluid at high temperatures and pressures – experimental and simulated data. *Fluid Phase Equilibria*. **2001**, *189*, 85-97.

Peng, D.Y.; Robinson, D.B.; A new two constant equation of state. *Ind. Eng. Chem. Fundam.,* **1976**, *15*, 59-64.

Piatkowski, N.; Wieckert, C.; Weimer, A.W.; Steinfeld, A., *Energy Environ. Sci.*, **2011**, *4*, 73.

Pinaud, B.A.; Benck, J.D.; Seitz, L.C.; Forman, A.J.; Chen, Z.; Deutsch, T.G.; James, B.D.; Baum, K.N.; Baum, G.N.; Ardo, S.; Wang, H.; Millere, E.; Jaramillo, T.F., *Energy Environ. Sci.*, 2013, *6*, **1983**.

Poling, B.E.; Prausnitz, J.M.; O'Connell, J.P. *Properties of gases and liquids*, 5ed; McGraw-Hill Education: New York, **2001**.

Rao, M. R.; Rao, C. V. Ternary Liquid Equilibria. IV. Various Systems. *J. Appl. Chem.* **1957***, 7*, 659-666.

Redlich, O.; Kwong, J.N.S.; On the thermodynamics of solutions: V. an equation of state: fugacities of gaseous solutions. *Chem. Rev.***1949**, *44*, 233-244.

Rodríguez Vallejo, D. F.; De Klerk, A. Improving the interface between Fischer—Tropsch synthesis and refining. *Energy Fuels* **2013**, *27*, 3137-3147.

Romero M.; Steinfeld, A., *Energy Environ. Sci.*, **2012**, *5*, 9234.

Rostrup-Nielsen, J.; Christiansen, L. J. *Concepts in Syngas Manufacture;* Imperial College Press: London, **2011**.

Schulz, H. A short history of Fischer—Tropsch and present trends of Fischer—Tropsch synthesis, *Applied Catalysis A: General*, **1999,** 3-12**.**

Soave, G. Equilibrium constants from a modified Redlich-Kwong equation of state. *Chem. Eng. Sci.* **1972**, *27*, 1197-1203.

Specht, M.; Bandi, A.; Baumgart, F.; Murray, C.N.; Gretz, J., In *Greenhouse gas control technologies*, B. Eliasson, P.W.F. Riemer and A. Wokaun Eds., Pergamon Press: Amsterdam, **1999**, 723

Stempian, J.P.; Ni, M.; Sun, Q., Chan, S.H. Thermodynamic analysis of combined Solid Oxide Electrolyzer and Fischer—Tropsch processes. *Energy* **2015**, Vol. 81, 682-690.

Steynberg, A.P.; Nel, Herman G., Clean coal conversion options using Fischer—Tropsch technology. *Fuel* **2003**, *Vol. 83*, 765-770.

Storch, H.H.; Golumbic, N.; Anderson, R.B. The Fischer—Tropsch and Related Syntheses, Wiley, New York, **1951**

Tsai, F.N.; Huang, S.H.; Lin, H.M.; Chao, K.C. Solubility of methane, ethane, and carbon dioxide in a Mobile Fischer—Tropsch wax and in n-paraffins. *The Chemical Engineering Journal* **1988**, *Vol. 38*, 41-46.

Ulrich, G.D.; Vasudevan, P.T. *Chemical engineering process design and economics: a practical guide*, Process Publishing: Durham, New Hampshire, **2004**.

Vallejo, D.F.R.; De Klerk, A. Improving the interface between Fischer—Tropsch synthesis and refining. *Energy and Fuels* **2013**, *Vol. 27*, 3137-3147.

Van der Waals, J.D. On the continuity of the gas and liquid state. Doctoral Dissertation, Leiden, **1873**.

Vosloo, A. C. Fischer–Tropsch: a futuristic view. *Fuel processing technology*, **2001**, *71*(1), 149-155.

Walas, S.M. *Phase Equilibria in Chemical Engineering*; Butterworth: Boston, **1985**.

Walpot, Henk. *Theoretical modelling of residue curve maps for a reactive distillation concept for the production of n-propyl propionate*; Master's Thesis, Technical University of Delft*;* **2011**

Wang, H.; Wang, Q.; Xiong, Z.; Chen, C. Liquid–liquid equilibria for ternary system water + toluene + benzaldehyde at (303.2–343.2) K. *Fluid Phase Equilibria.* **2014**, *383*, 43-48.

Wang, Y.N.; Li, Y.W.; Bai,L.; Zhao, Y.L, Zhang, B.J. Correlation of gas-liquid equilibrium prediction in Fischer—Tropsch synthesis. *Fuel* **1999**, *Vol. 78*, 911-917.

Appendix A: Derivation of phase equilibrium conditions for VLLE

The following is a derivation for the conditions at equilibrium for a VLLE system. VLE and LLE are simplified versions of the derivation which follow the exact same methodology, but are … simpler. Figure A.1 shows a schematic of a closed and isolated system. The methodology employed is based on reference 1.

1) Elliott, J. A. W. Advanced macroscopic and statistical thermodynamics, course notes (CH E 625), University Of Alberta, **2015**.

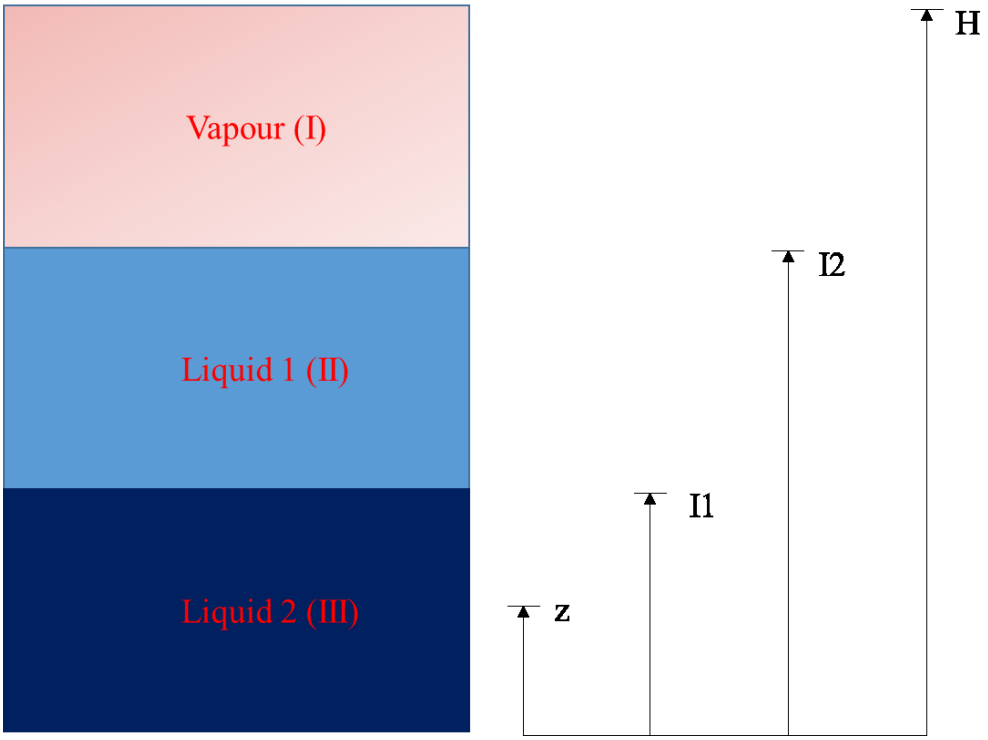

Figure A.1: Vapor—liquid—liquid Equilibrium system.

Solving for the conditions at equilibrium requires knowledge of the constraints. For a closed, isolated system, the number of moles of each component is constant and energy cannot flow into or out of the system i.e. energy is conserved.

$$N = Constant = A\left[\int_0^{I1} n^I dz + \int_{I1}^{I2} n^{II} dz + \int_{I2}^{H} n^{III} dz\right] \quad \text{A.1}$$

$$E = Constant = A\left[\int_0^{I1} u^I dz + \int_{I1}^{I2} u^{II} dz + \int_{I2}^{H} u^{III} dz\right] \quad \text{A.2}$$

Here A stands for area, n for number of moles in a given phase, and u for internal energy of a given phase.

At equilibrium the net change in entropy must be zero. The definition of the composite systems entropy is given below:

$$S^c = S^I + S^{II} + S^{III} \tag{A.3}$$

This leads to:

$$S^c = A\left[\int_0^{I1} s^I dz + \int_{I1}^{I2} s^{II} dz + \int_{I2}^{H} s^{III} dz\ \right] \tag{A.4}$$

The problem is now a maximization of A.4 with the constraints A.1 and A.2. While there are many ways to solve this mathematically, the most popular method is to use Lagrangian multipliers.

$$\partial[S^c - \lambda_0 E - \lambda_1 N] = 0 \tag{A.5}$$

Where "c" stands for composite system. Inserting equations A.1, A.2 and A.4 into equation A.5 leads to

$$\delta\left\{A\left[\int_0^{I_1}(s^I - \lambda_0 u^I - \lambda_1 n^I\ )dz + \int_{I_1}^{I_2}(s^{II} - \lambda_0 u^{II} - \lambda_1 n^{II})dz + \int_{I_2}^{H}(s^{III} - \lambda_0 u^{III} - \lambda_1 n^{III})dz\ \right]\right\} = 0 \tag{A.6}$$

It must be noted that the integrals are not over constant bounds; therefore Leibniz rule must be used when evaluating the integrals. Using Leibniz rule for differential integration:

$$\left\{\left[\int_0^{I_1}(\partial s^I - \lambda_0 \partial u^I - \lambda_1 \partial n^I\ )dz + (s^I - \lambda_0 u^I - \lambda_1 n^I)\ |_{I_1}\partial I_1 + \int_{I_1}^{I_2}(\partial s^{II} - \lambda_0 \partial u^{II} - \lambda_{1\partial} n^{II})dz + (s^{II} - \lambda_0 u^{II} - \lambda_1 n^{II})\ |_{I_2}\partial I_2 - (s^{II} - \lambda_0 u^{II} - \lambda_1 n^{II})\ |_{I_1}\partial I_1 + \int_{I_2}^{H}(s^{III} - \lambda_0 u^{III} - \lambda_1 n^{III})dz - (s^{III} - \lambda_0 u^{III} - \lambda_1 n^{III})\ |_{I_2}\partial I_2\ \right]\right\} = 0 \tag{A.7}$$

And inserting the following expressions:

$$s = \frac{u}{T} + \frac{P}{T} - \sum_i^{NC}\frac{\mu_i n_i}{T} \text{ and } \partial s = \frac{\partial u}{T} - \sum_i^{NC}\frac{\mu_i \partial n_i}{T}$$

Leads to:

$$\left\{\left[\int_0^{I_1}\left(\frac{\partial u^I}{T^I}-\sum_i^{NC}\frac{\mu_i{}^I\partial n_i{}^I}{T^I}-\lambda_0\partial u^I-\lambda_1\partial n^I\right)dz\right.\right.$$
$$+\left(\frac{u^I}{T^I}+\frac{P^I}{T^I}-\sum_i^{NC}\frac{\mu_i{}^I n_i^I}{T^I}-\lambda_0 u^I-\lambda_1 n^I\right)\Bigg|_{I_1}\partial I_1$$
$$+\int_{I_1}^{I_2}\left(\frac{\partial u^{II}}{T^{II}}-\sum_i^{NC}\frac{\mu_i{}^{II}\partial n_i{}^{II}}{T^{II}}-\lambda_0\partial u^{II}-\lambda_1\partial n^{II}\right)dz$$
$$+\left(\frac{u^{II}}{T^{II}}+\frac{P^{II}}{T^{II}}-\sum_i^{NC}\frac{\mu_i{}^{II} n_i^{II}}{T^{II}}-\lambda_0 u^{II}-\lambda_1 n^{II}\right)\Bigg|_{I_2}\partial I_2$$
$$-\left(\frac{u^{II}}{T^{II}}+\frac{P^{II}}{T^{II}}-\sum_i^{NC}\frac{\mu_i{}^{II} n_i^{II}}{T^{II}}-\lambda_0 u^{II}-\lambda_1 n^{II}\right)\Bigg|_{I_1}\partial I_1$$
$$+\int_{I_2}^{H}\left(\frac{\partial u^{III}}{T^{III}}-\sum_i^{NC}\frac{\mu_i{}^{III}\partial n_i{}^{III}}{T^{III}}-\lambda_0\partial u^{III}-\lambda_1\partial n^{III}\right)dz$$
$$\left.\left.-\left(\frac{u^{III}}{T^{III}}+\frac{P^{III}}{T^{III}}-\sum_i^{NC}\frac{\mu_i{}^{III} n_i^{III}}{T^{III}}-\lambda_0 u^{III}-\lambda_1 n^{III}\right)\Bigg|_{I_2}\partial I_2\right]\right\}=0$$

A.8

With a bit of rearrangement to put like terms together this becomes:

$$\left\{\left[\int_0^{I_1}\left(\left(\frac{1}{T^I}-\lambda_0\right)\partial u^I-\sum_i^{NC}\left(\frac{{\mu_i}^I}{T^I}-\lambda_1\right)\partial {n_i}^I\right)dz\right.\right. \tag{A.9}$$

$$+\int_{I_1}^{I_2}\left(\left(\frac{1}{T^{II}}-\lambda_0\right)\partial u^{III}-\sum_i^{NC}\left(\frac{{\mu_i}^{II}}{T^{II}}-\lambda_1\right)\partial {n_i}^{II}\right)dz$$

$$+\int_{I_2}^{H}\left(\left(\frac{1}{T^{III}}-\lambda_0\right)\partial u^{III}-\sum_i^{NC}\left(\frac{{\mu_i}^{III}}{T^{III}}-\lambda_1\right)\partial {n_i}^{III}\right)dz$$

$$+\left(\frac{u^I}{T^I}-\frac{u^{II}}{T^{II}}+\frac{P^I}{T^I}-\frac{P^{II}}{T^{II}}+\sum_i^{NC}\frac{{\mu_i}^{II}n_i^{II}}{T^{II}}-\sum_i^{NC}\frac{{\mu_i}^{I}n_i^{I}}{T^I}+\lambda_0u^{II}-\lambda_0u^I+\lambda_1n^{II}\right.$$

$$\left.-\lambda_1n^I\right)\Big|_{I_1}\partial I_1$$

$$+\left(\frac{u^{II}}{T^{II}}-\frac{u^{III}}{T^{III}}+\frac{P^{II}}{T^{II}}-\frac{P^{III}}{T^{III}}+\sum_i^{NC}\frac{{\mu_i}^{III}n_i^{III}}{T^{III}}-\sum_i^{NC}\frac{{\mu_i}^{II}n_i^{II}}{T^{II}}+\lambda_0u^{III}-\lambda_0u^{II}\right.$$

$$\left.\left.+\lambda_1n^{III}-\lambda_1n^{II}\right)\Big|_{I_2}\partial I_2\right]\right\}=0$$

From the first three integrals

$$\frac{1}{T^I}-\lambda_0=0,\frac{1}{T^{II}}-\lambda_0=0,\frac{1}{T^{III}}-\lambda_0=0$$

Therefore:

$$T^I=T^{II}=T^{III}=\frac{1}{\lambda_0}=constant$$

Comparing: $\frac{{\mu_i}^I}{T^I}-\lambda_1=0,\frac{{\mu_i}^{II}}{T^{II}}-\lambda_1=0,\frac{{\mu_i}^{III}}{T^{III}}-\lambda_1=0$ it is clear that

$${\mu_i}^I={\mu_i}^{II}={\mu_i}^{III}=\lambda_1T=constant$$

And after substituting the definitions just calculated into the last two terms most of the terms cancel out and it is readily found that

$$P^I=P^{II}\text{and }P^{II}=P^{III}$$

So that the conditions for equilibrium in a VLLE system has been derived. The same method is used to calculate the conditions at equilibrium for VLE and LLE. As a general expression:

$$\mu_i^I=\mu_i^{II}=,\dots,=\mu_i^{NP}\ for\ i=1,2,\dots,NC$$

$$T^I=T^{II}=,\dots,=T^{NP}$$

$$P^I=P^{II}=,\dots,=P^{NP}$$

Appendix B: Additional ternary LLE and VLLE figures.

Appendix B contains supplementary figures for the water—acetic acid—hexane ternary (LLE) and the water—ethanol—heptane ternary (VLLE). Both default and optimized values for parameters are shown.

(1) Arlt, W.; Sørenson, J. M. Liquid—liquid Equilibrium Data Collection: Ternary Systems. Vols. V Part 2; DECHEMA: Frankfurt, **1980**

(2) Gomis, V.; Font, A.; Saquete, M. D. Vapor—liquid—liquid and vapor liquid equilibrium of the system water + ethanol + heptane at 101.3 kPa. *Fluid Phase Equil.* **2006**, *248*, 206-210.

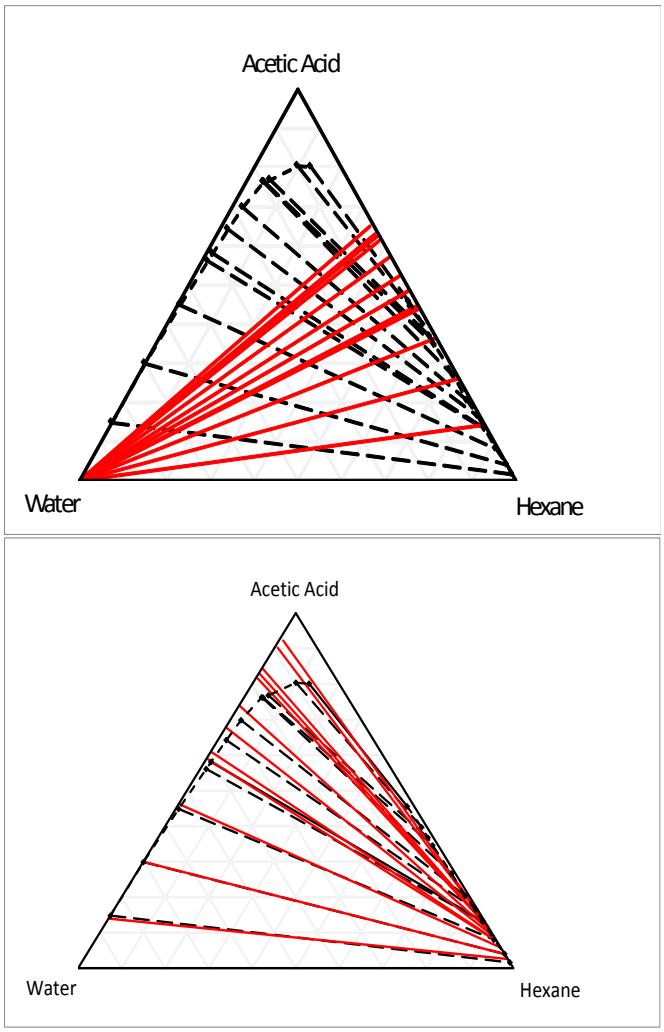

Figure B.1. Peng—Robinson calculation of LLE for water—acetic acid—hexane using (top) default parameters, and (bottom) optimized parameters. Calculated values are solid lines, experimental values are dashed lines.[(1)]

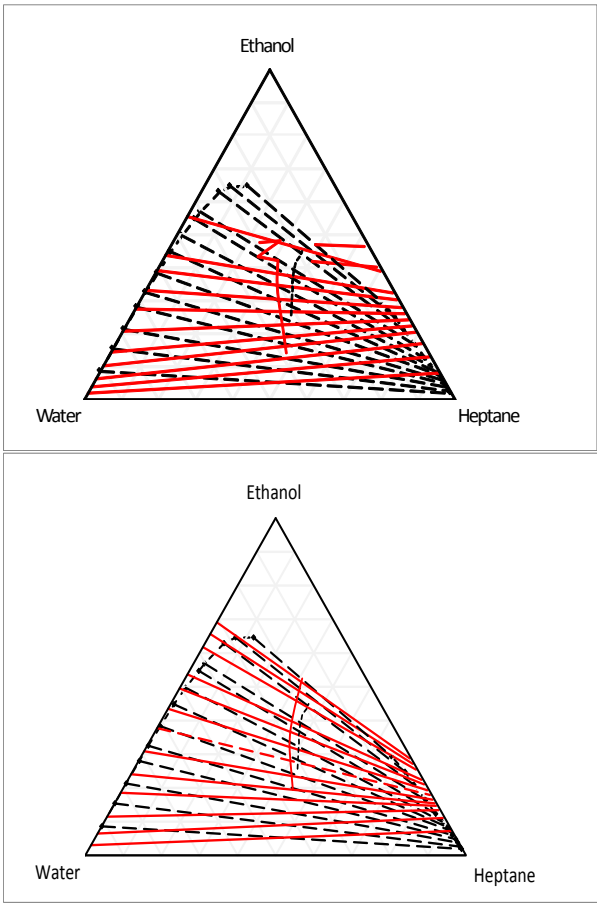

Figure B.2. Peng—Robinson calculation of VLLE for water—ethanol—heptane using (top) default parameters, and (bottom) optimized parameters. Calculated values are solid lines, experimental values are dashed lines.[2]

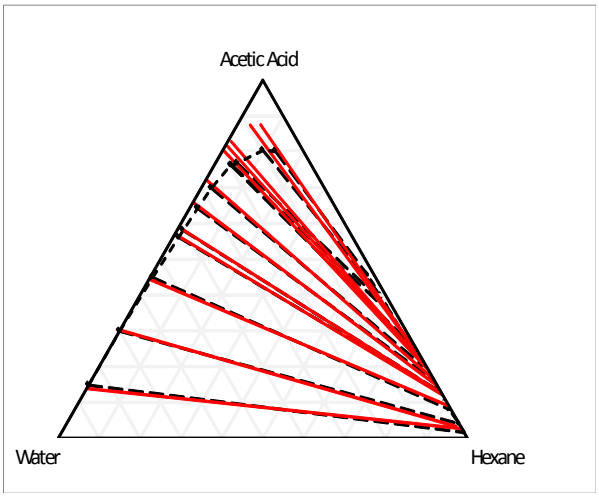

Figure B.3 Huron—Vidal Peng—Robinson calculation of LLE for water—acetic acid—hexane using optimized parameters; default parameters failed to predict LLE. Calculated values are solid lines, experimental values are dashed lines.(1)

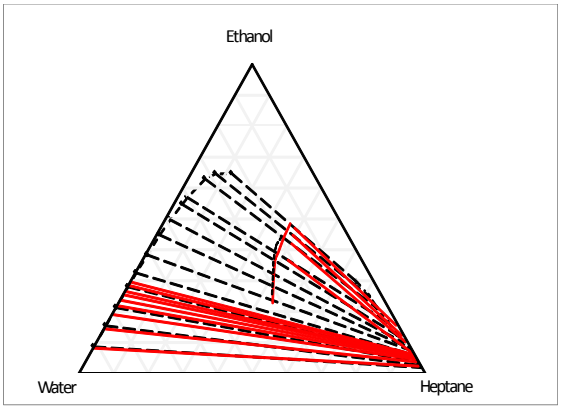

Figure B.4 Huron—Vidal Peng—Robinson calculation of VLLE for water—ethanol—heptane using optimized parameters; default parameters failed to predict LLE. Calculated values are solid lines, experimental values are dashed lines.(2)

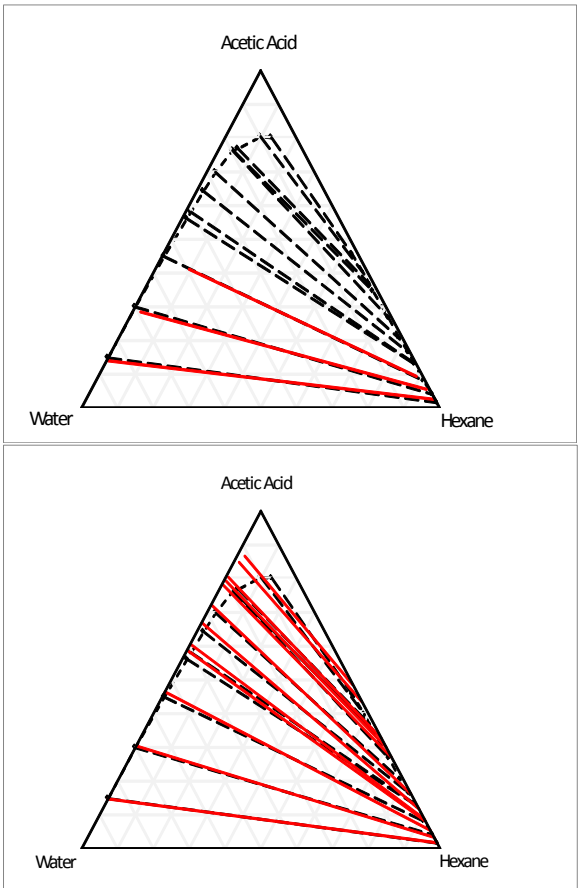

Figure B.5 NRTL with Hayden O'Connell calculation of LLE for water—acetic acid—hexane using (top) default parameters, and (bottom) optimized parameters. Calculated values are solid lines, experimental values are dashed lines.[1]

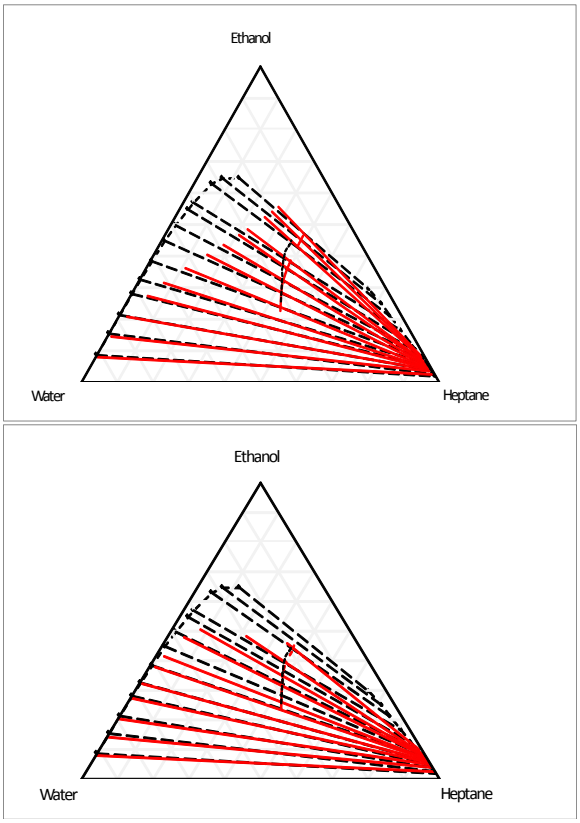

Figure B.6 NRTL with Hayden O'Connell calculation of VLLE for water—ethanol—heptane using (top) default parameters, and (bottom) optimized parameters. Calculated values are solid lines, experimental value are dashed lines.[2]

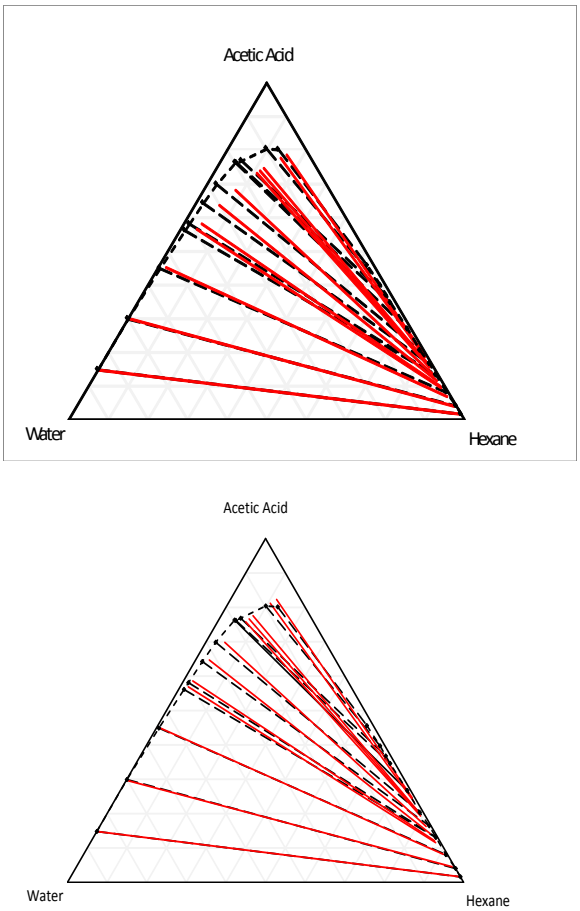

Figure B.7 UNIQUAC with Hayden O'Connell calculation of LLE for water—acetic acid—hexane using (top) default parameters, and (bottom) optimized parameters. Calculated values are solid lines, experimental values are dashed lines.[1]

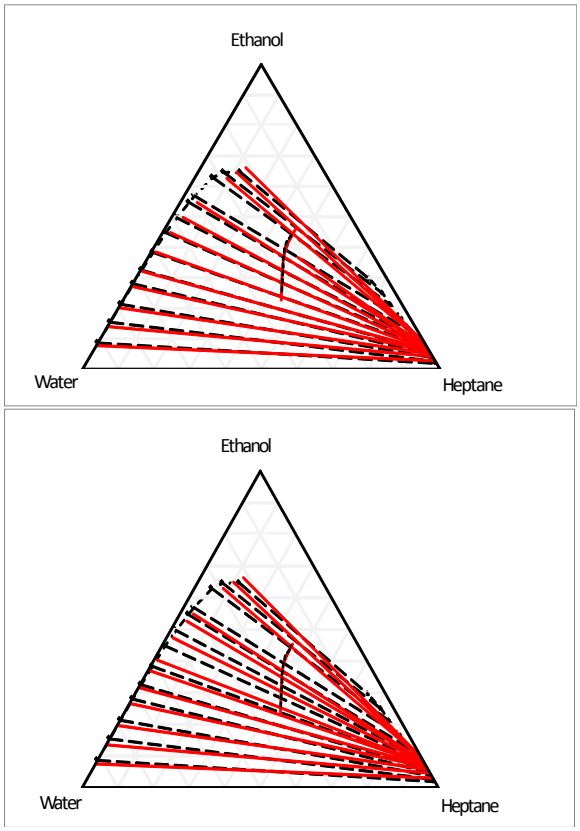

Figure B.8 UNIQUAC with Hayden O'Connell calculation of VLLE for water—ethanol—heptane using (top) default parameters, and (bottom) optimized parameters. Calculated values are solid lines, experimental values are dashed lines.[2]

Appendix C: Additional phase equilibrium error analysis

Appendix C contains the experimental data, model predictions, and error analysis for the tie-lines with under 10 % oxygenates. **Table B1** and contains the flash composition used to initiate calculations in VMGSim as well as the experimental results for the water—acetic acid—hexane LLE ternaries.[1][2] **Table B2** contains the model predictions for the flash compositions (**Table B1**), and the error analysis between the predicted and experimental results (**Tables B2 and B1** respectively).

References

(3) Arlt, W.; Sørenson, J. M. Liquid—liquid Equilibrium Data Collection: Ternary Systems. Vols. V Part 2; DECHEMA: Frankfurt, **1980**

(4) Rao, M. R.; Rao, C. V. Ternary Liquid Equilibria. IV. Various Systems. *J. Appl. Chem.* **1957***, 7*, 659-666

(5) Gomis, V.; Font, A.; Saquete, M. D. Vapor—liquid—liquid and vapor liquid equilibrium of the system water + ethanol + heptane at 101.3 kPa. *Fluid Phase Equil.* **2006***, 248*, 206-210.

Table B1 Experimental results and the corresponding flash compositions for Water—acetic acid—hexane tie-lines with less than 10 % acetic acid.

				Experimental Results					
Flash Composition				Organic Phase			Aqueous Phase		
Water	Acetic Acid	Hexane	T (K)	Water	Acetic Acid	Hexane	Water	Acetic Acid	Hexane
42.58	8.21	49.21	298	0	0.016	0.984	0.852	0.148	2.80E-04
48.03	2.11	49.86	304	0	0.003	0.997	0.961	0.039	0.00
46.74	3.54	49.73	304	0	0.006	0.994	0.935	0.065	2.41E-04
45.01	5.54	49.45	304	0	0.011	0.989	0.900	0.099	3.87E-04
43.24	7.52	49.24	304	0	0.016	0.984	0.865	0.135	5.50E-04

Table B2 Model predictions and AAPD for Table B1.

Model Predictions						AAPD Error (%)					
Organic Phase			Aqueous Phase			Organic Phase			Aqueous Phase		
Water	Acetic Acid	Hexane	Water	Acetic Acid	Hexane	Water	Acetic Acid	Hexane	Water	Acetic Acid	Hexane
Optimized Peng—Robinson Results											
0.000622	0.025851	0.973527	0.86037	0.13963	6.43887E-14	#DIV/0!	60.17013	1.050251	1.028604	5.7189	100
0.000616	0.011256	0.988127	0.968907	0.031093	4.68562E-19	#DIV/0!	292.5472	0.903118	0.854389	20.88542	#DIV/0!
0.000621	0.016216	0.983163	0.945033	0.054967	1.08934E-17	#DIV/0!	182.989	1.117045	1.09966	15.44209	100
0.000623	0.021064	0.978313	0.909533	0.090467	6.2441E-16	#DIV/0!	84.12295	1.036559	1.028158	8.928732	100
0.000622	0.024696	0.974682	0.873269	0.126731	2.09335E-14	#DIV/0!	57.19987	0.976174	0.979764	5.883719	100
Default Peng—Robinson Results											
0.000849	0.142824	0.856327	0.999885	0.000115	1.51298E-21	#DIV/0!	784.9092	12.96254	17.41111	99.92219	100
0.000593	0.040516	0.958891	0.999962	3.77E-05	1.64053E-21	#DIV/0!	1312.928	3.835171	4.086913	99.90403	#DIV/0!
0.000647	0.066311	0.933042	0.99994	5.96E-05	1.60732E-21	#DIV/0!	1057.244	6.158106	6.973663	99.90836	100
0.000729	0.100595	0.898676	0.999914	8.62E-05	1.56423E-21	#DIV/0!	779.3057	9.092426	11.06744	99.91327	100
0.000817	0.132275	0.866908	0.999892	0.000108	1.52558E-21	#DIV/0!	741.9821	11.92555	15.62162	99.91954	100
Optimized Huron—Vidal Peng—Robinson Results											
0.000725	0.026812	0.972463	0.861226	0.138774	4.44045E-11	#DIV/0!	66.12062	1.158429	1.12916	6.297124	99.99998
0.000647	0.007439	0.991914	0.965127	0.034873	9.11508E-12	#DIV/0!	159.4288	0.523328	0.460846	11.26532	#DIV/0!
0.000666	0.012135	0.987199	0.941053	0.058947	1.31084E-11	#DIV/0!	111.775	0.711163	0.67387	9.319372	99.99999
0.000692	0.018463	0.980845	0.907071	0.092929	2.19341E-11	#DIV/0!	61.38582	0.780393	0.7547	6.450422	99.99999
0.000717	0.024633	0.97465	0.873202	0.126798	3.68727E-11	#DIV/0!	56.80039	0.979395	0.971962	5.83361	99.99999
Optimized NRTL Results											
0.000621	0.017298	0.982082	0.852783	0.147216	9.51822E-07	#DIV/0!	7.172004	0.180732	0.137738	0.596857	99.66006
0.000627	0.004935	0.994438	0.962679	0.037321	4.45767E-07	#DIV/0!	72.10666	0.270245	0.206047	5.037926	#DIV/0!
0.000626	0.00805	0.991324	0.937138	0.062862	5.20038E-07	#DIV/0!	40.4858	0.296285	0.255054	3.297728	99.78418
0.000624	0.012147	0.987229	0.901218	0.098781	6.61037E-07	#DIV/0!	6.177283	0.134615	0.104646	0.559752	99.82907
0.000622	0.015982	0.983396	0.865444	0.134555	8.61482E-07	#DIV/0!	1.733291	0.090814	0.074902	0.072977	99.84347
Default NRTL Results											
0.004835	0.025743	0.969423	0.85552	0.139668	0.004811697	#DIV/0!	59.49778	1.467434	0.459121	5.69319	1618.463
0.002965	0.006487	0.990548	0.963136	0.035846	0.001017564	#DIV/0!	126.229	0.660372	0.25366	8.789872	#DIV/0!
0.003339	0.01093	0.985731	0.938282	0.060167	0.001550876	#DIV/0!	90.74034	0.858812	0.377416	7.442228	543.6394
0.003924	0.017202	0.978873	0.903221	0.094163	0.002616616	#DIV/0!	50.36578	0.979853	0.327042	5.20871	576.6093
0.004582	0.023499	0.971919	0.868049	0.127811	0.004139822	#DIV/0!	49.57855	1.256843	0.376133	5.081394	652.2205
Optimized UNIQUAC Results											
0.002818	0.016606	0.980576	0.851707	0.148086	0.00020722	#DIV/0!	2.887273	0.333804	0.011401	0.009666	25.9928
0.001079	0.002745	0.996175	0.960529	0.039458	1.304E-05	#DIV/0!	4.265331	0.095982	0.01771	0.399741	#DIV/0!
0.001381	0.005291	0.993328	0.934457	0.065514	2.94037E-05	#DIV/0!	7.657691	0.094721	0.031791	0.782579	87.79698
0.001917	0.009628	0.988455	0.898737	0.101188	7.52543E-05	#DIV/0!	15.84394	0.010587	0.171022	1.863497	80.54062
0.002566	0.014673	0.982762	0.863911	0.135927	0.000162575	#DIV/0!	6.602296	0.155272	0.10244	0.945888	70.45946
Default UNIQUAC Results											
0.003012	0.016767	0.980221	0.850946	0.147836	0.001217064	#DIV/0!	3.88284	0.369839	0.077917	0.17793	334.6659
0.001182	0.003469	0.995349	0.961032	0.038755	0.000213363	#DIV/0!	20.96826	0.178861	0.034583	1.388264	#DIV/0!
0.001539	0.006211	0.99225	0.935019	0.064638	0.000343749	#DIV/0!	8.386088	0.203147	0.02833	0.565508	42.66159
0.002119	0.01046	0.987421	0.898982	0.1004	0.000618739	#DIV/0!	8.567072	0.115163	0.143814	1.069806	59.9946
0.002768	0.015063	0.982169	0.863467	0.135502	0.001030871	#DIV/0!	4.119959	0.21547	0.153692	0.630213	87.31291

Table B3 and contains the flash composition used to initiate calculations in VMGSim as well as the experimental results for the water—ethanol—heptane VLLE ternary.[3] **Table B4** contains the model predictions for the flash compositions (**Table B1**), and Table B5 contains the error analysis between the predicted compositions (**Table B4**) and the experimental results (**Table B3**).

Table B3 Experimental results and the corresponding flash compositions for Water—ethanol—heptane tie-lines with less than 10 % ethanol.

				Experimental Results								
Flash Composition			T	Organic Phase			Aqueous Phase			Vapor Phase		
Water	Ethanol	Heptane	(K)	Water	Ethanol	Heptane	Water	Ethanol	Heptane	Water	Ethanol	Heptane
0.458	0.0525	0.48965	72.32	0.002	0.019	0.979	0.914	0.086	0.0003	0.313	0.257	0.429
0.4235	0.09	0.4858	70.83	0.002	0.026	0.971	0.845	0.154	0.0006	0.284	0.314	0.403

Table B4 Model predictions for Table B3.

Model Predictions								
Organic Phase			Aqueous Phase			Vapor Phase		
Water	Ethanol	Heptane	Water	Ethanol	Heptane	Water	Ethanol	Heptane
Optimized Peng—Robinson Results								
4.59E-03	7.21E-02	0.923344	0.969595	3.04E-02	1.57E-17	0.357674	0.194546	0.44778
4.71E-03	1.11E-01	0.884395	0.935368	6.46E-02	4.40E-16	0.325036	0.271332	0.403631
Default Peng—Robinson Results								
4.37E-03	8.06E-02	0.914997	0.979892	2.01E-02	3.11E-18	0.38436	0.14208	0.47356
4.60E-03	0.129919	0.865479	0.961014	3.90E-02	2.06E-17	0.357682	0.213138	0.42918
Optimized Gibbs Excess Peng Robinson Results								
3.02E-03	2.38E-02	0.97316	0.918415	8.15E-02	6.88E-05	0.32641	0.227176	0.446413
3.47E-03	3.76E-02	0.958957	0.85563	0.143989	3.82E-04	0.291116	0.293727	0.415157
Optimized NRTL Results								
2.92E-03	2.55E-02	0.971587	0.920052	7.99E-02	3.05E-05	0.32263	0.24018	0.43719
3.67E-03	3.96E-02	0.956768	0.857455	0.142196	3.50E-04	0.289886	0.302443	0.407671
Default NRTL Results								
0.008852	0.025217	0.965931	0.915842	0.080303	0.003855	0.330648	0.226863	0.442489
0.010312	0.035768	0.95392	0.844078	0.145251	0.010671	0.302316	0.279354	0.41833
Optimized UNIQUAC Results								
0.00309	0.027786	0.969123	0.922225	0.077711	6.33E-05	0.32574	0.234261	0.439999
0.003727	0.041326	0.954947	0.85919	0.140578	0.000233	0.291062	0.30041	0.408527
Default UNIQUAC Results								
3.84E-03	2.79E-02	0.968234	0.922119	7.76E-02	2.75E-04	0.330411	0.227323	0.442267
4.72E-03	4.20E-02	0.953261	0.859253	0.139989	7.58E-04	0.296419	0.292501	0.41108

Table B5 AAPD for Tables B3 and B4.

AAPD (%)								
Organic Phase			Aqueous Phase			Vapor Phase		
Water	Ethanol	Heptane	Water	Ethanol	Heptane	Water	Ethanol	Heptane
Optimized Peng—Robinson Results								
129.7314	279.2694	5.684965	6.082572	64.645	100	14.27276	24.30105	4.377614
135.4471	326.5244	8.919184	10.6944	58.03097	100	14.44942	13.58843	0.156655
Default Peng—Robinson Results								
118.5127	324.3822	6.537577	7.209205	76.61876	100	22.79882	44.716	10.3869
130.0964	399.688	10.86723	13.72947	74.68444	100	25.94443	32.12179	6.496341
Optimized Gibbs Excess Peng Robinson Results								
51.06368	25.3636	0.596564	0.483013	5.213419	77.06597	4.284496	11.60449	4.05899
73.43654	44.51586	1.240253	1.257962	6.500851	36.41172	2.505803	6.456396	3.016526
Optimized NRTL Results								
46.16237	34.15479	0.757166	0.662198	7.073286	89.82181	3.076656	6.544705	1.909081
83.69244	52.14483	1.465654	1.473919	7.665213	41.69809	2.072677	3.680723	1.159074
Default NRTL Results								
342.605	32.72259	1.334974	0.201544	6.624016	1184.846	5.638285	11.72648	3.14434
415.6214	37.56863	1.759039	0.109083	5.681288	1678.49	6.449309	11.03382	3.80401
Optimized UNIQUAC Results								
54.51812	46.24348	1.008848	0.899919	9.637843	78.90382	4.070361	8.847956	2.563873
86.32664	58.94709	1.653221	1.679273	8.715819	61.24966	2.486747	4.327903	1.371527
Default UNIQUAC Results								
92.08002	46.96889	1.099662	0.888263	9.759896	8.404628	5.562475	11.54764	3.092513
136.1872	61.59866	1.82692	1.686801	9.098132	26.27579	4.373026	6.846813	2.004863